Nitrogen Doped Highly Ordered Mesoporous Carbon as Catalyst and Catalyst Support for Oxygen Reduction

A Thesis Submitted By

Taiwo Olubunmi Alaje

For the Degree of Doctor of Philosophy

Supervisor: Professor Keith Scott

Dr. Eileen Yu

School of Chemical Engineering and Advanced Materials

Newcastle University

October, 2016

ABSTRACT

Fuels such as hydrogen, produced from renewable resources and efficiently utilized in environment friendly fuel cells are crucial to long term energy security. However, the lack of cost-effective catalysts, with a performance similar to that of platinum, is a major obstacle to the development of the fuel cell technology. This work researched cheap and environmental friendly oxygen reduction catalysts, based on carbon, which can replace platinum for oxygen reduction reaction (ORR) in the cathode of alkaline and microbial fuel cells. Nitrogen doped mesoporous carbon was prepared by pyrolyzing 1,2-diaminobenzene in a template of highly ordered mesoporous silica (KIT-6) at 700, 800 and 900 ^{o}C. Manganese oxides are active catalysts for ORR and as they are an earth abundant metal with widespread availability, this offsets a key drawback of the platinum group metals (PGM). A simple chemical deposition method (using $KMnO_4$) and physical deposition followed by heat treatment (using $Mn(NO_3)_2$) was used to prepare amorphous and crystalline manganese oxides which were separately deposited on ordered mesoporous nitrogen doped carbon (OMNC) and on ordered mesoporous carbon (OMC) without nitrogen doping respectively. The catalysts were characterized by Transmission Electron Microscopy (TEM), X-ray powder diffraction (XRD), Raman Spectroscopy, X-Ray Photoelectron Spectroscopy (XPS) and nitrogen adsorption-desorption.

Cyclic voltammetry and linear sweep voltammetry (LSV) with a rotating-ring disk electrode (RRDE) were used for electrochemical characterisation of the

oxygen reduction reaction (ORR). They were also tested as cathode catalysts in a microbial fuel cell. The best catalysts in alkaline media (0.1 M KOH) were amorphous manganese oxide on OMNC and OMC. They had onset potentials of 1.04 V and 1.05 V (RHE); half-wave potentials of 0.83 V and 0.82 V (RHE) respectively. This behaviour may be because the amorphous oxide maintained the ordered pore structure of the catalysts by depositing a thin coating of nanoparticle catalysts within them, thus causing a fast three phase reaction and excellent catalyst utilization. In the microbial fuel cell, the best catalysts were the amorphous MnO_2 on OMC and on nitrogen doped carbon pyrolyzed at 900°C with equal power densities of.

Dedication

To God only wise,

Creator, Redeemer and Friend;

to Him be all glory, now and forever,

Amen.

Acknowledgements

I wish to express my immense gratitude to my supervisor Professor Keith Scott for his excellent supervision and outstanding support throughout the duration of this doctorate degree. In addition to electrochemistry, I have learnt an enormous deal on how to deal with issues and people from you. Also to my second supervisor Dr Eileen Yu for her constant support. My heartfelt appreciation to Dr Katarina Novakovich (Director of Postgraduate Research Studies) for her unwavering support and also to Miss Justin McGruther(PGR Support Officer).

The members of the research group to which I belong played a defining role in my success. The Post-docs Dr. Mamlouk Mohammed, Dr Maryam Bayati and Dr. Terence Liu were helpful in so many ways. I also appreciate the friendship and academic support I received from my fellow PhD students Kemi, Osa , Ravi, Vinod, Chris, Ukrit and others who have graduated. I cannot but thank the "Microbial Quartet" Edward, Dorin, Martin and Su for the backing they gave while I ran my microbial fuel cell experiments.

I also appreciate my colleagues in my office C500 Merz Court especially Tolu and Chukwuma who helped in the last minute rolling out of my thesis.

My experiments would have meant little if I did not have access to equipment and personnel for the physical and chemical analysis of the materials and catalysts. In no particular order I wish to acknowledge the Leeds EPSRC Nanoscience and Nanotechnology Research Equipment Facility (LENNF) for granting me free access to carry out Transmission Electron Microscopy (TEM) analysis of my catalysts and especially Dr Zabeada Aslam who ran the machine and always had a friendly welcome whenever I visited. I also thank the National EPSRC XPS Users's Service (NEXUS) here in Newcastle University for access to XPS facilities. Special thanks to the staff, Dr. Naoko Sano and Dr. Anders Barlow who ran the machine and patiently taught me how to analyse my data. The XRD data were generated by Maggie White from

the Advanced Chemical and Materials Analysis (ACMA) also here in Newcastle University. Maggie also provided guidance (very patiently) on the basics of how to interpret my data. Mrs Sylvia Williamson from the School of Chemistry in St Andrews University obtained the data for BET analysis; thank you very much. Dr. Brian Ray graciously helped to obtain data for the Raman analysis – thanks Brian for being there when I really needed you.

My deep appreciation also goes to the body of Christ that assemble together at the Deeper Life Bible Church in the North East; the regional overseer, leaders and members. Thank you for the fellowship, encouragement, prayers and friendship.

Special thanks to my funding body, the Petroleum Technology Development Fund (PTDF) Nigeria, for their very generous financial support that made it possible for me to undertake this doctorate degree.

Thanks to the University of Lagos for granting me study leave and for their financial support too. Thank you to Professor Abiola Kehinde and late Professor Olu Ogboja who gave me the initial push into a research degree.

To the members of my family - mothers, brothers and sisters. I owe you more than a debt of gratitude. Thank you for always being there for me.

Special recognition goes to my wife Faith. Love, you have been to me a pillar, a shelter and a friend. Thank you for your loving sacrifice over these many years. I really appreciate it. To Jedidiah my son, even though you may not know it, your smile, laughter, and cries have contributed to the success of my PhD. I love you both.

Most importantly, I am grateful to Almighty God who has been my rock and my strength throughout this period and who has given me life and kept me this far. To Him be all the glory, in Jesus name. Amen.

Table of Contents

List of Figures

List of Tables

Chapter 1. **Introduction**

The environment, man's principal asset, is at risk. Much of the harm comes from the use of fossil fuels in internal combustion engines and power plants. Therefore, environment friendly fuels like hydrogen, ethanol and methanol are being developed. However, these would require the technology of fuel cells if they are to replace fossil fuels for power generation at different levels. The emergence of market ready fuel cells is being hindered by unavailability of inexpensive and widely available oxygen reduction catalysts amongst other reasons. This is because platinum being the catalyst of choice at the moment is not only very expensive, it is available only in a few countries. Hence, much effort is going into developing alternative non-platinum group metal catalysts. The setbacks encountered include poor activity, expensive precursor materials and complex procedures that do not lend themselves to widespread applicability. These were addressed in the course of this work.

The fuel cell is an electrochemical device that converts the chemical energy in a variety of fuels (and corresponding oxidant) directly into electricity, with negligible impact on the environment. There are different types and these include polymer electrolyte membrane fuel cells (PEMFC), solid oxide fuel cells (SOFC), molten carbonate fuel cells (MCFC), and phosphoric acid fuel cells (PAFC)(Mugikura and Asano, 2002). The PEMFC is the most researched because it has the highest number of potential applications. It can be divided into those that use acid or alkaline electrolytes. This work would be focused on alkaline electrolyte PEMFCs. To produce electricity PEMFCs use electrocatalysts like platinum at the anode and cathode. Despite having been around for decades, there remains much to be improved in them especially with respect to costs. A good proportion of this can be ascribed to the price of platinum which is used much more at the cathode than at the anode. Price aside, platinum is relatively very scarce, being available in limited amounts in a few nations. Hence, much research has gone into reducing the amount of platinum being used in fuel cells. However, as rightly pointed out by James

et al (2011) catalyst loading reductions with platinum and platinum group metals (PGM) are approaching a plateau and significant cost reduction in catalysis must be geared toward non-PGM catalysts. Good judgment will require, that alternatives, which though are less active but are also less expensive and more abundant, be used in solving the challenges posed by the cost and scarcity of platinum group metals (PGM). Carbon based catalysts can help (Gasteiger *et al.*, 2005).

Carbon based catalysts lend themselves as ready alternatives being more abundant, more durable than and not as expensive as PGM (Kobayashi *et al.*, 2011). Another advantage of carbon based catalyst is their selectivity for oxygen reduction at the cathode. This is vital in methanol fuel cells where there is the tendency for methanol to cross over from the anode to the cathode(Janarthanan *et al.*, 2015). The first set of carbon based catalysts considered prior to this time were the transition metal macrocyclic compounds specifically the phthalocyanines (Sen *et al.*, 1977), non-precious metal chalcogenides (Feng and Alonso-Vante, 2008) non-Precious metal based nitrides (Charreteur *et al.*, 2008) and electro-conductive polymers (Martínez Millán *et al.*, 2009; Othman *et al.*, 2012). It is interesting to note that most of these proposed alternatives contain nitrogen in one form or another. Indeed, the specific nature of the active sites of these alternatives has been a subject of debate. Nevertheless, recent findings by researchers like Kobayashi et al (2011), Liu et al (2011a) and Lyth et al (2011) point to the fact that their oxygen reduction capability is derived from nitrogen functional groups and perhaps carbon.

Therefore, recent efforts towards finding non-PGM catalysts for ORR tend to focus on nitrogen-doped carbons of different morphologies like carbon nanotubes, graphenes and ordered mesoporous carbon. Ordered mesoporous carbons (OMC) with high surface area and ordered pore structure would afford easy access of reactant molecules to active sites in addition to facile diffusion into and out of the pores. This is more so with the unique three-

dimensional network of pores present in KIT-6 template used in this work (Maiyalagan *et al.*, 2012a).

Much work has been done towards producing non-PGM catalysts for ORR in fuel cells (Faubert *et al.*, 1996; Xia and Mokaya, 2004; Kurak and Anderson, 2009; Wang *et al.*, 2010; Li *et al.*, 2012b). However, while some fall short in terms of activity others are simply too expensive to implement. Two examples are the works of Kim et al (2011b) and Wu et al(2011). Kim and co-workers made use of 5,9,14,18,23,27,32,36-octabutoxy-2,3-naphthalocyanine that costs £125.50/100 mg, while Wu's group used graphene oxide sheets that costs £260.5/g (sigma-aldrich UK; 13/03/16). 20 wt% platinum on Vulcan XC72 costs £98.40/g (sigma-aldrich UK; 13/03/16). Some others are too laborious, requiring several synthesis steps to obtain the final catalyst. An example being the work of Bikkarolla et al (2014) who deposited manganese oxide on nitrogenated graphene.

Hence, the need to develop non-PGM based catalysts which are active for ORR, low cost and easy to synthesize is the motivation for this research.

The aims of this work are

1. To develop a nitrogen doped carbon with the potential to replace platinum as an oxygen reduction reaction catalyst in alkaline and neutral media.
2. To use this nitrogen doped carbon as a support for manganese oxide thus harnessing the ORR activity of these two entities. This composite would also be tested for ORR activity in alkaline and neutral media.

Objectives

1. To use KIT-6 mesoporous silica for nanocasting nitrogen doped ordered mesoporous carbon using different reagents as simultaneous nitrogen and carbon source. Also, to optimize the pyrolysis temperature used.

2. To reduce the number of steps used to produce nitrogen doped carbon by eliminating the use of a template i.e.to employ a direct synthesis procedure. This should make the process less laborious and cheaper.
3. To optimize the deposition of manganese oxides on the best nitrogen doped carbons using different reagents and procedures.
4. Physical and chemical characterization of the catalysts synthesized.
5. To test the catalysts for oxygen reduction activity and stability in alkaline and neutral media.

The thesis is divided into the following chapters

Chapter One – Introduction to the work

Chapter Two – Literature Review

Chapter Three – Methodology

Chapter Four – Physical and Electrochemical Characterization of Ordered Mesoporous Nitrogen Doped Carbons used as ORR catalysts in Alkaline Media

Chapter Five - Physical and Electrochemical Characterization of Manganese Oxides Supported on Nitrogen-Doped Ordered Mesoporous Carbons

Chapter Six - Ordered Mesoporous Nitrogen doped carbon as catalyst and catalyst support in neutral media and their application in microbial fuel cells

Chapter Seven - Conclusions

Chapter 2. **Review of Literature**

2.1 Introduction

This chapter presents a review of literature that underpins the aims and objective of this research. Areas covered include the theoretical aspects of the oxygen reduction reaction (ORR), fuel cells and the challenge of durability and cost, the latter being largely dependent on the cost and amount of platinum. Also in the chapter, ORR activity of carbon based non-platinum group metal (PGM) catalysts is discussed along with the progress made hitherto. This is followed by an explanation of nitrogen doped carbon catalyst and the nature of their active sites. A justification for why highly ordered mesoporous carbon may make a difference is thereafter presented. At the end of the chapter, a review is presented on the application of carbon based catalysts and manganese oxide catalyst in microbial fuel cells. To conclude, a case is made based on literature, on why this work is worth doing.

2.2 Oxygen Reduction Reaction

In aqueous solutions, oxygen reduction reaction (ORR) occurs via two pathways. In acid electrolytes, one is the four-electron pathway from oxygen to water, while the other is the two-electron pathway from oxygen to hydrogen peroxide.

$$O_2 + 4e^- + 4H^+ \leftrightarrow 2H_2O \qquad E^o = 1.23V \qquad \text{eqn 2.1}$$

$$O_2 + 2e^- + 2H^+ \leftrightarrow H_2O_2 \qquad E^o = 0.67V \qquad \text{eqn 2.2}$$

The four-electron pathway is preferred in fuel cells that use oxygen as the oxidant. However, because of the very high O=O bond strength (498 kJ/mol) its activation requires a very large overpotential. The ORR is crucial not only to the overall fuel cell efficiency but also to cost. According to Gasteiger et al (2005), sluggish ORR kinetics is the major contributor to the overpotential experienced in fuel cells (**Figure 2-1**). This ultimately leads to a reduction in

efficiency and increase in cost due to the higher catalyst loading employed to generate appreciable current.

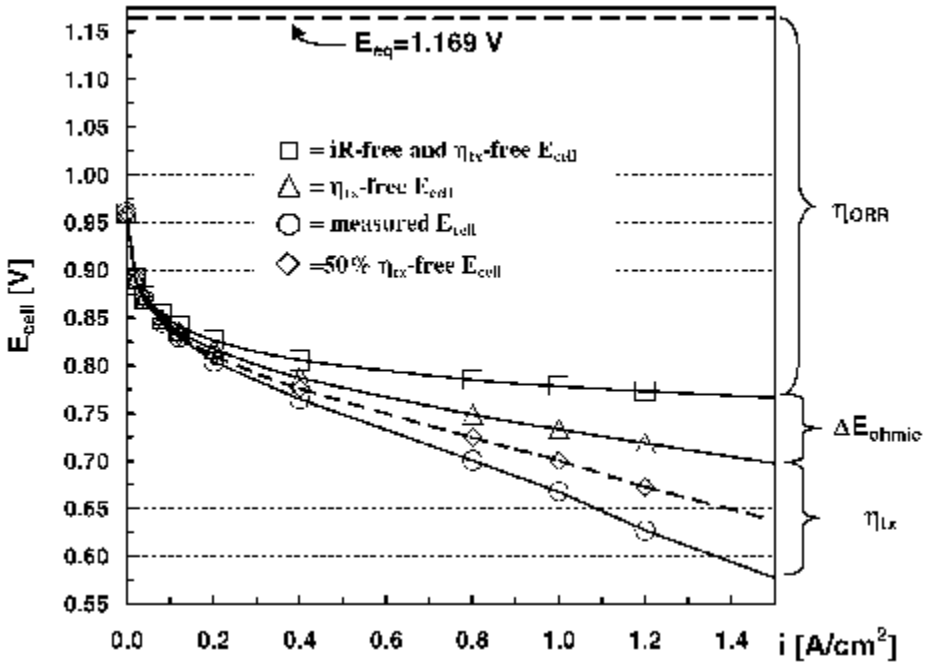

Figure 2-1 Effect of different voltage loss contributions on the output voltage of a H_2/O_2 fuel cell (Gasteiger *et al.*, 2005)

(a) Circular symbols: 50 cm^2 single-cell H_2/air performance at Tcell = 80 oC (80 °C dew points, i.e., 100% RH) at a total pressure of 150 kPa_{abs} and stoichiometric flows of s = 2.0/2.0. Catalyst-coated membrane (CCM) based on a ca. 25-mm low-EW membrane (ca. 900 EW) coated with electrodes consisting of ca. 50 wt.% Pt/carbon (0.4/0.4 mgPt/cm2 (anode/cathode)) and a low-EW ionomer (ca. 900 EW; ionomer/carbon ratio = 0.8/1).

▭ iR free and η_{tx}-free E_{cell}

△ η_{tx}-free E_{cell}

○ Measured E_{cell}(Gasteiger *et al.*, 2005)

◇ 50% η_{tx}-free E_{cell}

2.3 ORR Catalysts

So far, platinum and other platinum group metals (PGM) have proven to be the best catalysts for hydrogen oxidation and oxygen reduction in fuel cells. Therefore, much research efforts have gone into increasing their activity (A/mg_{pt}) while reducing the loading (mg_{pt}/cm^2) of membrane electrode assembly (MEA)). The end is to reduce the cost of fuel cells especially the

PEMFCs because the catalyst cost contributes significantly to its not being market competitive. However, regarding how much activity can be extracted out of the PGM, researchers seem to be approaching an asymptote. This is well documented in a report prepared by James et al (2011) to track the advances in fuel cell technology and corresponding cost of the car fuel cell system. The trends observed in **Figure 2-2** and **Figure 2-3** are pointers to the fact that there is a need to explore other options.

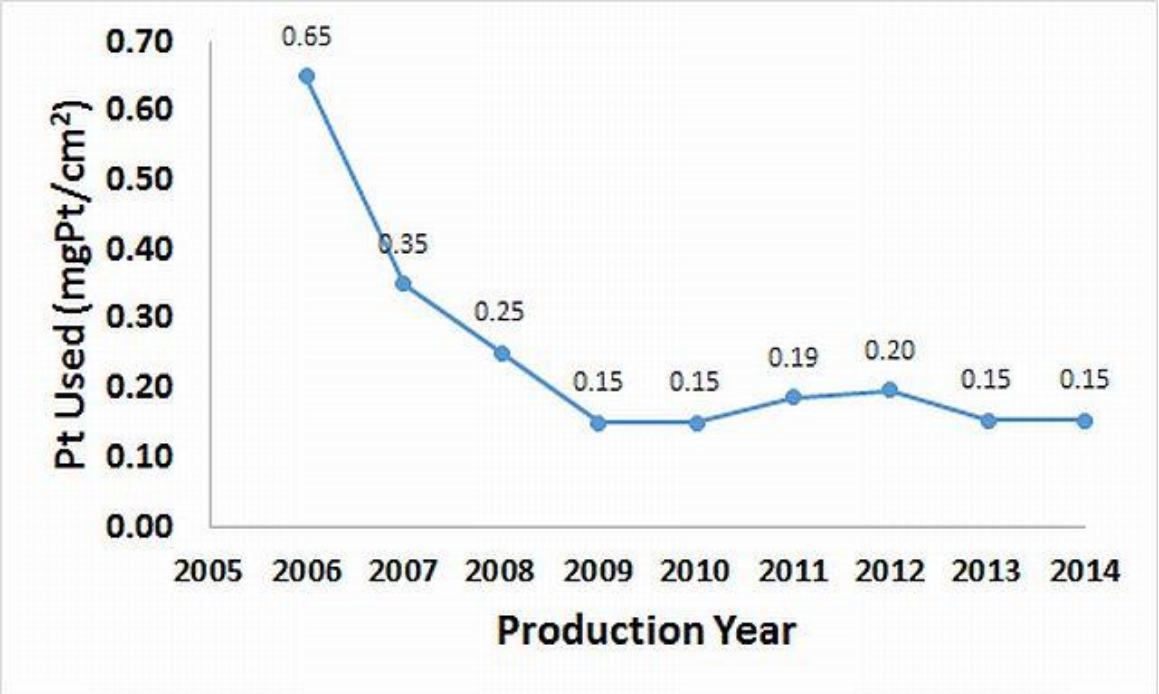

Figure 2-2 Reductions in total catalyst loading for automotive fuel cell systems from 2006 - 2011*Source (James et al., 2011; James et al., 2012; James et al., 2014; James et al., 2015)*

At the end of 2014, the optimized loading of platinum in automotive fuel cells remained at 0.153 mgPt/cm^2. The amount of platinum required to produce a KW of power did not improve either, increasing to 0.22 gPt/KW$_{net}$ at the end of 2014(James *et al.*, 2015). This further confirms the fact that the reduction of platinum loading in fuel cell systems has peaked and further cost reduction measures might need to be sought with non-PGM catalysts.

Hitherto, a means of increasing the mass activity of platinum catalysts was to increase its dispersion i.e. reducing particle size and increasing surface area.

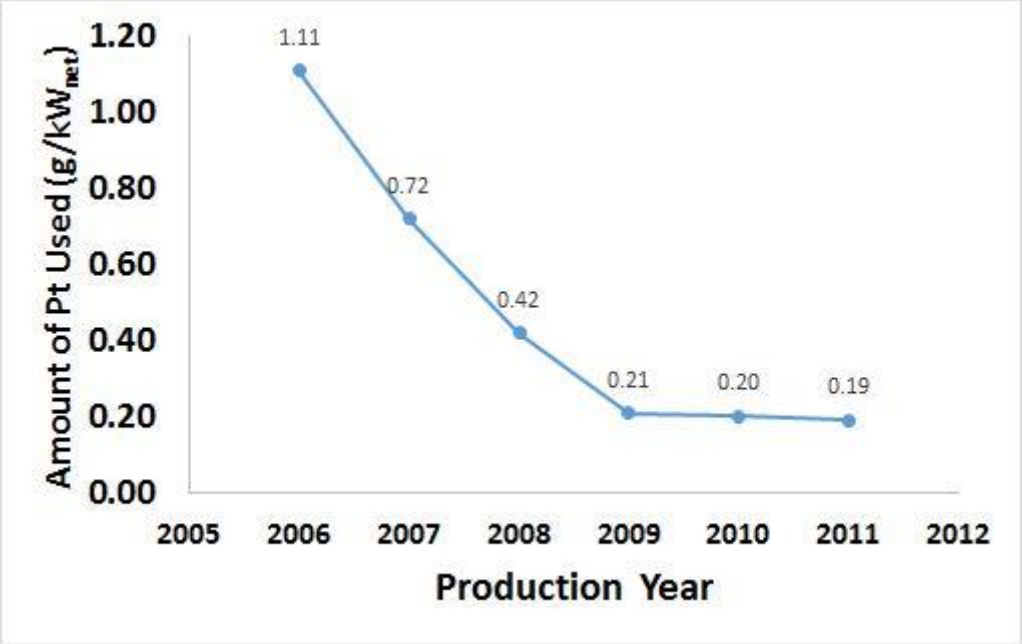

Figure 2-3 Reduction in total platinum usage for automotive fuel cell systems from 2006 - 2011Source (James et al., 2011)

However, it was established by Gasteiger (2005) that the mass activity would peak at a specific surface area of ca 90 m^2/mg_{pt} (**Figure 2-4**) which has already been attained.

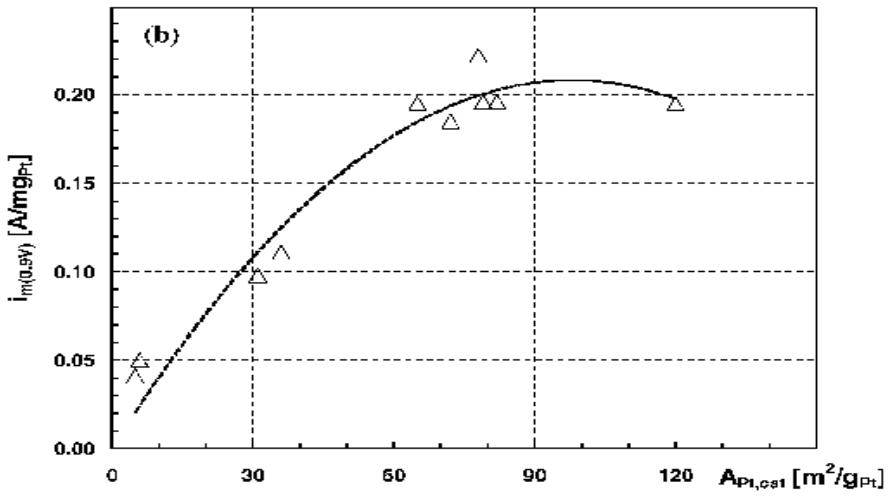

Figure 2-4 Variation in ORR mass activity, i_m (0.9V) with specific surface area of $Pt_{Apt,cat}$

(polycrystalline Pt, Pt-black and Pt/C catalysts at 0.9 V and 60 °C determined via RDE measurements in O_2 saturated 0.1M $HClO_4$. (20mV/s going from 0 to 1.0V))

This is because the adsorption strength of OH_{ads} (which blocks active sites) increases as the specific surface area increases (Mayrhofer *et al.*, 2005). **Table 2-1** gives an appreciation of the gap that needs to be filled.

Table 2-1 Technical targets: Electrocatalyst for transport applications

Characteristic	Unit	2015 Status	2020 target
Platinum group metal (PGM) total loading	mg PGM /cm2 electrode area	0.13	0.125
Mass activity	A / mg Pt @ 900 $mV_{IR\text{-}free}$	>0.5	0.44
PGM free catalyst activity	A/cm^2 @ 900 $mV_{IR\text{-}free}$	0.024	>0.044

Source ('Multi-Year Research, Development, and Demonstration Plan - Fuel Cells,' 2016)

According to a US Department of Energy Report report (James *et al.*, 2011), the hope for possible significant improvements lies in improving the power density or switching to non-platinum catalysts.

2.4 Non-platinum ORR catalysts

Good judgment will require, that alternatives, which though are less active are also less expensive and more abundant, be used in solving the challenges posed by the cost of platinum group metals (PGM). This is because being much cheaper than the platinum group metals, a larger amount can be applied to the electrode to make up for their reduced activity. The upper limit of how much can be loaded will be guided by mass transfer constraints. The understanding that the increased loading can make up for reduced activity has led to the use of transition metal containing compounds like phthalocyanines, porphyrins, chalcogenides and metal nitrides as ORR catalysts.

Another advantage of non-PGM catalysts is their specificity for oxygen reduction which is important in direct methanol fuel cells. Direct methanol fuel cells suffer from the challenge of methanol cross-over from the anode to the cathode (Yu and Scott, 2004). When platinum is used at the cathode, methanol cross-over can lead to a decrease in OCV of as much as 0.1V (Bunazawa and Yamazaki, 2009). However, non-PGM catalysts have been shown to demonstrate exceptional tolerance to methanol cross over (Janarthanan *et al.*, 2015). Hence they would perform better than platinum in direct methanol fuel cells.

Phthalocyanines and porphyrins are macrocyclic transition metal complexes with pyrrole as the building block. Phthalocyanines have a benzene ring fused to the pyrrole group to form isoindoles, as shown in **Figure 2-5** and **Figure 2-6**

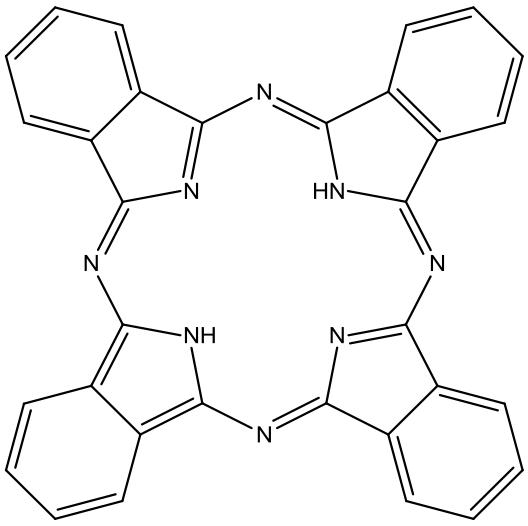

Figure 2-5 Basic structure of phthalocyanine

Jasinski (1964) carried out the first reported oxygen reduction in a fuel cell using phthalocyanines. Interestingly, this was performed with an alkaline electrolyte which generally affords a more facile kinetics compared with acid electrolytes (Ramaswamy and Mukerjee, 2011). Zagal (1992) Chen et al (2009) and Morozan et al, (2011) are amongst several researchers who have investigated the use of phthalocyanines and porphyrins for ORR. Most of them proposed that the ORR activity is a function of the conjugated transition metals like Fe and Co present within the macrocycle.

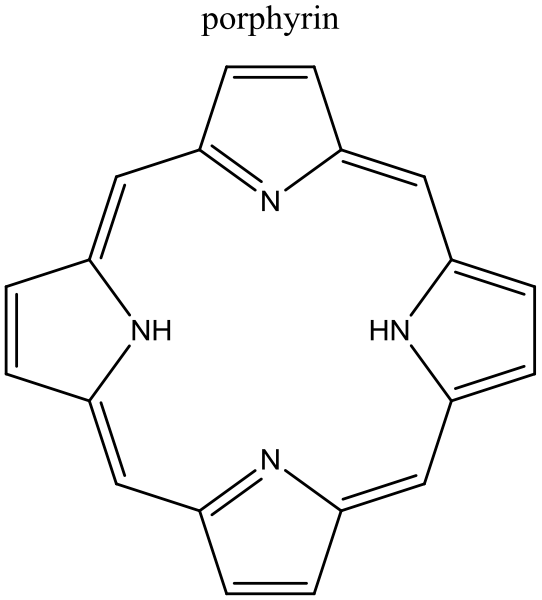

Figure 2-6 Basic structure of porphyrin

However, a number of researchers have also proposed that the nitrogen present in the macrocyle and not the metals are responsible for ORR activity. Among them is Kobayashi et al (2011)who in a well-structured experiment probed the electronic structure and coordination number of cobalt in pyrolyzed CoPc both before and after acid washing. The acid washing helped to remove ca 40% of the total quantity of cobalt which ironically gave rise to a slight improvement in the electrochemical properties of the catalyst. In addition, analysis revealed that the cobalt in the pyrolized CoPc consisted of metallic and not oxidized cobalt, which do not contribute significantly to ORR

activity. Hence, they concluded that the ORR activity of the catalysts comes from carbon and nitrogen, not the residual Co atoms in pyrolyzed CoPc. The group also carried out a similar research on FePc (Kobayashi *et al.*, 2012) which threw up the same conclusion, namely that the conjugated metals were converted to the metallic states after pyrolysis. According to Toda *et al* (1999) and Bashyam and Zelany (2006), metals in their metallic states do not exhibit significant ORR activity. Remarkably, the conversion of the conjugated metals to their metallic state was also confirmed in the work carried out by Faubert et al (Faubert *et al.*, 1996). Their XRD analysis confirmed that the Fe and Co in the catalysts (porphyrins being starting material) were present in their metallic state. The TEM analysis also revealed that most of the metals were coated in a graphitic layer exactly as was shown by Kobayashi et al. These two references establish that Fe and Co in porphyrins and phthalocyanine are converted to the metallic state after pyrolysis. Therefore, nitrogen and carbon are responsible for the ORR activity exhibited by macrocyclic compounds like phthalocyanines and porphyrins after pyrolysis.

Much of the argument for or against the metal centre being the active site seems to revolve around the nature of the metal after pyrolysis. Nevertheless, the fact remains that without the metal centres, nitrogen doped carbons have proven to be active for oxygen reduction reactions.

2.5 Nitrogen Doped Carbon as ORR Catalysts

The possibility of replacing carbon atoms in a sp^2 structure with nitrogen atoms (**Figure 2-7**) has opened up many areas of application for nitrogen-doped carbons.

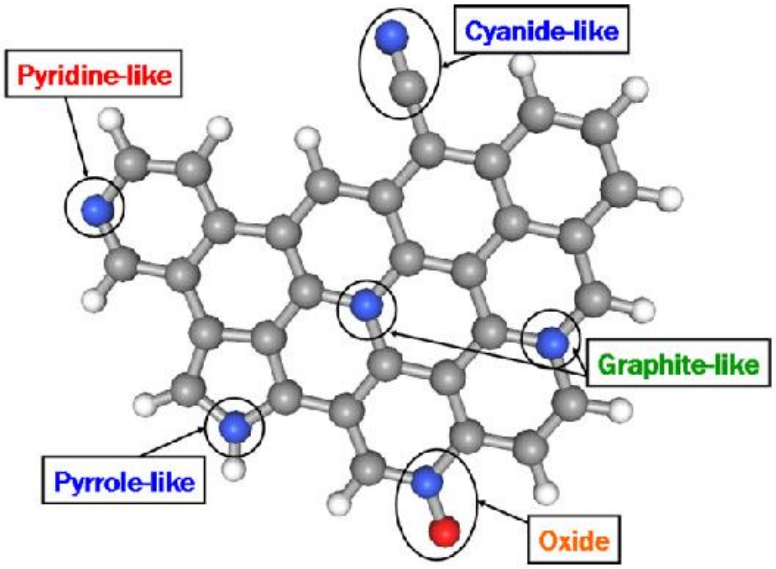

Figure 2-7 Schematic of various nitrogen moieties in N-doped graphene(Niwa *et al.*, 2011)

(Blue- N_2; white-H_2; red-O_2; grey-C)

This includes the possibility of modifying their mechanical, electronic and chemical properties (Terrones *et al.*, 2004). The ORR activity of N-doped carbons is one of such. Two major methods used in preparing nitrogen doped carbon materials are

i. The pyrolysis of nitrogen containing carbon precursors like phenylenediamine (Lu *et al.*, 2003; Xia and Mokaya, 2004; Liu *et al.*, 2010a). Nitrogen containing carbon precursors are heated at temperatures between 600 and 1050 ^{o}C under an inert atmosphere. This results in conversion into ORR active nitrogen moieties (**Figure 2-7**) specifically the pyridinic and quaternary structures. Stanczyk et al (1995) with the aid of X-ray Photoelectron Spectroscopy (XPS) analysis elucidated the transformation of nitrogen functionalities during carbonization of nitrogen containing carbon materials between 400 – 800 ^{o}C. They discovered that pyridinic structures possess a greater stability than pyrrolic ones with an increasing ratio of pyridinic to pyrrolic nitrogen as temperature increases. As the calcination temperature is increased further (ca 800 ^{o}C) both are converted to

quaternary or graphitic nitrogen. A significant outcome from their work is that similar nitrogen structures are obtained (although in different ratios) after calcination at 800 ^{o}C, irrespective of nitrogen functionality of the starting material.

ii. The second means of preparing n-doped carbon involves treatment of carbon or carbon precursors with gaseous ammonia at elevated temperatures (Wang *et al.*, 2010).This method has also proven effective in producing ORR active pyridinic and quaternary structures. During pyrolysis, ammonia decomposes to form free radicals like NH_2 and NH, which are capable of attacking carbon structures. This can lead to gasification as well as the inclusion of nitrogenous functional groups within the structure (Stöhr *et al.*, 1991; Rahinov *et al.*, 2003). Mangun *et al* (2001) carried out an investigation to find out the type of functional groups introduced during ammonia treatment of carbon. They also studied how the amount and type of functional groups change with treatment temperature and time. Their results revealed that the treatment successfully incorporated pyridinic, quaternary and amide groups into the carbon structure. A probable mechanism set forth was that of oxygen functional groups decomposing, thus leaving behind vacant sites that are attacked by the radicals. They concluded that substantial etching does not take place below 700 ^{o}C even though results from other researchers seem to contradict this (Wang *et al.*, 2010), perhaps this very aspect of their conclusion is specific to the type of carbon that was used.

2.6 Ordered Mesoporous Carbon

The nature of pores within any carbon material often determines its transport properties and structural functions. Pore sizes are categorised into three namely; micropores (pore dia < 2 nm), mesopores (2 nm <pore dia> 50 nm) and macropores (pore dia>50 nm). While micropores are known for maximizing surface area, they also suffer from pore blockage in the presence of bulky molecules. Macropores on the other hand are good for the transport

of bulky molecules but do not afford large surface areas. Mesopores therefore create a middle ground where significantly large surface areas are obtainable without undue pore blockage when bulky molecules are used (Shrestha and Mustain, 2010). Mesoporous materials have found applications in catalysis (Liu *et al.*, 2010c; Salgado *et al.*, 2010; Shresthaa and Mustaina, 2010; Slanac *et al.*, 2010; Su *et al.*, 2010; Calvillo *et al.*, 2011; Guo *et al.*, 2011; Li *et al.*, 2011; Liu *et al.*, 2011b; Maiyalagan *et al.*, 2012b) being that it is a surface phenomenon that requires the facile transport of reactants and products to and from active sites.

Ordered mesoporous carbon (OMC) have an array of periodically ordered pores, which is dependent on the structure of the ordered mesoporous silica template. Generally, they also possess a large surface area, large tuneable pores and narrow pore size distribution (Lee *et al.*, 2006). The periodically ordered array of mesopores results in a reduction in tortuosity. This enhances diffusion in OMCs compared with ordered microporous materials or even disordered mesoporous materials.

CMK-8 is a type of OMC that is synthesized by using the ordered mesoporous silica (OMS) KIT-6 as template. KIT-6 consists of a system of two continuous, interconnected and interwoven cylindrical chiral channels (Figure 2.8).

2.6.1 **Effect of pore structure on electrochemical activity**

Many researchers have investigated the effect of pore structure on the electrochemical performance of catalysts and fuel cells. Maruyama and Abe (Maruyama and Abe, 2007b; Maruyama and Abe, 2007a) in two separate investigations looked into the effect of catalysts/support structure on ORR in fuel cells.

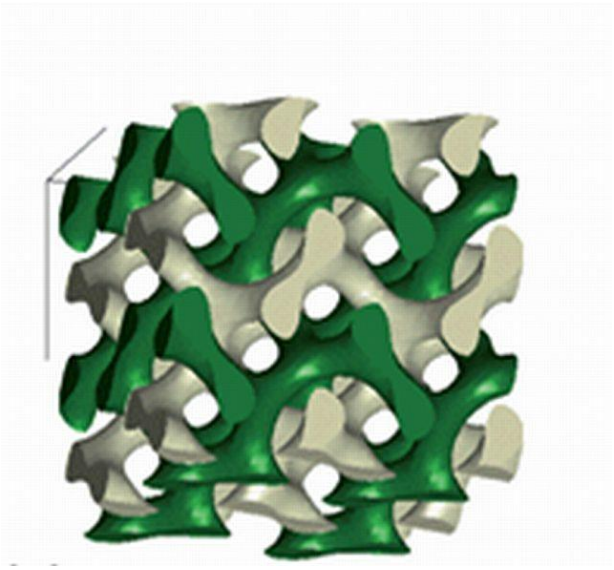

Figure 2-8 Sketch of ordered mesoporous KIT-6 template source (Almar *et al.*, 2013)

In the first, they synthesized three non-noble metal-based catalysts for ORR whose structure ranged between a graphene-layered structure and a very porous amorphous structure. The latter displayed a better output in half-cell rotating disks experiment (RDE) as well as in the fuel cell. In the second, they carried out ORR in a fuel cell using Pt supported on four different types of activated carbon, the main difference being in their pore structure and surface area. Here, the catalysts support with the largest mean pore diameter gave the best output at low voltages. Along the same line, Maiyalagan *et al* (Maiyalagan *et al.*, 2012b) carried out a study using two types of highly ordered mesoporous carbon (OMC) of different pore sizes as support for Pd in formic acid oxidation. The OMC with the larger pore size exhibited a higher specific mass activity of 486 mA/mg_{Pd} compared to 470.3 mA/mg_{Pd} for the smaller. Interestingly, they claimed that these performed better than Pd supported on carbon materials like CNT and graphene whose reported output from other researchers were 200 mA/mg_{Pd} and 210 mA/mg_{Pd} respectively. These findings underscore the importance of ordered mesoporous carbons as catalysts/support in electrochemical reactions. You and co-workers (You *et al.*, 2009) also developed glucose biosensors using OMC with different spatial

dimensions to immobilize glucose oxidase. Results showed that the CMK-8 (with an Ia3d symmetry) based biosensor had a better output than the CMK-3 (with p6mm symmetry) based biosensor and then earlier reported CNT biosensors.

2.7 Nitrogen doped ordered mesoporous carbon: State-of-the-art

OMCs with ordered pore structure and larger pore diameters compared with conventional carbon supports like Vulcan XC-72, graphene and CNT can facilitate easy molecular transport of products and reactants in ORR.

A large and increasing body of researchers have investigated the synthesis of doped OMC. One of such is Liu *et al* (2010a). They synthesized N-doped OMC with diaminobenezene (DAB) as both carbon and nitrogen precursor and ammonium peroxydisulfate (APDS) as oxidant. The synthesis was carried out in a template of highly ordered mesoporous silica SBA-15 at temperatures between 70^{o}C and 100^{o}C while the final product was pyrolyzed at 600^{o}C. TEM, SEM and small angle XRD showed that the N-doped carbons were a faithful replica of the SBA-15 template. XPS analysis also confirmed the presence of pyridinic and nitrile groups in the carbon. Peaks which correspond with the presence graphitic or quaternary (Q3) nitrogen were absent. While they obtained one of the highest overall nitrogen content reported in literature i.e. 26 wt%, same might not be said of the "quality" or chemical states of the nitrogen species vis their ability to catalyse ORR. This is because the ORR activity of N-doped carbon does not depend on the total amount of nitrogen present but rather on the type of nitrogen functional groups.

An analysis of the chemical states of the N_2 would have shed more light on the usefulness or otherwise of these results. Optimization of carbonization temperature could also have improved the outcome. This is because the percentage of pyridinic and quaternary groups that enhance ORR activity increases with temperature of pyrolysis (Stańczyk *et al.*, 1995). In addition, the authors did not use the catalyst in any typical ORR application. Thus,

investigating the effect of carbonization temperature on the type of N_2 functional groups and using the N-doped catalysts for ORR will enhance the applicability of results from this study.

Liu *et al* (2010b) also employed the nanocasting technology to prepare N-doped OMC. They impregnated the pores of SBA-15 with an aromatic dye N,N'-bis(2,6-diisopropyphenyl)-3,4,9,10-perylenetetracarboxylic diimide (PDI) dissolved in tetrahydrofuran (THF). The composite was dried at 60°C and pyrolyzed at 600, 700 and 900°C respectively. TEM analysis confirmed the highly ordered structure of the carbon obtained after removal of the template. Also, the XPS analysis revealed in **Table 2-2** that while there was a reduction in total nitrogen content with increasing pyrolysis temperature, the percentage of graphitic (or quaternary) nitrogen increased.

Table 2-2 Total nitrogen and chemical states of PDI prepared at different pyrolysis temperatures (source (Liu *et al.*, 2010b))

	Total N_2 (wt%)	Pyridinic	Quarternary
PDI-600	3.5	36.0	52.3
PDI-750	2.8	31.4	62.4
PDI-900	2.7	28.1	70.9

The N-doped catalysts were used in ORR experiments where their performance was compared with that of 20 wt% Pt/C in 0.1M KOH solution. Looking at Figure 2-9, PDI-900 had the best performance for oxygen reduction. This was attributed to the highly graphitic nature of the carbon as well as the increased amount of quaternary nitrogen atoms. It is obvious from this result that ORR activity does not depend on total nitrogen content. A major setback for this otherwise very good result is that the chemical used i.e. PDI is very expensive, perhaps more expensive than platinum (PDI costs 142GBP/100 mg while 20 wt% Pt costs 80 GBP/1000 mg (Sigma Aldrich)). Therefore, it is not likely to address the challenge of bringing down the cost of fuel cells. It would be worthwhile to find cheaper precursors with similar configuration as a means of reducing the final cost of ORR catalysts.

The positive side notwithstanding, the platinum polarisation curve raises a pertinent question on the validity of these results. Platinum is very active and has been known to achieve limiting current in 0.1 M KOH. This result contradicts that. The platinum used does not attain the diffusion limiting current.

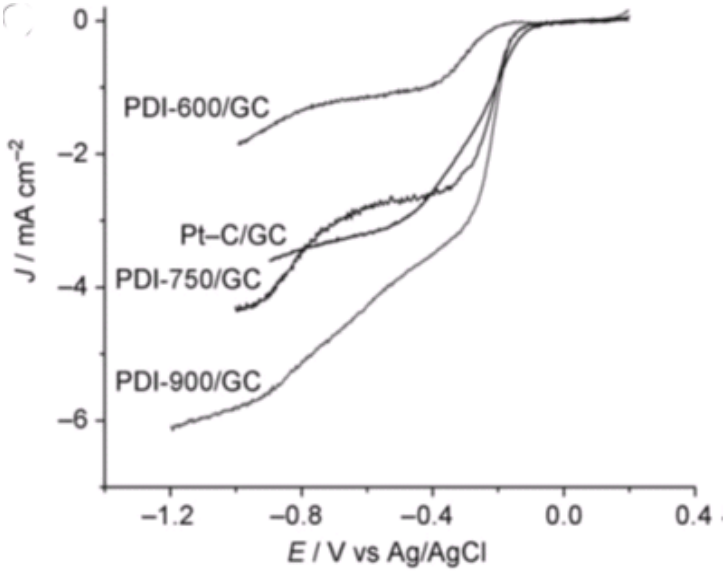

Figure 2-9 RDE voltammogramms of the series of PDI-NOMGAS and Pt/C supported on GC electrode at a rotation rate of 1600 rpm in an O_2 saturated 0.1M KOH, scan rate 10 mVs^{-1}Source (Liu *et al.*, 2010b)

Yang et al (2010) also investigated the synthesis of N-doped carbon and their use as ORR catalysts. Using nucleobases as simultaneous carbon and nitrogen source and spherical silica nanoparticles as template, they carbonized the composite at 1000 ^{o}C for 1hr before removal of the template. The investigation made use of four different nucleobases namely adenine (A), guanine (G), cytosine (C), thymine (T), and uracil (U). The total nitrogen content varied from 10.1 wt% for mesoEmC to 13.2 wt% for meso-EmU. As seen in Figure 2-10, the onset potential for all the N-doped catalysts in alkaline media was very close i.e. ca -35 mV with an overpotential of about 35 mV compared to that of 20 wt% Pt/C. However, the limiting current of Meso-EmT and Meso-EmU exceeded that of platinum. Using Koutecky-Levich analysis,

the number of electrons transferred was determined to be 4.1 for Meso-EmU, which is similar to that for platinum.

The authors also used the catalyst for ORR in an acid electrolyte (Figure 2-11) where the 20 wt% Pt/C performed much better. Meso-EmG that was used had an overpotential of 197 mV (Ag/AgCl) compared with 20 wt% Pt/C which also had a higher limiting current. This confirms the fact that N-doped carbon materials are more active in alkaline solutions than in acid electrolytes.

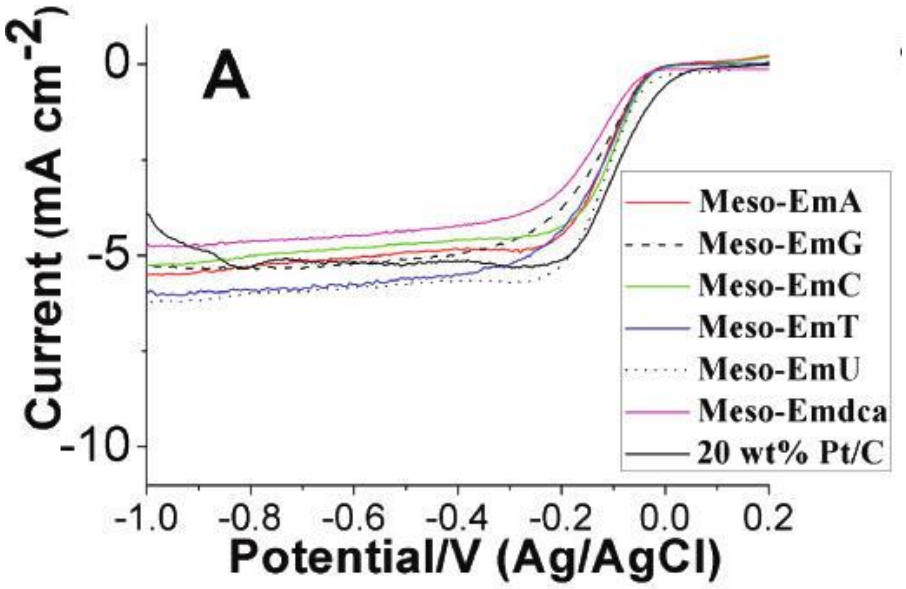

Figure 2-10 Polarization curves on a glassy carbon RDE for N-doped carbons, as compared with 20 wt% Pt/C in O_2 saturated 0.1M KOH; $10mVs^{-1}$, 1600rpm

Source (Yang *et al.*, 2010)

The scheme looks promising considering that the nucleobases used are much cheaper than Pt and have a performance that is relatively close to that of platinum in alkaline medium. However, the result would have been more explicit had the researchers performed an analysis to determine the chemical state of nitrogen groups present on each catalyst. Also an optimization of the carbonization temperature might have been useful because the nitrogen functional groups are converted into more ORR active forms with increasing temperature (Stöhr *et al.*, 1991).

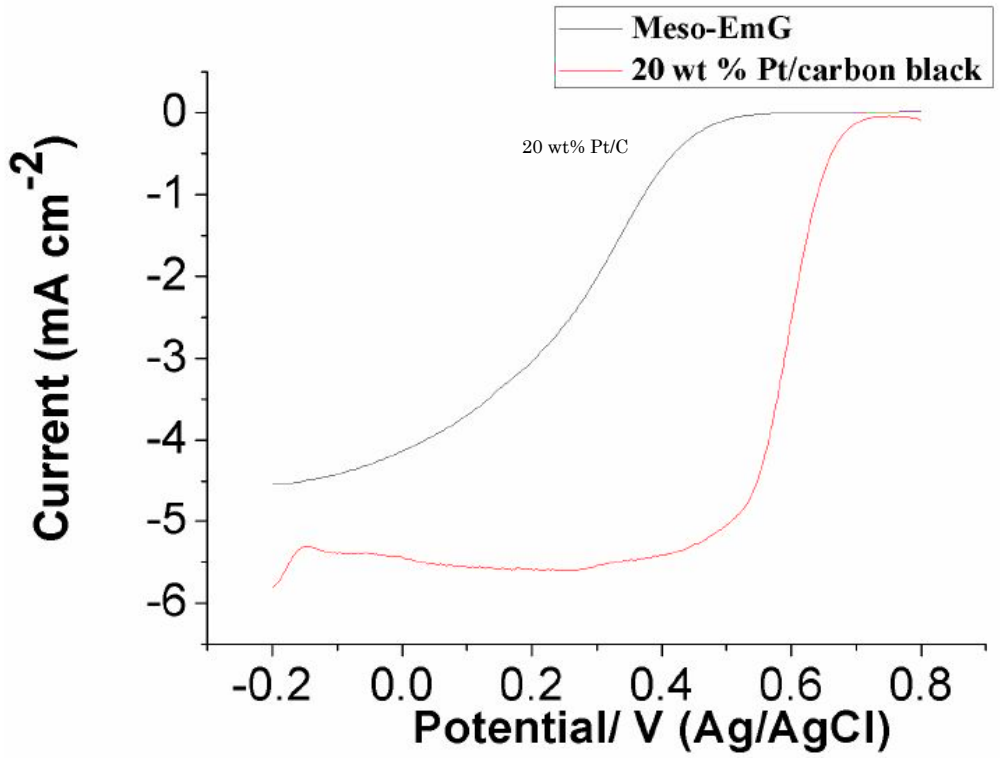

Figure 2-11 Polarization curves for oxygen reduction in O_2 saturated 0.1M $HClO_4$ at 10 mVs^{-1} and 1600 rpm source(Yang et al., 2010)

The possibility of producing N-doped catalysts by treating carbon with ammonia at elevated temperatures was explored by Wang et al (Wang *et al.*, 2010). Ordered mesoporous carbon (OMC) was heated in a quartz tube under flowing NH_3 for 1hr at target temperatures of 950, 1000 and 1050°C respectively. **Table 2-3** shows the structural and textural properties of the N-doped OMC. It also shows the RDE performance relative to 20 wt% Pt/C.

Though not as good as 20 wt% P/C, the authors claim that N-OMC-1050 performed better in acidic media than the other N-doped metal free ORR catalysts reported earlier.

Table 2-3 Textural properties of surface-etched mesoporous carbon membranes Source (Wang *et al.*, 2010)

materials	yield %	S_{BET} (m^2/g)[a]	w (nm)[b]	N content (%)[d]	Percentage (%) pyridinic	graphitic	E_{onset} (mV)[e]	n[f]
C-ORNL-1		658	6.9	0				
N-OMC-950	37.4	1681	6.5	6.0±0.3	44.0	8.6	669.0	3.5
N-OMC-1000	23.4	2121	6.6	3.6±0.3	45.2	9.0	703.0	3.7
N-OMC-1050	4.0	1923	4.0	4.6±0.4	46.9	10.0	720.0	3.4

[a]S_{BET}: BET surface area. w: BJH mesopore diameter [d]-determined by XPS; [e]onset potential (vs NHE) point of 5% increase in current. [f]N electron transfer number.

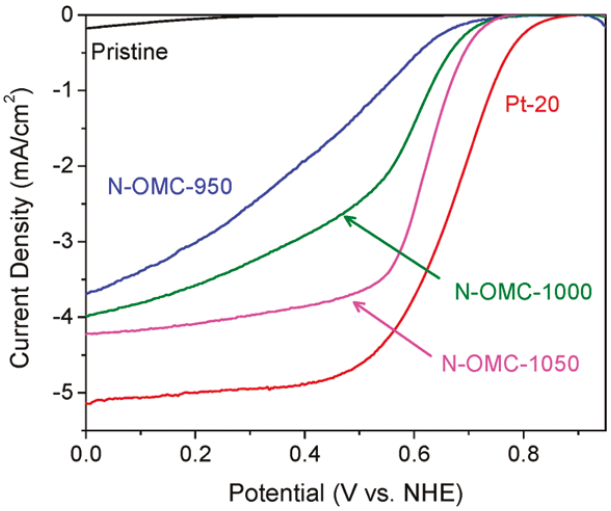

Figure 2-12 Polarization curves of oxygen reduction on N-OMC-X (X=950, 1000, 1050 °C) source(Wang et al., 2010)

(ORR tests were carried out in oxygen-saturated 0.05M H_2SO_4, the rotation rate of RDE was 1600 rpm, and the potential scan rate was 10mV/s. Non-faradaic currents obtained in N_2 saturated electrolyte under identical conditions were subtracted. Catalysts loading for Pt-20 and N-OMC-x were 352 and 312 µg/cm², respectively.)

The authors identified the pyridinic and quaternary types of N_2 as being responsible for the ORR activity. It is worth noting, that the trend of ORR activity was at variance with that of increasing nitrogen content. This emphasizes the fact that ORR activity is not dependent on total nitrogen content but rather on the chemical states of the nitrogen moieties. Considering that N-doped carbons are known to perform poorly in acidic media, the results are commendable. Notwithstanding, the treatment time under ammonia at high temperature could be increased. Perhaps this may lead to an increase of the N_2 content and subsequently enhance its performance to make it as good as or even better than Pt/C.

Shrestha and Mustain (2010) using SBA-15 as template and pyrrole as the nitrogen containing carbon precursor, developed an N-doped ordered mesoporous carbon catalysts that showed ORR activity. The monomers were polymerized in the presence of $FeCl_3$ over 24 h after which the $FeCl_3$ was washed out and the sample carbonized at 800 ^oC for 3 h.

The results of the RDE confirmed the ORR activity of the carbon material. However, the onset potential of ca 350 mV (NHE) in acidic medium was quite low compared to that of 20 wt% Pt/C which occurs around 900 mV (NHE). The study might have been more insightful if the authors had performed further electrochemical analysis especially the Koutecky-Levich and Tafel plot. As it is, the key parameters needed to assess an electrocatalysts of this sort are missing. It might also be possible to improve the obtainable activity by carbonizing at a higher temperature where ORR active groups like the pyridinic and quaternary N_2 bonds are dominant.

Kim *et al* (2008) synthesized N-doped carbon by heat treating with ammonia. This was used as an electrode in electrochemical double layer capacitor. The authors performed polymerization of the carbon source, sucrose, in ordered mesoporous silica (SBA-15) template. Two methods were employed for the ammonia treatment. In the first, the polymerized sucrose was heat treated with NH_3 at 300 ^oC before carbonization at 850 ^oC denoted as NC. The second method entailed carbonization at 850^oC after polymerization; this was followed by NH_3 treatment at 300 ^oC and denoted as CN.

It is evident from Tables 2.6 and 2.7 that the amount and functionality of the nitrogen depends on the sequence of NH_3 treatment

Table 2-4 Elemental composition of carbon and N-doped carbon materials obtained by ammonia treatment Source (Kim *et al.*, 2008)

sample	C(wt %)	H (wt%)	N (wt%)
AC	92.0	1.0	0
MC	95.0	0.8	0
CN	91.0	1.0	1.6
NC	74.0	1.6	8.0

AC-activated carbon, MC- mesoporous carbon

Table 2-5 Chemical states of nitrogen in N-doped carbon materials obtained by ammonia treatment. source (Kim *et al.*, 2008)

SAMPLE	$N_{Quaternary}$(%)	$N_{pyrrolic}$ (%)	$N_{pyridinic}$ (%)
AC	0	0	0
MC	0	0	0
CN	9.5	61.9	28.6
NC	31.1	35.6	33.3

The higher nitrogen content of NC was ascribed to the ammonia treatment which took place when the carbon bonds were relatively weak. Considering the high wt% of nitrogen and the proportion of the chemical states of nitrogen which are said to be ORR active it will be worth replicating this for use as an ORR catalysts. The chemical states better suited for ORR applications are obtained at higher temperatures (above 850 ^{o}C). Therefore, it might also be worth exploring the effects of carbonization at temperatures above 850 ^{o}C. It may be interesting to study the effect on nitrogen content should the polymerization step be carried out under flowing NH_3. **Table 2-6** is a summary of critical parameters from past research involving the use N-doped OMC for ORR.

Li *et al (Li et al., 2015)* using Pluronic F127 as a soft-template, phenol resin as carbon source and dicyandiamide as nitrogen source synthesized nitrogen doped ordered mesoporous carbon spheres. These were confirmed to have good catalytic activity and stability. The activity was ascribed to the ordered mesoporous design of the pores, the amount of graphite and the different nitrogen functional groups present.

By employing a two-step nanocasting technique with SBA-15 as the hard template, Sheng and co-workers (Sheng *et al.*, 2015) synthesized nitrogen doped ordered mesoporous carbon catalysts. These were only capable of catalysing the reduction of oxygen to hydrogen peroxide.

Table 2-6 Summary of parameters from past research involving the use N-doped mesoporous carbon for ORR

Synthesis method	Types of N_2 Groups	Onset potential(E_{ons})	J mA/cm^2	N_{e-}	Contrast With 20wt% Pt	ref
Pyrolysis of N,N'-bis(2,6-diisopropyphenyl)-3,4,9,10-perylenetetracarboxylic diimide (PDI-900)	Nitrogen at % 1.93 Pyridinic 28.90% Quaternary % 70.10%	0.89 V RHE 0.1 M KOH ;	6.2	3.9	Ca 130 mV over potential	(Liu *et al.*, 2010b)
Heat treatment of OMC under flowing NH_3 at 1050 ^{oC}	Nitrogen at % 5.00 Pyridinic 46.90% Quaternary 10.00%	720mV (NHE) 0.05M H_2SO_4,	4.2	3.4	Ca 180mV over potential	(Wang *et al.*, 2010)
Pyrolysis of Nucleobases in SBA-15 template	meso-EmT 12.1 Nitrogen wt% meso-EmU 13.2 Nitrogen wt%	0.99 V RHE 0.1 M KOH ;	ca 6.2	4.1 Meso-EmU	Ca 30 mV Over potential	(Yang *et al.*, 2010)
Pyrolysis of polypyrrole in an SBA-15 template	Nitrogen at % 8.30 Pyridinic 36.00% Quaternary 39.00%	ca 0.4 mV (NHE) 0.5 M H_2SO_4	Not Stated	NS	Ca 500 mV Over potential	(Shrestha and Mustain, 2010)
one pot hydrothermal route using resol and dicyandiamide (DCDA) as the carbon and nitrogen source	Nitrogen at % $_{N\text{-}OMCS\text{-}1.5\text{-}900}$ 2.16 Pyridinic 40.40% Quaternary 16.50% Others 43.10%	0.91 V RHE 0.1 M KOH	Not Stated	3.76 (at -0.3V) N-OMCS-1.5-900	Not Stated	(Li *et al.*, 2015)
Aniline and dihydroxynaphthalene were polymerised inside the pores of SBA-15	Nitrogen wt % $_{NOMC\text{-}L}$ 3.4 Pyridinic 1.00% Quaternary 1.60% Others 0.8%	0.92 V RHE 0.1 M KOH (NOMC-L)	16.0 NOMC-L	2.3 NOMC-L	Not Stated	(Sheng *et al.*, 2015)

Table 2-7 Summary of parameters from past research involving the use N-doped mesoporous carbon for ORR (continued)

Synthesis method	**Types of N_2 Groups**	**Onset potential(E_{ons})**	**J_{mA/cm^2}**	**N_{e^-}**	**Contrast With 20wt% Pt**	**ref**
Prepared a mixture of graphene oxide, colloidal silica nanoparticle, melamine and benzyl disulphide which was heated under argon at 900 °C after which the silica was removed.	They confirmed the presence of pyridinic, pyrolic and graphitic nitrogen but the composition was not stated.	0.964 V RHE 0.1 M KOH	15 (-0.4 V)(Ag/AgCl)	3.6 (-0.6V) (Ag/AgCl)	30 mV Over potential	(Liang *et al.*, 2012a)
Nanotube mesoporous carbon doped with nitrogen and sulphur was prepared using nano-$CaCO_3$ as hard template, and binuclear cobalt phthalocyanine hexasulfonate as simultaneous nitrogen, sulfur, carbon source. This same reagent served as catalyst for the growth of CNT.	Nitrogen at % 4.97 Pyridinic 2.38% Quaternary 1.29% Pyrolic 1.30%	0.953 V RHE 0.1 M KOH	Not stated	3.56 (-0.4V) (Ag/AgCl)	10 mV Over potential	(Nie *et al.*, 2014)
Mixing of amino acids with SBA-15 mesoporous silica followed by heat treatment at 900 °C	They confirmed the presence of pyridinic, pyrrolic, graphitic and oxidized nitrogen but the composition was not stated.	0.964 V RHE 0.1 M KOH	Not stated	Not stated	30 mV Over potential	(Gao *et al.*, 2016)

The two step technique help to ensure that the pores were completely filled thus resulting in a very uniform distribution of pores when the template was removed.

2.8 Nature of the Active Site in N-Doped Catalysts

The chemical state of nitrogen that is responsible for oxygen reduction has been an issue of controversy. Some authors (Matter *et al.*, 2007; Kundu *et al.*, 2009; Rao *et al.*, 2010) have argued that the pyridinic nitrogen is the active site for ORR. Others (Liu *et al.*, 2010b; Kim *et al.*, 2011a; Niwa *et al.*, 2011) say it is the graphitic or quaternary state where nitrogen is bonded to three carbon atoms. Both parties have a similar approach in predicting the active site. They carry out ORR with a range of N-doped carbon materials and try to correlate the performance with the trend of chemical states as evidenced in physico-chemical analysis.

An example is Rao et al (2010) whose data is shown in **Table 2-8**.

Table 2-8 XPS results and ORR onset potential obtained by using undoped CNTs and N-doped CNTs in acid electrolyte Source (Rao et al., 2010)

		Surface Concentration at%			
Catalysts	**Total Surface nitrogen content**	**N1**	**N2**	**N3**	**Onset Potential for ORR (V) Ag/AgCl**
CNT_{PPA}	0	0	0	0	0.05
$CNTP_{4VP}$	4.3	1.7	0.4	2.2	0.20
CNT_{PMPY}	5.6	2.8	0.5	2.5	0.31
CNT_{PMM}	8.4	5.2	0.4	2.8	0.46
CNT_{PPP}	10.7	4.3	0.7	5.7	0.39

For them, the fourth catalyst, which had the best performance in terms of onset potential, also had the highest ratio of pyridinic nitrogen (N1). Therefore, pyridinic nitrogen must be responsible for ORR activity.

On the other hand, for Liu and co-workers (2010b) PDI-900 showed the highest ORR activity and from the analysis, it had the highest proportion of

quaternary nitrogen. Therefore, quaternary nitrogen must have influenced the exceptional activity.

Others still, believe that though the pyridinic site is active, it is only capable of a two-electron transfer and not the whole four as observed in very good ORR catalysts. In an excellent investigation carried out by Luo *et al* (2011) they prepared N-doped graphene made up of only pyridinic nitrogen moieties, i.e. without quaternary nitrogen bonds. Hence, any observed activity, could only be due to the pyridinic nitrogen specie. Their results showed that pyridinic species though active for ORR are only capable of the two electron reaction that produces peroxide.

A better perspective is acquired when the theory is considered (Robertson and Davis, 1995; Terrones *et al.*, 2004; Dommele, 2008). Looking at Figure 2-13, for the nitrogen in pyridine, there are three sp^2 orbitals having four electrons

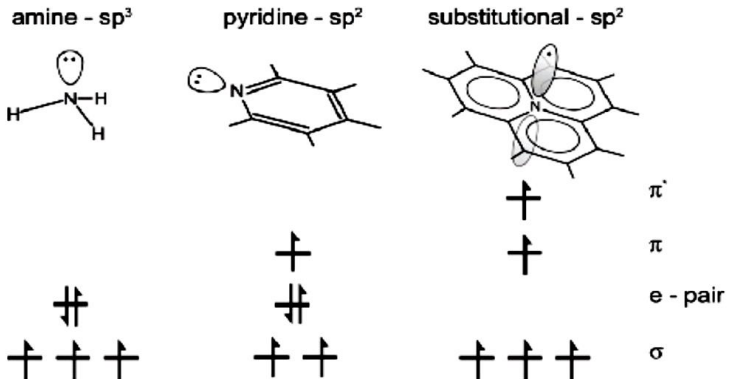

Figure 2-13 Electron structure of nitrogen in pyridinic and quaternary formations
Source (Dommele, 2008)

and a p-orbital with an electron. It uses two to form σ bonds with two carbon atoms while the electron in the p-orbital forms a π-bond with one of the two carbon atoms. This leaves a localized lone pair of π electrons (from the sp^2 orbital), which can be electron donating. For the quaternary or graphitic nitrogen, it has three electrons in the sp^2-hybridized orbital and two in the third p-orbital. The three electrons are used to form σ-bonds with three adjacent carbon atoms while one of those from the p-π orbitals forms a π-bond with one of the carbon atoms. The fifth cannot remain in the same orbital according to rules guiding electron orbitals. Therefore it occupies a π* state

which has a higher energy than the π state and becomes delocalized. It is this delocalized π* electron that actually "dopes" the carbon structure.
Another view that corroborates this considers the band gap between the highest occupied molecular orbital (HOMO) and lowest unoccupied molecular orbital (LUMO) as an indicator of chemical activity (Zhang and Xia, 2011). According to (Zhang *et al.*, 2012) the band gap calculated for NCNT containing quaternary nitrogen sites is 0.39 eV, which is smaller than 0.48 eV for pyridinic nitrogen sites. The value for pure CNT is 0.61 eV. Therefore the quaternary nitrogen is energetically most favoured to add an electron to a higher lying LUMO.

An additional reason that has been proposed for the enhanced activity through nitrogen doping is the ability of nitrogen dopants to increase the Fermi energy level of the carbon hosts (Czerw *et al.*, 2001; Carvalho and Dos Santos, 2006). This will follow from the previous theory of HOMO and LUMO considering that the Fermi energy level can be considered as that state closest to the conduction band where electrons can be found. Hence nitrogen doping which places electrons closer to the conduction band increases the metallic character of the carbons.

2.8.1 **Mechanism of ORR on Nitrogen Doped Carbon Catalysts**

Combining computational techniques with experimental observations enhances the possibility of arriving at a general description of the ORR mechanism on carbon alloy catalysts. There are two general pathways for the ORR mechanism, which are depicted in scheme 1 and 2 (Figure 2-14) adapted from (Ruvinskiy *et al.*, 2011). Both are similar in almost all respects, the difference being in the 2*2 pathway where water is formed from hydrogen peroxide. It is worth noting that along the entire pathways are many high energy and short-lived intermediates which can appear or be used via several different mechanisms.

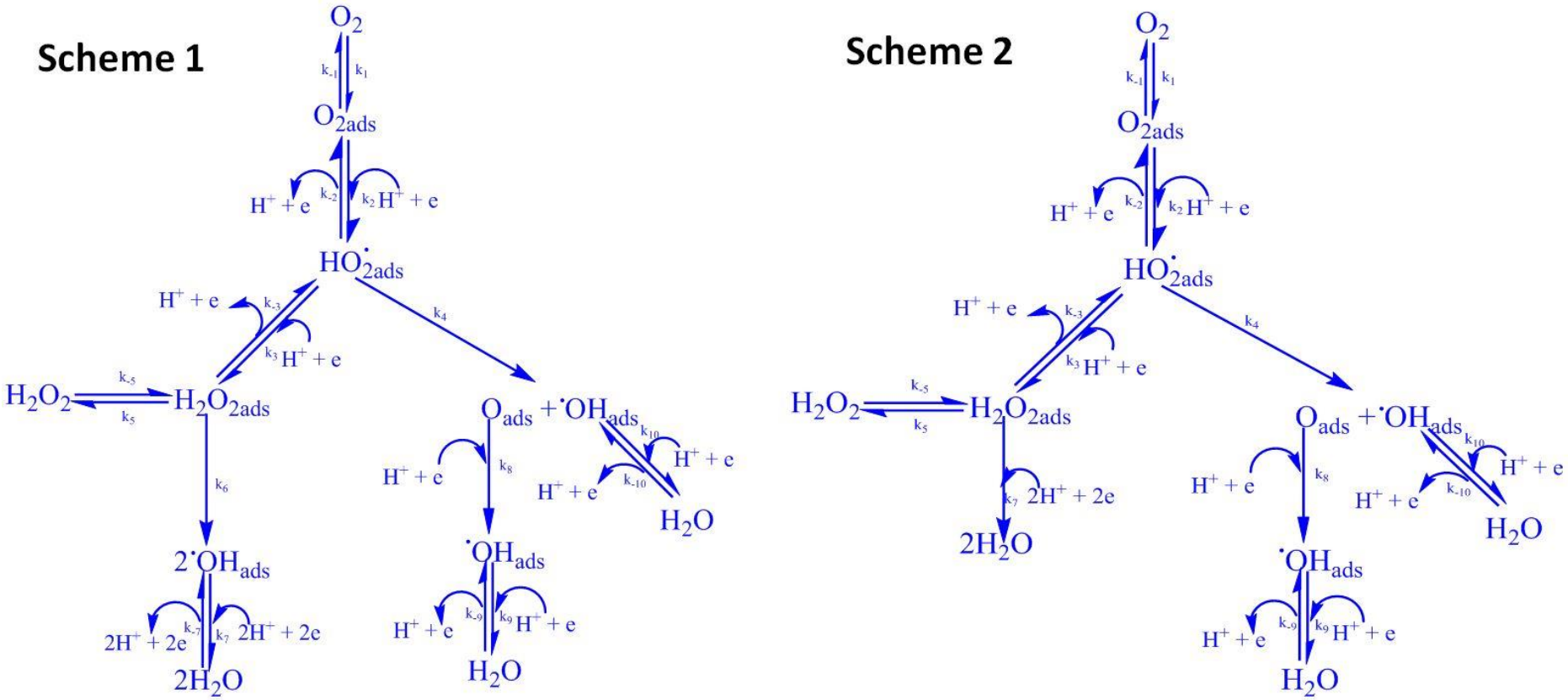

Figure 2-14 Oxygen reduction pathway on nitrogen doped carbon catalysts (in scheme 1,the 2x2 pathway has water being formed from the reduction of hydroxides produced after the dissociation of H_2O_2 i.e. steps 6 and 7; in scheme two, the 2x2 pathway has water being formed from the direct reduction of H_2O_2, step 7) (Ruvinskiy *et al.*, 2011)

The first step is commonly believed to be the adsorption of molecular oxygen (Feng *et al.*, 2011b) which preferentially occurs in a chemisorbed non-dissociated form as confirmed by simulations of the ORR on carbon catalysts. This is followed by the formation of HO_{2ads} (Ikeda *et al.*, 2008; Okamoto, 2009) through the addition of a proton and an electron. From the simulations of Okamoto(2009) on nitrogen doped graphene and Zhang and Xia (2011) on nitrogen doped carbon nanotubes, there is a likelihood of two different pathways proceeding concurrently from the HO_{2ads}.

The first is the breaking of the O-OH bond to produce O_{ads} + OH_{ads} from where two molecules of water are generated by the addition of 3 protons and 3 electrons. This is the direct 4 electron pathway. The second pathway from HO_{2ads} is the formation of HOOH by the addition of an electron and a proton. This is the two electron pathway. The peroxide can accept two hydrogen ions to form water i.e. scheme two or can dissociate into 2OH which proceeds to form water through the addition of two electrons and two protons, i.e. scheme one. The last two steps in both schemes would represent the termination of the 2 * 2 pathway to a four electron transfer. Going by the argument put forward by Ramaswany et al (2012), provided that there exists an active site that further reduces the intermediate peroxide product to water, this mechanism will likely be the same in both alkaline and acidic media. Occasionally on some non-noble metal catalysts in acidic media, the active site necessary for the reduction of the peroxide intermediate is not present. This gives rise to the high percentage of peroxides observed when a rotating ring disc electrode (RRDE) is used to investigate their ORR in acidic media.

2.9 Carbon based ORR catalysts-Preparation and Performance in MFCs

The upsurge of interest in microbial fuel cells has been driven chiefly by the need to improve the overall energy efficiency of water treatment plants. As humanity is becoming more urban, this will reduce the cost of water through making water treatment systems cost effective. It will also boost the possibility of designing rural water treatment plants. Generally, a

breakthrough in the development of MFCs will increase access to sanitation and reduce water pollution thus helping to address pertinent global water challenges. Although called fuel cells. MFCs are essentially "energy recovery devices" as in most applications they are not used for power generation because their power densities are very low. **Figure 2-15** is a schematic diagram of a microbial fuel cell.

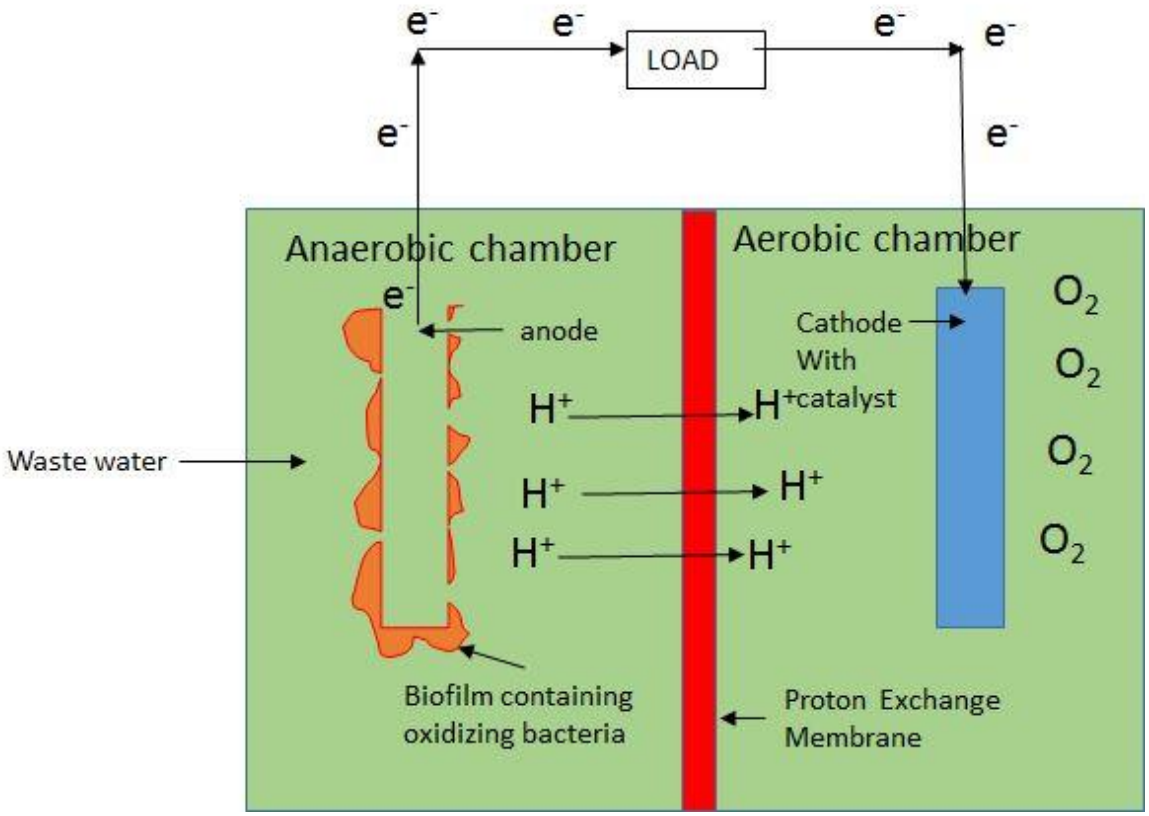

Figure 2-15 Schematic of a Microbial Fuel Cell

For a more logical discussion, the carbon based catalysts used in neutral media have been grouped into two classes; nitrogen doped carbon and manganese oxide catalysts.

2.9.1 **Nitrogen Doped Carbons in MFC's**

Feng et al (Feng *et al.*, 2012) reasoned that due to the benefits of low cost, relatively good electrical conductivity and strong oxidation resistance,

nitrogen-doped carbons are likely substitutes for noble metals in microbial fuel cells (MFCs) for wastewater treatment. **Table 2-9** summarises the preparation routes and performances of nitrogen doped carbons in MFCs. While high activity is desirable in a potential commercial catalyst, other factors like stability and reproducibility on a large scale are equally important. Furthermore, the cost of reactants and their widespread availability must be also considered.

While the high activity exhibited by the nitrogen doped graphene, produced by Feng et al (2011a) is desirable, same may not be said for the preparation method; detonation of reactants. This is a procedure which may not be easily reproducible on a large scale. In addition as argued by Li et al (2012a) the reactants are toxic or highly explosive which makes them unsafe for manufacturing purposes. Furthermore, Jeon and co-workers(2013),argued that the CVD used to produce CNTs and Hummers method used to prepare graphene oxide though common place in laboratories, are likely to be expensive and perhaps hazardous on an industrial scale.

Sulfate is a common component of waste water and when acted upon by microbes in MFCs produces sulphides which are detrimental to the operation of MFCs (Zhao *et al.*, 2008). Hence the good performance of nitrogen doped carbon powders prepared by Feng et al (2012) in the presence of hydrogen sulphide is commendable. However nitric acid used in preparing the n-doped powders is very corrosive and extremely hazardous and boiling it will also produce harmful vapour. This could be a set-back for commercial scale production of the catalyst.

Table 2-9 Synopsis of results from using nitrogen doped carbon in MFCs

Catalyst and Ref	Nitrogen Doped Graphene (Feng *et al.*, 2011a)	N-doped carbon nanofibre grown on stainless steel mesh (Chen *et al.*, 2012)	Nitrogen doped graphene sheets (Ci *et al.*, 2012)		Nitrogen doped CNT (Feng *et al.*, 2011b)
Preparation and reactants	Detonation of reactants at momentary pressure of 60 MPa and equilibrium pressure of 30MPa temp of 320 oC; Cyanuric Chloride and tri-nitrophenol	Chemical treatment of substrate Stainless steel mesh (SSM) followed by CVD of pyridine at 750oC; Stainless steel mesh and pyridine vapour	Graphene oxide likely to have been prepared by hummer's method. Pyrolysis of reactants at 750 – 900oC. Cyanamide and graphene oxide solution		CVD (800oC) using Fe-containing SBA-15 molecular sieve as catalyst. Etheylene Diamine
Anode Medium	Acetate synthetic waste water	Secondary artificial wastewater with 10 mM sodium acetate as substrate medium in the anode chamber	Phosphate buffer (PBS, pH 7.0) with Acetate		PBM were inoculated with 20% domestic wastewater collected from a municipal wastewater treatment plant
Max power density in a MFC	N-G 1350 mW/m^2 Pt/C 1420 mW/m2	N-CNF Ca 960 mW m2 in air & 1900 mW m2 in O2	NGNSs-900 4.06 W/m3 Pt/C 3.77 W/m3 (oxygen)		N-CNT 1600 mW/m2 Pt/C 1393 mW m2 (air cathode)
Cost and performance comparisons	Proved more stable than Pt. Cost much less than 20 wt% Platinum on a reagent basis.	The performance was close to that of Pt/SSM. The authors claimed it is cheaper than Pt/SSM	NS. But claims it will produce cheaper catalysts. NGNSs-900 performed better than platinum		Cost analysis was not stated. N-CNT performed better than platinum

Table 2-10 Synopsis of results from using nitrogen doped carbon in MFCs (continued)

Catalyst and Ref	Nitrogen doped carbon powders (NDCP) (Feng *et al.*, 2012)	Mesoporous graphitic carbon nitride implanted with N_2 active sites (I-NG) (Feng *et al.*, 2013)	Activated nitrogen doped carbon nanofiber (ANCNF) (Yang *et al.*, 2014)	Nitrogen doped carbon derived from rice straw (NC). (Liu *et al.*, 2015b)
Preparation and reactants	A three-step procedure of heat treatment followed by acid treatment and finally refluxing in HNO_3 at 120 ^oC.; Carbon powder, HCl and HNO_3.	N-doped graphene and graphitic carbon nitride were sonicated in HNO_3 followed by drying at 80 ^oC; Graphite, $NaNO_3$, $KMnO_4$, H_2SO_4, NH_4 solution, cyanamide, HNO_3	ANCNF was prepared through a modified oxidative assembly route and activated with KOH; CTAB, pyrrole, HCl, and KOH	The rice straw was converted via hydrothermal carbonization, freeze drying and heat treating in NH_3. Rice straw, NH_3, HF and HCl
Anode Medium	A mixture of domestic wastewater and phosphate-buffered medium	Suspended bacteria from an acetate fed MFC in synthetic waste water laden with acetate.	Mixed culture, carbon granules and sodium acetate culture medium	Secondary inoculum initially from wastewater treatment plant and acetate nutrient medium
Max power density in a MFC	N-CP ca 215 mW/m^2(from plot) Pt/C 254.8 ± 8 mW/m^2 In presence of sulfide N-CP 222.5 ± 8 mW/m^2 Pt/C 199.7± 4 mW $/m^2$	I-NG – 1618 $\pm$ 50 mW $/m^2$ Pt-C – 1423 $\pm$ 25 mW/m^2	ANCNF-900 1377 $\pm$ 46 mW/m^2 Pt-C 1307 $\pm$ 43 mW/m^2	H-NC-900 2300 mW/m^2 Pt-C 1634 mW/m^2
Cost and performance comparisons	The cost of NDCP preparation was ca 1% that of Pt/C. 20% when cost of Nafion and carbon cloth were factored. The N-doped powder had a better performance in the presence of H_2S.	I-NG is expected to be much cheaper than platinum. I-NG performed better than 20 wt% Pt-C in a MFC.	The reactants for the catalysts are cheaper than platinum and more accessible. ANCNF-900 displayed a slightly better activity in an MFC when compared with platinum	Evidently, the rice straw would be far cheaper than Platinum although the processing may increase overall cost slightly. H-NC-900 had a better performance relative to platinum

Moreover because of the strong oxidative influence of nitric acid, the carbon powder is very likely to be oxidized in the boiling acid. This piece of research would have carried more weight if the authors had characterized the catalysts using such tools as elemental analysis, XPS or EDX to confirm the presence and extent of doping of nitrogen atoms within the carbon structure

2.10 Manganese Oxide Catalysts in MFC's

For many years, manganese oxide has been known to catalyse the decomposition of hydrogen peroxide into water and oxygen (Dolhun, 2014). It is believed that it accelerates the decomposition more than 1000 times compared with the uncatalyzed reaction. This perhaps has influenced its choice as an oxygen reduction catalysts often used to shore-up the catalytic activity of carbon catalysts well known for peroxide production during ORR. A notable study of the ORR of manganese oxides in neutral media is that of Roche et al (Roche and Scott, 2009). Although they claimed that the MnO_2 deposited on the carbon catalysts acted mainly to bring about a four electron transfer with an addition role of decomposing the peroxide produced by the carbon, not much improvement was observed in the number of electrons transferred during the ORR. The number transferred when only carbon (Vulcan and monarch) was used was ca 1.7 and when MnO_2 was deposited the number rose marginally to ca 2.3 at -0.1 V (vs SHE). The onset potential with the oxides deposited was +0.25 on Monarch and +0.29 (vs SHE) on Vulcan. This seems to be a poor performance compared with that of other carbon catalyst like nitrogen doped CNT (Feng et al., 2011b) which have shown close to four electron transfer in neutral media. One is quick to note however that the support in both cases might be what makes a difference considering that CNTs are known to be more active compared with Vulcan and Monarch carbon.

A number of investigations have been carried out on the performance of manganese oxides in microbial fuel cells, some of which are summarized in Table 2-1111.

Table 2-11 Preparation routes and performances of manganese oxide catalysts in MFCs

Catalyst and Ref	Manganese Oxide (Roche *et al.*, 2010)	CNT supported MNO_2 (Lu *et al.*, 2011)	Graphite supported α, β, and ɣ MnO_2 (Zhang *et al.*, 2009)	Carbon cloth supported MnOx (Liu *et al.*, 2010d)
Preparation and reactants	Chemical oxidation of manganese sulphate by permanganate in the presence of carbon Carbon black Monarch, $MnSO_4$, $KMnO_4$	Chemical oxidation of manganese sulphate by permanganate –α-MnO_2 Chemical oxidation of $MnSO_4 \cdot H_2O$ by $(NH4)_2S_2O_8$ – β-MnO_2 Chemical oxidation of $MnSO_4 \cdot H_2O$ by $(NH4)_2S_2O_8$ – ɣ-MnO_2 β and ɣ were prepared under different reaction conditions Catalysts were prepared by mixing MnO2, CNT and PVDF binder.	Chemical Reaction between $MnSO_4 \cdot H_2O$, $(NH)_2S_2O_8$ and $(NH_4)_2SO_4$ –α-MnO_2 Reaction between KMnO4 and ethanol - β-MnO_2 Chemical oxidation of $MnSO_4 \cdot H_2O$ by $(NH4)_2S_2O_8$ – ɣ-MnO_2 Catalysts were prepared by mixing MnO2, graphite and PVDF binder.	Carbon cloth was kept in an electrolyte made up of 0.1M $Mn(CH_3COO)_2$ and 0.1M Na_2SO_4 at pH 6 and the voltage cycled btw +0.6 and +0.1V (vs SCE) at 400, 500, and 600 mV/s to deposit MnOx electrochemically.
Anode Medium	anaerobically digested sewage sludge from an anaerobic digester at a local municipal sewage treatment in Synthetic waste water containing acetate	Mixed culture in Domestic waste water	*K.pneumoniae* strain L17 (CCTCC AB 208106) with 3.0g/L glucose as electron donor	Diverse anaerobic sludge in acetate laden synthetic waste water.
Max power density in a MFC	At pH 7 MnOx/C 161 mW/m^2 Pt/C 193 mW/m^2	α-MnO2 – 22.1 mW/m^2 β-MnO_2 - 97.8 mW/m^2 ɣ-MnO_2 – 82.6 mW/m^2 Pt/Carbon – 152.7 mW/m^2	α-MnO2 – 125±11 mW/m^2 β-MnO_2 - 172±7mW/m^2 ɣ-MnO_2 – 88±8mW/m^2 Pt/Carbon – 268±7 mW/m^2	CV-400– 772.8 mW/m^3 CV-500 - 548.5 mW/m^3 CV-600 – 393.1 mW/m^3
Cost and performance comparisons	The cost of manganese is at least 100 times cheaper than that of Platinum(Roche and Scott, 2009)	Not stated, but it is expected the cost of CNT may significantly increase overall cost.	Not Stated	Not Stated but it is expected that the reactants used would be much cheaper than Pt.

Table 2-12 Preparation routes and performances of manganese oxide catalysts in MFCs (continued)

Catalyst and Ref	**Manganese oxide functionalized CNT (Liew *et al.*, 2015)**	**MnO_2 modified activated carbon (Zhang *et al.*, 2014)**	**α-MnO2 nanotubes on graphene (Khilari *et al.*, 2013)**	**MnO_2-graphene hybrid (Wen *et al.*, 2012)**
Preparation and reactants	MWCNT was functionalized with hydroxyl and carboxyl functional groups and reacted with $KMnO_4$ to obtain MnO2/Functionalized CNT. HNO_3, H_2SO_4, HCl, MWCNT, $KMnO_4$	MnO_2 was electrodeposited on the activated carbon electrode using Na_2SO_4 and $Mn(CH_3COO)_2$ as electrolyte. Activated carbon, Na_2SO_4 and $Mn(CH_3COO)_2$	α-MnO_2 was synthesized by reacting KMnO4 with HCl in an autoclave at 150 °C for 12 hours. The precipitate was dried at 70 °C for 6 h. $KMnO_4$ and HCl	Graphene nanosheets (GNS) were synthesized by reducing graphite oxide (obtained from natural graphite) with hydrazine. MnO_2/GNS nanocomposite was obtained by reacting GNS with $KMnO_4$ under microwave irradiation. Natural graphite, hydrazine, $KMnO_4$,
Anode Medium	Modified *Geobacter* medium with municipal waste water anaerobic sludge as inoculum	Enriched nutrient medium in 50 mM PBS with sodium acetate as carbon source.	Anaerobic sludge from a septic tank was added to synthetic acetate waste water.	Inoculum was anaerobic sludge from another MFC. This was added into acetate laden nutrient buffer solution
Max power density in a MFC	MnO_2/f-CNT 520 mW/m^2	MnO_2 modified activated carbon – 1554 mW/m^2	α-MnO_2/graphene 4.68 W/m^3 Pt/C – 5.67 W/m^3	MnO_2/GNS 2084 mW/m^2 Pt/C 1714 mW/m^2
Cost and performance comparisons	Not stated	The cost is expected to be lower than that of platinum. Though the power density of platinum was not stated, this was said to compare favourably.	It had a better cost-to-performance ratio compared with 10 wt% platinum	MnO_2/GNS had a better performance but it also had a loading that was 10 times that of platinum, i.e. 5 mg/cm^2 compared with 0.5 mg/cm^2 for platinum.

Compared with other MFCs using carbon catalysts, the average power density obtained from the use of MnOx catalysts seems rather low. It is worth mentioning though that so many factors like cell architecture and nature of anode also contribute to the maximum power and hence making a direct comparison difficult. Worthy of commendation is the fact that with the exception of (Lu et al., 2011) who used CNT, the other catalysts were synthesized using reactants that are much cheaper than Pt and therefore hold a promise of being able to generate power at a relatively affordable rate. Paralleled with other carbon catalysts in terms of cost and nearness to the market, MnOx catalysts will compete favourably due to the relative ease of synthesis and cost of materials.

2.11 Summary of Literature Review

Considering the finite nature of fossil fuels as well as the grave environmental damage that results from its use in internal combustion engines and power plants, there is an urgent need to develop alternatives. This is true both for the fuel as well as for the fuel conversion technology and fuel cells readily lend themselves to meet this need. A gap exists between the present state-of-the-art with respect to ORR catalyst and the target catalyst loading that is expected to make fuel cells market competitive. Considering that researchers are getting to a plateau with respect to platinum loading, expectations are high that sufficiently active non-PGM ORR catalysts will help bridge this gap and one of such is nitrogen-doped carbon catalysts.

From the literature review, it can be concluded that the synthesis of nitrogen-doped carbon catalysts has recorded significant progress but there is room for improvement. The first, is in selecting the right material; in addition to considering the chemical state of nitrogen in the precursor; cost should also be a key criteria. Hence, this research will be looking at selecting less expensive precursors with the right nitrogen functional groups. Considering past investigations, it is obvious that the pore structure of catalyst/support plays an important role in the activity of the catalyst. Therefore, the periodically ordered pore structure of ordered mesoporous carbons can help improve the activity of N-

doped carbons especially in the diffusion-controlled regions of oxygen reduction reactions.

Furthermore, there are investigations, which have been carried out to develop n-doped carbons whose results though good have not been applied in ORR. This research will be replicating as well as optimizing them for use as ORR catalysts. Carbon based catalysts have the potential to replace platinum in neutral media generally and MFC's specifically. However, a number of issues need to be addressed for this to be done in a cost effective manner, reproducible on a commercial scale. In the search for better catalysts, this research would adopt procedures that make use of reactants which are readily available and affordable on a commercial scale. Otherwise there might be the need to wait for another generation to perfect the science required to produce such reactants at an affordable scale. The world needs an urgent solution. Therefore, the use of reactants or supports or catalysts which are still at the development stage in terms of commercial exploitation will not result in an attainment of the goal within the shortest time possible. Hence in the course of this work, thought would be given to ease of scaling up the procedures used to synthesize the catalysts. Hence this work would make use of reactants that are relatively inexpensive and readily accessible. The procedures used would also be such as can be easily scaled-up for commercial purposes.

Chapter 3. **Methodology**

3.1 Introduction

In this chapter, the method and the materials used to achieve the stated objectives are described. Procedures adopted for synthesizing the catalysts are presented followed by the techniques used for electrochemical analysis. How the microbial fuel cell experiments were approached and the materials used are detailed next. Subsequently, an explanation of the parameters and equipment used for physical and chemical characterization of the catalysts is presented. Finally, the chapter gives an appraisal of the methods of analysis.

3.2 Procedures used for synthesis of the catalysts

i. Ordered mesoporous Silica (OMS) KIT-6
This was prepared using the procedure adapted from Kim *et al* (Kim *et al.*, 2005). Typically 4 g of P123 (MW 5800 – Aldrich) was added to 144 g of deionized water under stirring at a temperature of ca 32 ^{o}C. After the dissolution of the P123, 6.4 ml HCl (37wt%- Sigma Aldrich) was added followed by the addition of 4 g of N-Butanol (99.4%, Sigma Aldrich). After one hour, 8.6 g of TEOS (98%- Aldrich) was added at once to the homogenous solution. This was left stirring for 24 hours. Thereafter the hydrothermal treatment was performed in an oven at 100 ^{o}C for 24 h. The next step entailed washing and drying the precipitate. To remove the template, the dried precipitate was stirred in ethanolic-HCl for ca 3 h. This was followed by heating in an oven at 550 ^{o}C for 5 h. The entire reaction was carried out in a closed polypropylene bottle (250 ml).

ii. Ordered mesoporous Carbon (OMC) CMK-8
This was prepared using a procedure adapted from Jun *et al* (Jun *et al.*, 2000). Typically, to a solution of 0.162 mg of H_2SO_4 and 5 ml of water was added 1.25 g of sucrose (Fisher Scientific UK) and 1 g KIT-6. The mixture was heated to 100 ^{o}C at a ramp rate of 1 ^{o}C/min in an oven. After 6 h, it was heated to 160 ^{o}C at the same ramp rate and left for another 6 h. To

the partially polymerised sucrose was added a solution of 5 ml H_2O, 0.77 g sucrose and ca 6 drops H_2SO_4. The heating at 100 ^oC and 160 ^oC was then repeated. Thereafter, the composite was heated up to 900 ^oC with a ramp rate of 2 ^oC/min under flowing nitrogen and left for 4 h. To remove the silica template, the product from the furnace was dissolved in a warm solution of 200 ml 1 M ethanolic NaOH (50% water/ethanol v/v) and left to stir over night. Thereafter, the precipitate was centrifuged and washed repeatedly with ethanol. The final product was dried overnight at ca 80 ^oC.

iii. Nitrogen doped carbon prepared from O-phenylene diamine (NDAB)

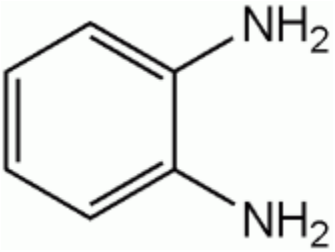

Figure 3-1 O-Phenylene diamine

The procedure was adapted with modifications from the work of Liu *et al* (Liu *et al.*, 2010a). Typically 0.5 g calcined KIT-6 together with 1.62 g of O-phenylenediamine (Sigma Aldrich) and 2.3 g ammonium persulfate, APDS (Sigma Aldrich) were added to 20 ml toluene solution AnalaR NORMAPUR® ACS (VWR), with the aid of ultrasonication for 15 min, the resultant mixture was refluxed at 80 ^oC for 14-16 h. The solution obtained was left overnight during which it solidified. The solid samples were carbonized at 750, 950 and 1050 ^oC in a nitrogen flow of 100 mL/min with a ramp rate of 2.0 ^oC/min and kept under these conditions for 5 h. The silica framework was removed by dissolving the composite in 1M ethanolic NaOH (50 wt% water-50 wt.% ethanol) and leaving to stir overnight at a slightly elevated temperature of ca 45 ^oC. Thereafter the precipitate was centrifuged and washed several times with ethanol. The final samples were dried overnight at ca 80 ^oC.

iv. Nitrogen doped carbon prepared from 1,3,5-Tris(diphenylamino)benzene (NTDAB).

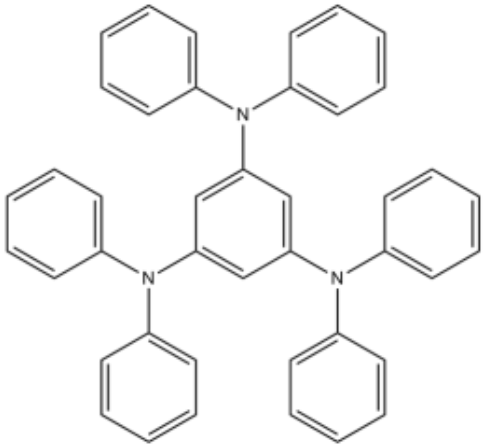

Figure 3-2 1,3,5-Tris(diphenylamino)benzene

This was adapted from the work of Liu *et al* (Liu *et al.*, 2010b) though they used a different precursor. Typically 500 mg KIT-6 is mixed with 750 mg 1,3,5-tris(diphenylamino)benzene (Sigma Aldrich) in 30 ml tetrahydrofuran (THF) (Sigma Aldrich) at room temperature under stirring in an open beaker. After evaporation of the THF, the obtained TDAB/KIT-6 composite is dried overnight at 60 ^{o}C in an oven and subsequently calcined at 900 and 1050 ^{o}C for 5 h, respectively. The silica template is removed by dissolving the composite in 200 ml of warm 1M ethanolic-sodium hydroxide overnight. Thereafter the precipitate was centrifuged, washed severally with ethanol and dried overnight to obtain the N-doped carbon.

v. Direct Synthesis of Nitrogen-Doped Ordered Mesoporous Carbon (adapted from (Yu *et al.*, 2014))

Typically, 4.4 g Pluronic F127 (Sigma), 2.2 g resorcinol (Sigma Aldrich), 1.4 g hexamethylenetetramine (Sigma-Aldrich) and 4 ml ammonium hydroxide solution (ACS reagent 28-30% NH_3 -Fluka) is added into 108 ml of DI water. This was stirred for 1 hour at ca 25 ^{o}C. Thereafter, 1.2g urea (Sigma) was added after ca 10 mins, 0.7g hexamethylenetetramine was added. This gave a very dark green solution. This mixture was stirred for

24 hours at ca 80°C. The reddish brown precipitate was cooled and collected by centrifugation at 5000 g. The particles were then washed copiously with water until the supernatant from centrifuging had a near neutral pH. The reddish brown precipitate was air-dry at room temperature in a fume cupboard. Total weight of sample recovered after drying was 3.1 g. The sample was divided into five batches to be pyrolyzed at 600 °C, 700 °C, 800 °C and 900 °C all for 3 hours under nitrogen with a ramp rate of 1 °C/min.

vi. Manganese oxide from $Mn(NO_3)_2$

The procedure is modified from that Lin and Kuo (2013). Typically 40 mg of NDAB-900 was poured into aqueous $Mn(NO_3)_2$ (Purum; Sigma Aldrich) solution (2500mg in 5ml) and sonicated for ca 2 hours. This was centrifuged and the carbon/ $Mn(NO_3)_2$ composite recovered. The wet composite was placed in the oven at ca 80 °C to cure. This was left overnight i.e. ca 14 hours. Finally, the product was carbonized at 250 °C and 350 °C for 2h, with a heating rate of 1 °Cmin^{-1}under nitrogen gas. This was repeated for CMK-8 with heat treatment at only 350 °C for 2h.

$$\boldsymbol{Mn(NO_3)_2 \rightarrow MnO_2 + 2NO_2} \qquad \text{eqn 3.1 (Stern, 1972)}$$

vii. Manganese oxide from $KMnO_4$

This was adapted (and modified) from (Ma *et al.*, 2006; Fischer *et al.*, 2007; Huang *et al.*, 2007). The chemical oxidation method was adopted here because of the desire to maintain the ordered mesoporous structure of the support.

Typically to 35 ml of DI water was added 23 mg of $KMnO_4$ (AnalaR BDH Prolabo); 24.5 mg of K_2SO_4 AnalaR 99.5 % (BDH) and 68 mg of NDAB-900. The $KMnO_4$ and K_2SO_4 were in a mole ratio of 1:1. This mixture was stirred at a temperature of ca 80 °C. The mixture turned colourless or almost colourless after ca an hour indicating the completion of the oxidation reaction or rather the total depletion of $KMnO_4$. The solution

was centrifuged to recover the solid (the supernatant had a golden yellow colour). The precipitate was washed twice with DI water. The supernatant or filtrate from these was colourless.

The final precipitate was dried overnight (ca 20 hours) at ca 53 ^{o}C. This was used without any modification for ORR analysis.

The exact amount of reagents will vary depending on the amount of manganese oxide to be deposited. The calculation is done on the assumption that the final amount of manganese oxide would be 20 wt% (or 10 or 35wt%) of the final mass of carbon (without nitrogen)after oxidation by $KMnO_4$. This was repeated for CMK-8 and Vulcan XC72R using the quantities calculated for 20 wt%. This is because it gave the best activity of the three different classes i.e. the 10 wt%, 20 wt% and 35 wt%.

3.3 Procedures for Electrochemical Analysis

I. Tests for the oxygen reduction activity of catalysts

With the exception of the tests for methanol stability, all the electrochemical analysis were performed using a half-cell within a rotating ring-disc electrode (RRDE) system. The system was an RRDE-3A manufactured by ALS co. The electrode had a Pt ring combined with a glassy carbon disc also from ALS co. In alkaline solution, the ring was set to a potential of 0.35 V. The potentiostat used was an AUTOLAB PGSTAT302N, made by Echochemie. The LSV was performed by sweeping from 0.05 V to -0.8 V except for platinum that started from 0.2 V.

A platinum wire was used as the counter electrode and Ag/AgCl (saturated KCl) was used as the reference electrode.

Except otherwise stated, the ink was prepared by dissolving 5 mg of catalysts in 0.8 ml of ethanol, 165 ml of DI water and 0.035 ml of Nafion. This was mixed ultrasonically. Thereafter a 5 µl drop was placed on the disc section of the RRDE.

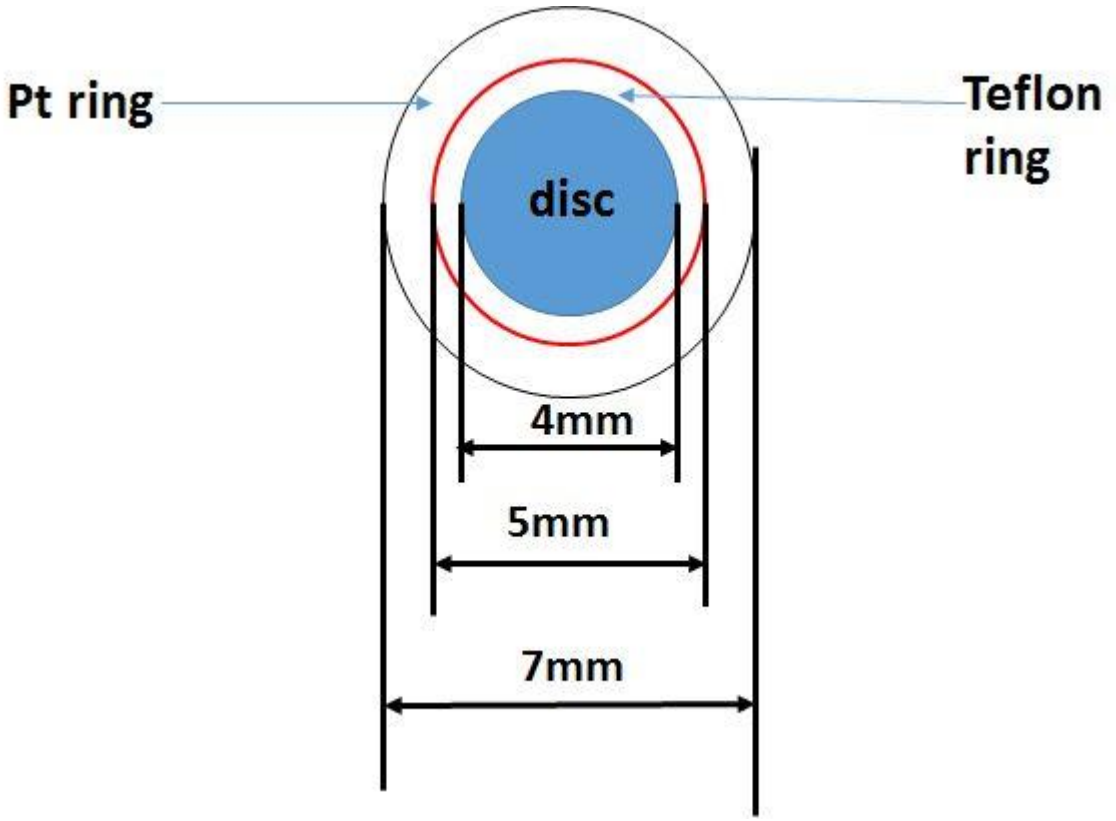

Figure 3-3 Dimensions of RRDE ring and disc

The electrolyte solution was purged prior to the tests with pure oxygen for at least twenty minutes. In alkaline solution, the ring was set to a potential 0.35 V. A 5 mV/s scan rate was used for all the RRDE experiments. A typical half-cell RRDE half-cell is shown

3.4 Accelerated degradation test (ADT)

This was performed by running cyclic voltammetry at 100 mV/s between 0.05 V and -0.5 V (vs Ag/AgCl) for ca 1000 cycles in 0.1 M KOH **(85%, Aldrich)**. This range was chosen because it covered the region where the catalysts had the best activity.

Though the electrolyte was purged with oxygen at the onset, it was necessary that it be sparged lightly with oxygen as the test progressed.

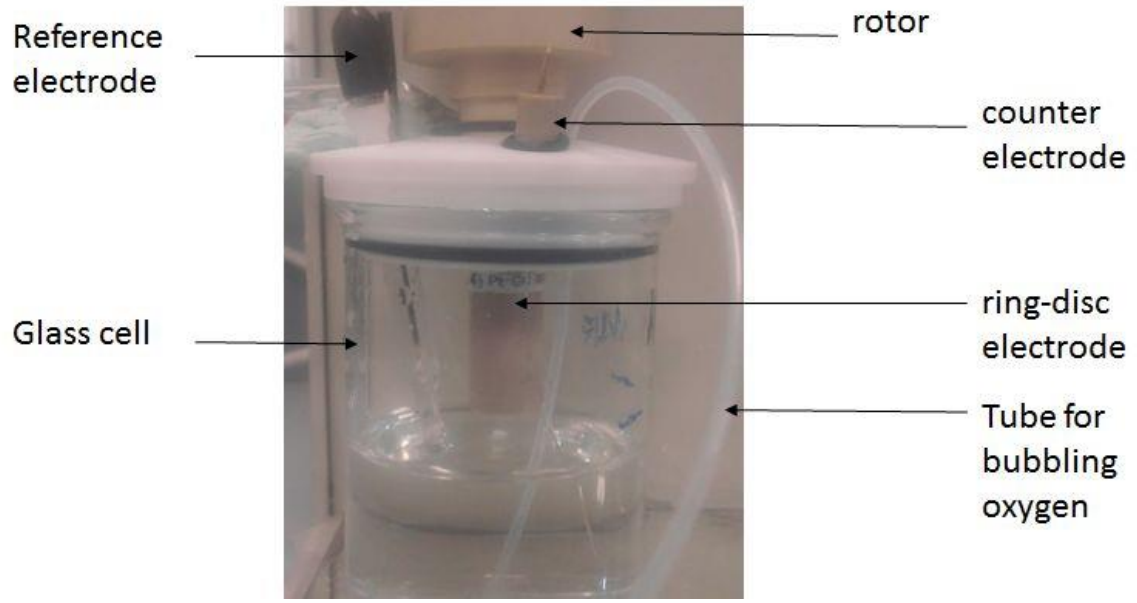

Figure 3-4 A typical RRDE half-cell

LSV in an RRDE system was performed at a rotation rate of 1600 rpm before and after the ADT. The plots of the LSV before and after were compared.

3.5 Chronoamperometry

This was performed in 0.1 M KOH at a fixed voltage, selected to be the voltage at which the catalyst attains limiting current density (ca 0.30 V for NDAB-900 and ca 0.32 V for DNOMC-900). 900 rpm was used for the rotation rate. Data was collected in 2 seconds interval. The electrolyte was also sparged lightly with oxygen as the test progressed.

3.6 Methanol stability tests using a rotating disc electrode (RDE)

The catalyst ink was prepared by mixing 5 mg of catalysts with a 1 ml solution consisting of 800 µl ethanol (absolute, Fisher-Scientific), 165 µl water and 35 µl Nafion (5 wt % in a mixture of lower aliphatic alcohols and water- Aldrich). This was sonicated to obtain a homogenous mixture (20 -30 minutes of sonication seem ideal). 6 µl of the catalyst ink was pippeted onto a glassy carbon electrode and dried under a lamp.

Oxygen was sparged through 75 ml of 0.1 M KOH (85 % ACS reagent -Sigma Aldrich) in a flask for ca 30 minutes. The electrode with the catalyst was then dipped in the solution and the open circuit voltage of the system measured. A test CV of 200 mV/s was performed for ten cycles. This was followed by three cycles of cyclic voltammetry at 100 mV/s (used the third), an LSV of 5 mV/s and RDE of 2500, 1600, 900, 400, and 100 rotations per minute (rpm) (sometimes it was the other way from 100 increased to 2500). The solution was sparged with oxygen for ca 5 minutes in between the rotating disk experiment (RDE) runs.

After running through the stated rotation speeds, the solution was sparged with oxygen again and 300 µl of methanol (Fisher Specified Laboratory Grade (SLR) grade) was added to make up a 0.1 M methanol (Absolute; Fisher Scientific-Specified Laboratory Reagent) concentration in the electrolyte. A RDE experiment was performed at 1600 rpm and a CV at 100 mV/s. This was repeated after each addition of an appropriate amount of methanol to make up a methanol concentration of 0.3 M, 0.5 M and 1 M respectively.

3.7 Methodology for Microbial Fuel Cell Experiments

3.7.1 **Structure of the microbial fuel cells**

A 50 cm3 single chamber cell was used. The anode was separated from the cathode by a Nafion membrane.

Structure of anode

Carbon cloth was placed directly against the wall, with platinised titania wire inserted into the cloth and curved into a spiral to improve contact with the cloth. The anode medium was made of a secondary inoculum from an MFC that was initially inoculated with waste water from a water treatment plant and acetate laden nutrient media.

Structure of cathode

The current collector (stainless steel) was placed on the air facing side, next to this was the catalyst on carbon paper which was hot pressed with Nafion 117.

The back of the carbon paper was in contact with the stainless steel, while the Nafion face of the composite was in contact with the anode medium. The titania wire (carrying current from the stainless steel to the electrode clips) was connected to the stainless steel mesh.

The reference electrode was adapted in a 5 ml pippete filled with agar- 3 M NaCl gel up to three quarter level and topped with 3M NaCl solution. The actual electrode was dipped into the top via a rubber bung (so that it stayed in the NaCl solution above the gel). The pippete was then dipped into the cell through the bigger hole at the top.

The anode medium used was made of 250 mg of sodium acetate, 250 µl of a 1ml/litre vitamin solution, 500 µl of a 2 ml/litre micro nutrients solution, 2.5 ml macro nutrients solution, 12.5 ml of 1 M PBS pH 7 and 50 ml of fresh inoculum. This was topped up with DI water up to and slightly above 250 ml.

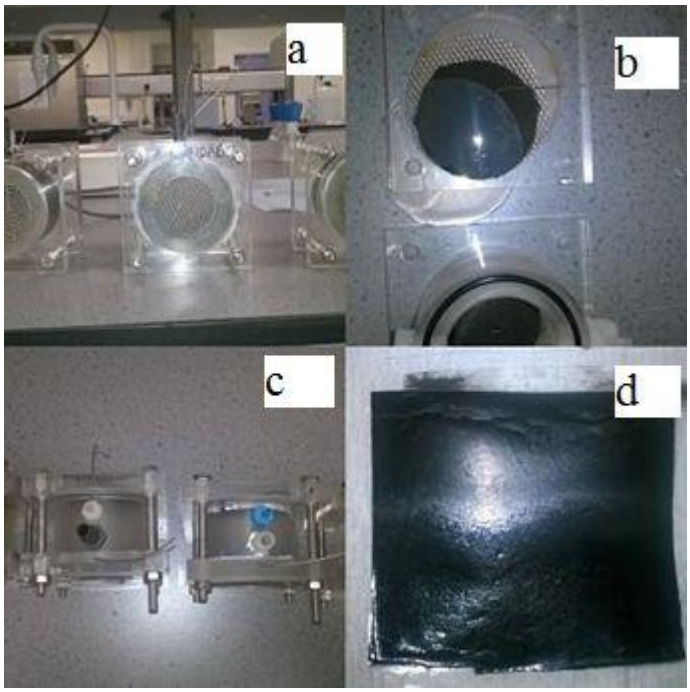

Figure 3-5 MFC cell, a,c; cathode components, b and membrane electrode assembly, d

This mixture was sparged with nitrogen for ca 30 minutes. A 500 ohm resistor was connected across all the four cells for building up the biofilm. The substrate in the cells were changed whenever the voltage was ca 0 V. To do this the old substrate was drawn out using a syringe and the new was introduced also using a different syringe. The data logger continued logging. After about two weeks, a temperature controller was added to the set up with temperature fixed at ca 35 ^{o}C. For the duplicate cells a 100 ohm resistor was used in the process of building up the biofilm.

3.7.2 **Treatment of Nafion membrane**

Typically the Nafion 117 membrane was boiled in 3% H_2O_2 for 1 hour at 90 ^{o}C (allowed to cool normally). It was then submerged in deionized water for 15 minutes at room temperature. Thereafter, the membrane was boiled in 0.5 M sulphuric acid for 1 hour at 90 ^{o}C (allowed to cool). It was again submerged in deionized water for 15 minutes at room temperature. This was followed by boiling in deionized water for 1 hour at 90 ^{o}C. Finally it was kept in deionized water for 15 minutes at room temperature.

3.7.3 **Preparation of ink to be used in air-brushing (spray gun) electrodes (carbon paper)**

10 ml ethanol for every 100 mg of catalysts and 33 wt% actual Nafion and not the Nafion solution (wt % of the catalyst) was used. 16.5 vol% water i.e the ethanol constitutes 80 % was added. This was used because that is the formulation being used for the inks in the half-cell experiments. 2.5 times the actual amount of ink need was prepared, i.e. 2.5 times the mass of catalyst actually required was used. This covers for wastage during spraying.

The actual diameter of the exposed region of the catalyst when inserted into the acrylic cell is 4 cm which gives an area of 12.56 cm^2. Carbon paper with dimensions of 5*5 cm was used. 5*10 cm piece was used so that two squares can be sprayed at the same time. A loading of 0.5 mg/cm^2 was aimed for. Due to inexperience with spraying, it was not possible to get this exact loading calculated for.

3.7.4 **Polarization tests**

When all the cells attained their maximum capacity shown by the regular height reached by the cell voltage plot cycle after cycle, the polarization tests were performed.

The 500 Ω resistor on which the biomass had been grown was removed from all the cells thus allowing them to get to their OCP over time. This took about three hours. Thereafter different sizes of resistors were introduced and the cell voltage was monitored to know when it had attained a stable value. The first resistor 52 500 Ω was left on for about one hour it did not attain a stable value as rapidly as the subsequent ones. On the average, each resistor was left for at least 20 minutes. 52500, 25600, 10000, 5100, 1000, 500, 300, 200, 100, 52, 10 ohms resistors were used. For the duplicate, the 5100 ohms resistor was omitted during polarization tests.

3.8 Physical and Chemical Analysis

3.8.1 **X-ray photoelectron spectroscopy analysis**

When x-ray photons impinge on a sample, photoelectrons are emitted. The kinetic energy as well as binding energy of this photoelectron can be calculated. These are typical not only of the element but also of the atomic level from which the photoelectron was ejected (Watts, 1994). Hence they can be used to identify the chemical state of elements on the surface of a sample. Catalysis being a surface phenomenon, it was important that the chemical species on the surface of catalysts synthesized in this work be determined. The Equipment used was a K-Alpha manufactured by Thermo Scientific, East Grinstead, UK. The X-ray was Microfocused monochromatic AlKα with an X-ray Energy of 1486.6 eV, spot size of 400 x 800 microns (Emission angle: take-off angle of 90 degrees) and pass energy: surveys 200 eV, High resolution regions 40 eV. Charge neutralisation was on during the characterization.

3.8.2 **X-ray powder diffraction analysis (XRD)**

The equipment used was PANalytical X'Pert Pro Multipurpose Diffractometer The anode material was copper, K-Alpha1 wavelength was 1.540598 nm, K-Alpha2 wavelength was 1.544426 nm and ratio K-Alpha2/K-Alpha1 was 0.5. The divergence slit (fixed) was 0.38 mm, generator voltage was 40 kV and tube current 40 mA. No monochromator was used.

3.8.3 **Transmission Electron Microscopy (TEM)**

The transmission electron microscope is much like the visible light microscope in that they both depend on the wavelength of the incident electrons/light. The former depends on the wavelength of accelerated electrons and the latter on the wavelength of light. TEM functions by generating electrons that are accelerated and focused by electromagnetic lenses. Being focused, the electrons are directed on to the specimen. Similar to light waves and depending on the density of the specimen some will be absorbed, diffracted and others will pass through the sample. Those that pass through create an image on a detector. The image is viewed photographically on a screen capable of converting electron intensity to light intensity and is called the Transmission Electron Micrograph (Williams and Carter, 2009). The TEM was used in this work to ascertain the highly ordered pore structure of the template and the ordered mesoporous carbon.

The specific microscope used was a Philips CM200 FEGTEM operated at 200kV. Typically the samples were dispersed in acetone and placed in an ultrasonicator. After they were thoroughly homogenised, a drop was placed on the carbon grid and the grid placed in the microscope.

3.8.4 **Nitrogen adsorption-desorption (BET analysis)**

This was used to determine the surface area and pore structure i.e. pore size, pore volume and surface area of pores. Typically the samples were heated to 120 ^{o}C and vacuumed down to about $10x^{-2}$ torr then the nitrogen was passed in.

3.8.5 **Raman Analysis**

The machine used was a Horiba LabRam HR Evolution. The wavelength of the laser was 532 nm with a power of 500 mW, set to 90 % and a laser power at the sample of about 170 mW. Acquisition time was 60 second and 2 acquisitions were made. The pinhole opened up 200 μm (no confocality) and the focus was adjusted for maximum intensity on the surface. Spectral center of 1400 cm^{-1} and a 600 gr/mm grating.

3.9 Methods of Analysis

3.9.1 **Voltammetry**

Cyclic and linear voltammetry are widely used to acquire qualitative information in the study of electrochemical reactions. Their main objective is to obtain a current output that corresponds to the concentration of the target analyte. This is obtained by studying the rate and quantity of electron transferred throughout the redox process and can be represented by

$$\boldsymbol{O + ne^{-} \leftrightarrow R} \qquad \text{eqn 3.2}$$

O is the oxidized state and R the reduced state of the analyte of interest. The concentrations of these species during an electrochemical process is governed by the Nernst equation i.e. eqn 3.3 (Wang, 2006)

$$\boldsymbol{E = E^{o} + \frac{2.3RT}{nF} log \frac{C_o\,(0,t)}{C_R\,(0,t)}} \qquad \text{eqn 3.3}$$

E^{o} is standard potential for the redox reaction, T the Kelvin temperature, R the universal gas constant, n the number of electrons transferred and F is the Faraday constant. $C_O(0,t)$ represents the concentration of oxidant and C_R (0,t) the concentration of the reductant at the surface of the electrode respectively. The usefulness of voltammetric techniques lies in their ability to give rapid information on the thermodynamics of oxidation-reduction processes as well as on the kinetics of heterogeneous electrochemical processes.

Voltammetry entails increasing (or decreasing) at a constant rate the potential of a stationary working electrode in a quiescent solution and monitoring the

corresponding change in electron density. In such a system, the concentration gradient is given by eqn 3.4 (Wang, 2006)

$$\frac{\partial c(x,t)}{\partial x} = \frac{(C_O\,(b,t) - C_O\,(0,t)}{\delta} \qquad \text{eqn 3.4}$$

$C_O(b,t)$ represents the concentration of O in the bulk solution and δ the thickness of the diffusion layer. The concentration gradient determines the flux of oxidant, which in turn determines the quantity of current. As the peak potential is approached, concentration of oxidant on the surface tends to zero. Therefore, the only force on the flux is the increasing thickness of the diffusion layer that serves to lessen it. Just before this point, a peak current is attained and the current gradually diminishes afterwards.

As scan rate is increased, the peak current increases but the voltage at which the peak occurs remains the same. This is characteristic of fast or reversible processes. For a quasi-reversible electron transfer reactions or slow process the same phenomenon of increasing peak currents occur with increasing scan rates but the voltage at which it occurs changes.

Linear sweep voltammetry (LSV) entails scanning the potential in one direction only while cyclic voltammetry entails scanning the potential in forward and reverse direction. Cyclic voltammetry can involve repeated scans depending on the property under investigation.

In this work, the LSV was used to compare the limiting current for the synthesized catalyst and 20 wt% Pt/Carbon commercial catalyst.

3.9.2 **Rotating Disk Electrode (RDE) and Rotating Ring Disk Electrode (RRDE)**

Voltammetry with the aid of a rotating disk electrode (RDE) allows for a well-defined diffusion layer with constant thickness and a mass transfer process whose theoretical basis is well investigated and the equations related to relevant electrocatalytic parameters (Town *et al.*, 1991).

The electrode rotates at a constant angular velocity ω=2π*f* about this axis (*f* is rotation speed in revolution per second). Some equations used to extract electrocatalytic oxygen reduction relevant parameters from the RDE data include:

3.9.3 **The Levich equation**

This relates the limiting current i_l to the square root of the angular velocity, ω in a reversible system.

$$\boldsymbol{i_l = 0.62nFAD^{2/3}\omega^{1/2}v^{-1/6}C^b} \qquad \text{eqn 3.5}$$

n is the number of electrons transferred ; F is Faraday's constant ; A is the geometrical surface area of electrode; D is the diffusion coefficient of the analyte, v is the kinematic viscosity and C^b is the concentration of the analyte in bulk solution. This equation was developed with an assumption that the concentration of the analyte is zero at the electrode-solution interface. It therefore implies a mass transfer controlled process. A plot of i_l *vs* $v^{-1/2}$ is used to determine n, the number of electrons transferred as well as D, the diffusion coefficient; a kinetic limitation exists when it does not pass through the origin.

3.9.4 **The Koutecky-Levich equation**

Similar to the Levich equation is the Koutecky-Levich. This was developed to accommodate quasi-reversible systems that are controlled by mass-transfer and kinetic limitations. The cathode current I_c is represented by equation 3.6

$$\frac{\mathbf{1}}{\boldsymbol{I_c}} = \frac{\mathbf{1}}{\mathbf{0.62}\boldsymbol{nFAD^{2/3}v^{-1/6}\omega^{1/2}C^b}} + \frac{\mathbf{1}}{\boldsymbol{nFAk_hC^b}} \qquad \text{eqn 3.6}$$

k_h with units of cm/s is the heterogeneous reaction rate constant or charge transfer constant that typifies the ease of electron transfer between the catalysts material and oxygen, the larger the value of k_h the faster the kinetics. From the equation, a plot of $1/I_c$ vs $1/\omega^{1/2}$ should be a straight line. Equation 3.6 can also be represented as

$$\frac{1}{I_c} = \frac{1}{j_m} + \frac{1}{j_k}$$ eqn 3.7

with j_m being the mass transfer limiting current while j_k is the kinetic current. The Koutecky-Levich equation is used to determine the number of electrons transferred n, which also defines if the ORR is proceeding to form water, terminates in the formation of hydrogen peroxide or combines both.

The uniqueness of the RRDE lies in the presence of a concentric ring around the disc, both being separated by an insulating non-catalytic material. Its principal benefit during ORR is its ability to detect peroxide, the ORR intermediate. This is achieved by setting the ring at a voltage that is sufficient to oxidize peroxide as it is swept outwards by the rotating motion of the disc. Hence the RRDE is useful for clarifying the predominant mechanism during oxygen reduction. Two key equations for the RRDE are the number of electrons transferred eqn 3.8 and the mole fraction of peroxide formed eqn 3.9,

$$n = \frac{4I_D}{I_D + I_R/N}$$ eqn 3.8

Where n is the average number of electrons transferred per molecule of oxygen, I_D is the disk current, I_R the ring current generated as a result of the oxidation of hydrogen peroxide and N is the collection efficiency which captures the ratio of the amount of peroxide reduced to the total which was produced at the disc. Using data from RRDE, the mole fraction of peroxide can also be calculated from the equation 3.9

$$X_{H_2O_2} = \frac{2I_R/N}{I_D + I_R/N}$$ eqn 3.9

X_{H2O2} is the mole fraction of peroxide which is an indication of catalytic efficiency in terms of how much of the ORR proceeds to complete four electron reduction.

3.9.5 **Butler-Volmer Analysis**

For the reaction represented by

$$O + ne^{-} \leftrightarrow R \qquad \text{eqn 3.10}$$

When the ORR current is controlled by the rate at which electrons are being transferred (charge transfer of electrons is sufficiently fast), the rate of the forward reaction is represented by a first order equation with respect O

$$V_f = k_f C_o(0,t) \qquad \text{eqn 3.11}$$

and that of the backward reaction by a first order equation with respect to R

$$V_b = k_b C_R(0,t) \qquad \text{eqn 3.12}$$

k_f and k_b tell the speed of the reactions and are known as the forward and backward heterogeneous rate constants respectively. The unit of the heterogeneous rate constant for first order reactions is cms^{-1}.They depend on the overpotential and are represented as

$$k_f = k^o \exp\left[\frac{\alpha nF(E-E_o)}{RT}\right] \qquad \text{eqn 3.13}$$

$$k_b = k^o \exp\left[-\frac{(1-\alpha)nF(E-E_o)}{RT}\right] \qquad \text{eqn 3.14}$$

Where k_o is the standard heterogeneous rate constant and α the transfer coefficient. The net reaction rate can be represented by

$$V_{net} = V_f - V_b = k_f C_o(0,t) - k_b C_R(0,t) \qquad \text{eqn 3.15}$$

The current output is proportional to the rate of reaction and can be represented as

$$i_f = i_c = nAFV_f = nAFC_o\, k^o \exp\left[\frac{\alpha nF(E-E_o)}{RT}\right] \text{ eqn 3.16}$$

$$i_b = i_a = nAFV_b = nAFC_R k^o \exp\left[-\frac{(1-\alpha)nF(E-E_o)}{RT}\right] \qquad \text{eqn 3.17}$$

$$i_{net} = i_f - i_b = nFA[k_f C_o(0,t) - k_b C_R(0,t)] \text{ eqn 3.18}$$

Substituting for the heterogeneous rate constants in eqn 3.18 gives

$$i_{net} = nFAk^o \left(\exp\left[\frac{\alpha nF(E-E_o)}{RT}\right] C_o(0,t) - \exp\left[-\frac{(1-\alpha)nF(E-E_o)}{RT}\right] C_R(0,t) \right)$$ eqn 3.19

This is the Butler-Volmer equation and is used to represent a purely kinetic faradaic current. That is a Faradaic current that is controlled wholly by the rate of chemical reaction or charge transfer. Such a current is a function of the overpotential ($E - E_o$) which is the additional potential beyond the equilibrium potential that is required for the movement of electrons.

At equilibrium $E - E_o = \eta = 0$ and $C_o = C_R = C$, and eqns 3.16 and 3.17 simplify to

$$i_o = i_f = i_b = nFAk^oC \qquad \text{eqn 3.20}$$

i_o is called the exchange current density.

Also at large negative overpotential, $i_c >> i_a$ therefore eqn 3.19 becomes

$$i_{net} = i_c = nAFC_o k^o \exp\left[-\frac{\alpha nF(E-E_o)}{RT}\right] \quad \text{eqn 3.21}$$

$$i_c = i_o \exp\left[-\frac{\alpha nF(E-E_o)}{RT}\right] \qquad \text{eqn 3.22}$$

Equation 3.22 is referred to as the Tafel equation and can be represented alternatively as

$$lni_c = lni_o - \frac{\alpha nF}{RT}\eta \qquad \text{eqn 3.23}$$

i_o is referred to as the exchange current density. It is the current which flows at dynamic equilibrium and also characterizes the activity of an electrocatalysts.

3.9.6 **Half-Wave Potential**

The half-wave potential can be defined as the voltage at which the reduction current attains half of its value at the limiting current region. It serves as a good measure of the charge transfer kinetics particularly when differences in onset can be ambiguous. In essence, it gives information on the relative closeness to

thermodynamic predictions of the electrochemical activity in question. Therefore, for two or more catalyst being tested on the same reaction, the one with the smaller half-wave potential is closer to the thermodynamically predicted performance and adjudged to be better.

3.9.7 **Coulombic Efficiency (CE)**

This calculation was done for the microbial fuel cells. CE is defined as the amount of electrons that goes to produce current divided by the theoretical amount of electrons available for producing current (Logan *et al.*, 2006) expressed in percentage. It is calculated thus (HaoYu *et al.*, 2007)

$$\boldsymbol{CE = \frac{CE_{exp}}{CE_{theoretical}} x100} \qquad \text{eqn 3.24}$$

CE_{exp} is the experimental value of the total charge gotten from the substrate used. This was calculated by multiplying the current at a particular time by the time interval at which data is logged. The values were then summed up over a particular cycle common to all the catalysts. $CE_{theoretical}$ is the theoretical amount of charge obtainable from the substrate if it were completely consumed over the cycle being considered.

Chapter 4. **Physical and Electrochemical Characterization of Nitrogen Doped Carbons**

In this chapter, the use of nitrogen doped ordered mesoporous carbons as alternatives catalysts to platinum for oxygen reduction reactions in fuel cells is explored. Nitrogen doped ordered mesoporous carbon was synthesized using two methods. In the first method, O-phenylenediamine was polymerized and then carbonized using highly ordered mesoporous silica (KIT-6) as template. The template was removed after the carbonization step. For the purpose of attaining an optimal material property nitrogen doped carbon, carbonization was performed at three different temperatures of 700 ^{o}C, 800 ^{o}C and 900 ^{o}C to give NDAB-700, NDAB-800 and NDAB-900 respectively. In the second experiment, a reduction in the number of steps and materials involved in the production of ordered nitrogen doped carbon was explored through a direct synthesis approach that made use of a soft template instead of a hard one (i.e. KIT-6 silica) was adopted; here also the materials were carbonized at three different temperatures of 700 ^{o}C, 800 ^{o}C and 900 ^{o}C to give DNOMC-700, DNOMC-800 and DNOMC-900 respectively. For a proper understanding of what was responsible for catalysis, characterization was carried out. These include, X-ray photoelectron spectroscopy (XPS), transmission electron microscopy (TEM), Raman spectroscopy, nitrogen adsorption-desorption analysis and x-ray powder diffraction. The two groups of catalysts revealed average activity but good stability.

4.1 Introduction

Nitrogen doped carbons have been known to possess ORR activity. However certain issues are preventing their use on a large scale. This include the poor activity compared with platinum, expensive precursors that make the final product not to be market competitive, stability and complex synthesis procedures being used.

One promising work was that of Yang et al (2010). They synthesized N-doped catalysts that were used in alkaline media. The onset potentials were very close

i.e. ca -35 mV with an overpotential of about 35 mV compared to that of 20wt% Pt/C. Using Koutecky-Levich analysis, the number of electrons transferred was determined to be 4.1 for the best catalyst, which is similar to that for platinum. Why the choice of O-phenylenediamine in this work? It was used by Liu et al (2010a) to produce the highest nitrogen content of N-doped carbon reported in literature, i.e. 26.5 wt% at 600 ^{o}C. However, this high nitrogen content mesoporous carbon was not put to any practical use. Hence the need to investigate the possible advantages of nitrogen doped carbons obtained from this procedure. Furthermore, though many non-platinum catalysts have been synthesized the challenge of tedious synthesis procedures and expensive materials remains.

4.2 Physical and Chemical Characterization

4.2.1 **XPS Analysis**

To understand the chemical components responsible for the activity of these catalysts, they were analysed using high resolution X-ray photoelectron spectroscopy.

XPS analysis of nitrogen doped carbon prepared by carbonizing poly-o-phenylenediamine in ordered mesoporous silica template

The survey spectra in Figure 4-1**Error! Reference source not found.** are summarized in Table 4 -1

Table 4 -1 Chemical composition of NDAB catalysts obtained from XPS analysis (atomic %)

	Atomic %					
	C 1s	N 1s	O 1s	S 2p	Si 2p	Na 1s
NDAB-900	85.47	5.31	6.98	0.84	1.23	0.17
NDAB-800	79.49	8.15	8.59	1.67	1.31	0.78
NDAB-700	74.95	11.79	8.96	1.37	1.91	1.01

The presence of the desired elements carbon and nitrogen is confirmed, albeit with some impurities like sulphur, sodium and silica. These i.e. sulphur, sodium and silica are likely artefacts from the synthesis process. Silica and sodium are from the silica template and the NaOH used to etch the silica respectively. They are not expected to have any oxygen reduction activity either A common trend in the carbonization of nitrogen containing compounds is the reduction in total nitrogen content as temperature of carbonization increases (Stańczyk *et al.*, 1995). This is evidenced here as the synthesis temperature is increased from 700 to 900 ^{o}C and agrees with the works of Nagaiah et al and Wang et al (2010; 2012). Expectedly, the total amount of carbon increases with the carbonization temperature. It is worth mentioning that the C/N at% ratio obtained here 6.4 – 16.9 was lower than that claimed to have been obtained in the literature (Liu *et al.*, 2010a) 3.25–3.65.

In making use of binding energies for the identification of elements, there is often the need to have a charge reference otherwise referred to as calibration of the energy scale. The binding energy of adventitious carbon at 284.8 eV or near 285 eV is mostly used as the charge reference (Miller *et al.*, 2002; Biesinger *et al.*, 2010) . In this analysis, the main peak of the C1s spectrum for each row of elements were duly calibrated by adding a few eV to bring them to 248.8eV. The binding energy (BE) of the other elements in the row were adjusted accordingly.

Sulphur can be potentially doped into carbon with a concomitant oxygen reduction activity. However, the sulphur quantified in this work as S-2p (electrons from the 2p shell were used for quantification) at a binding energy (BE) of 164.08 eV is expected to be elemental sulphur or sulphur existing as a thiol physisorbed on the catalyst. (XPS simplified; (Fabianowski *et al.*, 1989). This is as opposed to sulphur that is doped into the carbon structure and is capable of possessing catalytic activity. This would have been identified as a C-S-C configuration appearing at 283.4-283.7 eV (Wan *et al.*, 2010) (Liang *et al.*, 2012a; Li *et al.*, 2014). Deconvolution of the respective spectra's yields more useful information as to the functionality of the species present.

Each C1s carbon was deconvoluted into six separate components, with the exception of NDAB-700. The Full width at Half Maximum (FWHM) was constrained to 1.4±0.2 eV (Gelius *et al.*, 1970). The first component occurs at a binding energy of 284.8 eV in all three samples. It corresponds to pure carbon C-C or C-H (Bhattacharyya *et al.*, 1998). The second component occurs at 286±1 eV and is assigned to the **C-N** sp2 bond. The third major component which is assigned to C-N sp3 bond occurs at a BE of 287±3 eV (Boyd *et al.*, 1995; Bhattacharyya *et al.*, 1998). Surface oxidized carbon species like carboxyl and carbonyl functional groups were also identified as being present on the surface of pyrolyzed NDAB (Song *et al.*, 2014) . This occurred at binding energies of 288.4±3 eV and 289.5±2 eV (Gelius *et al.*, 1970; Buchwalter and Czornyj, 1990) for the carbonyl and carboxyl groups respectively. For NDAB-700, at 290.5 eV is the carbonate functional group (Gardner *et al.*, 1995). The shift in BE suggest variations in the chemical composition of the surface oxidized carbon species. A pi to pi* transition of valence electrons is captured as a shake-up peak within the NDAB-900 and 800 samples at BE of 291.3±1 eV (Gardella *et al.*, 1986; Doren *et al.*, 1994; Brena *et al.*, 2004).

N-1s nitrogen spectrum was also deconvoluted into four components; graphitic or substitutionary nitrogen, pyridinic nitrogen, pyrolic nitrogen and nitrogen-oxides.

The binding energy of graphitic nitrogen is somewhat controversial. A nitrogen containing carbon molecule that typifies this structure is fullerene $C_{59}N$.

Fullerene has only one substituted nitrogen atom having a binding energy of 400.7 eV (Pichler *et al.*, 1997; Schulte *et al.*, 2007). Hence components in the synthesized materials with BE of ca 400.7 eV have been identified as substituted nitrogen. There seems to be a consensus about the BE of pyridinic nitrogen occurring at 398.3 ± 0.3 eV (Liu *et al.*, 2010a; Susi *et al.*, 2015). Hence the components occurring at 398.2 – 398.4 eV are labelled as pyridinic nitrogen. It is expected, that as carbonization temperature increases, the pathway for the transformation of nitrogen structures shifts from pyrrolic to pyridinic to

graphitic (Stańczyk *et al.*, 1995) with graphitic nitrogen considered as the most stable.

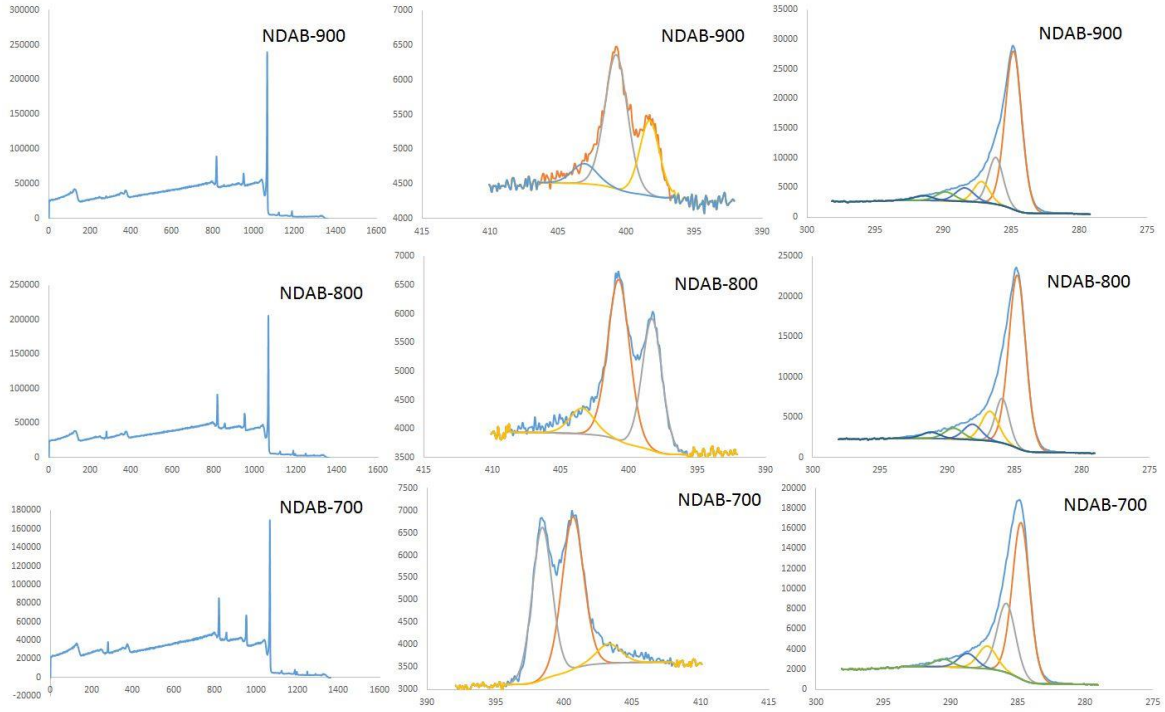

Figure 4-1 Survey and deconvoluted spectra of nitrogen doped carbon obtained from O-phenylenediamine

Here, nitrogen functional group with a BE 400.1 $\pm$ 0.3 and 402 – 403.5 eV (Susi *et al.*, 2015) are labelled as having the pyrrolic and nitrogen oxide functionality respectively. A summary of the types of nitrogen functional groups present in each sample and their percentages is shown in **Table 4-2**.

Table 4-2 Chemical composition and nitrogen functional groups of N-doped carbon from o-phenylenediamine using KIT-6 as template

Catalysts	Carbon (%)	Nitrogen (%)	Oxygen (%)	Nitrogen (%)		
				Pyridinic	Graphitic	Nitrogen oxides
NDAB-900	85.47	5.31	6.98	29.6	60.6	9.8
NDAB-800	79.49	8.15	8.59	38.6	52.1	9.3
NDAB-700	74.95	11.79	8.96	44.4	48.6	7.0

XPS analysis of direct nitrogen doped carbon prepared using a surfactant as soft template

For the direct nitrogen doped mesoporous carbon (DNOMC) the main C1s peak was calibrated to 284.8 eV and used for charge referencing. Other components and compound were adjusted accordingly. A predominance of the C-C single bond

is highlighted by the fact that C1s with a BE of 284.8 eV constitutes ca 69 % of all forms of carbon present. The possibility of overlaps within XPS spectra is common place (Artyushkova *et al.*, 2007; Lewin *et al.*, 2008). Hence the BE of 285.8 eV can be assigned to carbon species combined with oxygen in an ether configuration (Jordan *et al.*, 1987) as well as to carbon joined to nitrogen in an sp2 configuration (Boyd *et al.*, 1995) the aliphatic ether configuration is confirmed by the O1s binding energy of 532.2 eV (Ackeret and Ratner, 1992). Carbon bound to nitrogen in an sp3 configuration can be identified via the BE 287eV (Boyd *et al.*, 1995). An obvious left-shoulder peak is present in the spectra of the three DNOMC samples. Occurring at a BE of ca 288.9 eV the closest relevant match would be a carbonyl group of a ketone or ester, this confirms the presence of oxygen functional groups (Hantsche, 1993).

Oxygen was deconvoluted into 3 components. The BE at 532.2 eV represents the oxygen bound to two carbon atoms in an ether configuration (Ackeret and Ratner, 1992) , that at 533.6 eV characterizes oxidized carbon species namely carbonyl (Lhoest *et al.*, 1995) and ether (Jordan *et al.*, 1987). The likely presence of water or other hydroxides is suggested by the BE at 529.9 eV (Jin and Atrens, 1987).

From the survey spectrum, it is evident that the overall amount of nitrogen doped into the DNOMCs is relatively small. This, notwithstanding the work of Niwa et al (2011) shows that nitrogen doped carbon catalysts have been known to show oxygen reduction activity even at compositions as low 0.4 at%. Due to the very low amount of nitrogen present, the XPS peaks were noisy and did not yield fine distinctions of nitrogen functionalities. The N1s core level spectrum was deconvoluted into four components. The BE of 398.3$\pm$0.3 eV can be ascribed to pyridinic nitrogen (Susi *et al.*, 2015). Pyrolic nitrogen is amongst the first product in the pyrolysis of nitrogen containing carbon compounds. Here, they are confirmed to be present in all the DNOMC samples by the BE of 399.6-400.4 eV (Artyushkova *et al.*, 2007; Susi *et al.*, 2015). Substituted nitrogen, which is nitrogen combined with three carbon atoms in a sp2 hybridized configuration is seen in DNOMC-800 and DNOMC-900 at a binding energy of 400.8-401.1 eV.

The component represented by the BE of 401.5 eV is somewhat equivocal falling between values often referenced for substituted nitrogen at the lower end 400.7-401.5 eV (Pichler *et al.*, 1997; Raymundo-Piñero *et al.*, 2002) and those for oxidized nitrogen species at the upper end 402-405 eV (Susi *et al.*, 2015). However, there is an obvious presence of the oxides of nitrogen represented by the BE of 402.5 – 403.9 eV. Temperature of pyrolysis was also a factor that influenced overall activity though it did not produce a trend in the amount of nitrogen functional groups present (**Table 4-3**).

Table 4-3 Chemical composition and nitrogen functional groups of N-doped carbon from the direct synthesis procedure (atomic %)

Catalysts	Carbon	Nitrogen	Oxygen	Nitrogen			
				Pyridinic	Graphitic	Nitrogen oxides	Pyrrolic
DNOMC-900	92.44	0.62	6.95	17.11	28.32	13.69	40.88
DNOMC-800	92.48	0.78	6.75	14.52	36.1	14.46	34.93
DNOMC-700	91.04	0.78	8.19	22.89	23.04	9.22	44.84

4.2.2 **BET Analysis**

According to the IUPAC classification, most physisorption isotherms can be classed into six types (Sing, 1985) with type IV being typical of mesoporous materials. Following this, the three physisorption isotherms **Figure 4-2** a, c, and e are type IV, thus confirming their mesoporous nature. KIT-6 the hard template used to synthesize NDAB-900 was itself made from a so-called soft-template Pluronic 123. The sharp and vertical nature of the adsorption and desorption isotherms (H1 hysteresis) is a validation of the very narrow pore size distribution. This is corroborated by the pore size distribution (PSD) in **Figure 4-2**b.

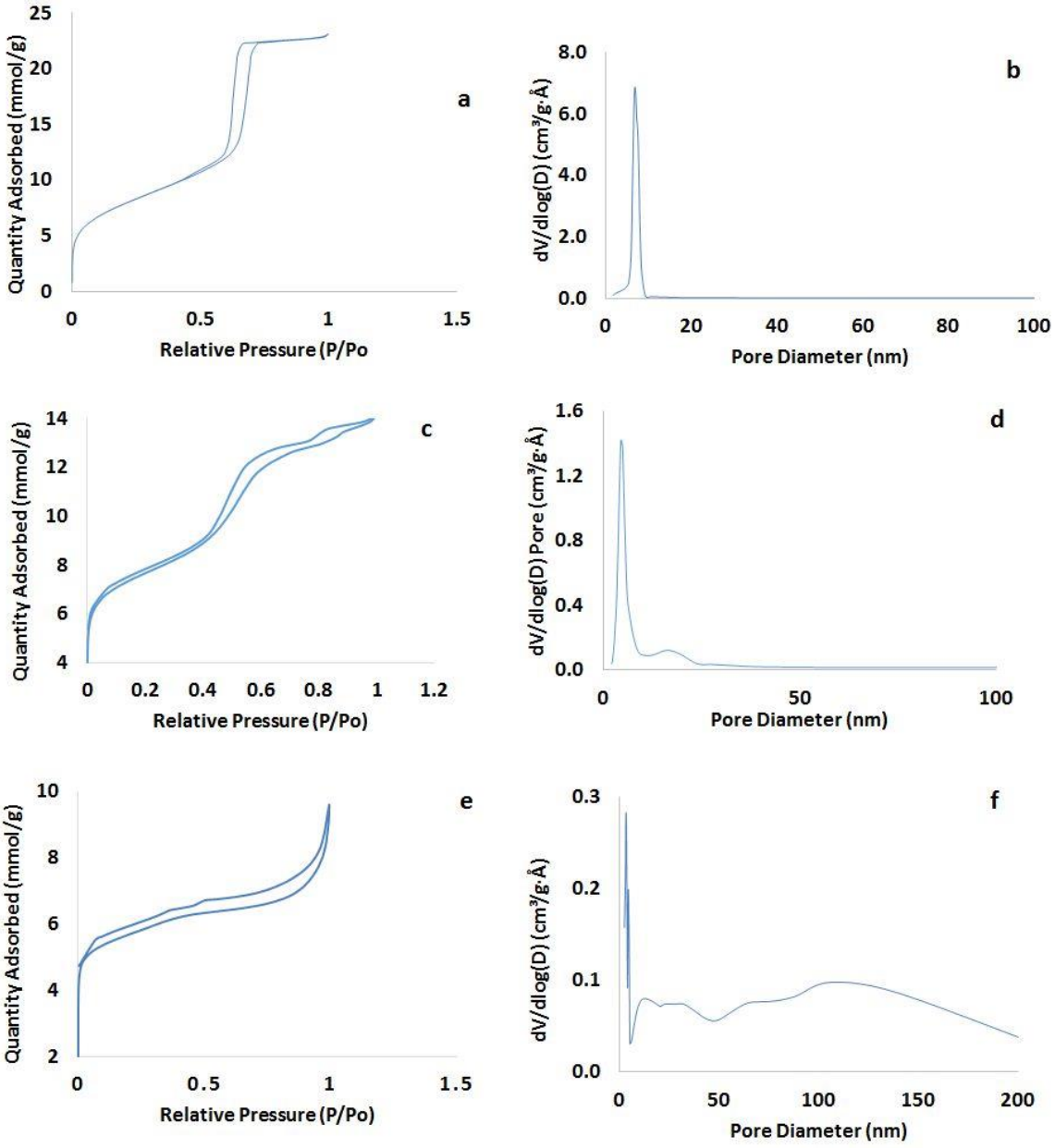

Figure 4-2 Physisorption Isotherm and Pore Size Distribution for a, b KIT-6 silica; c, d NDAB-900; e, f DNOMC-900

The area of the hysteresis also points to a relatively large mesopore volume. Though the isotherm of NDAB-900 is also a type IV, its H3 hysteresis loop is a departure from that of the parent template. This might be a pointer to the need to improve on the impregnation procedure as well as the template dissolution step. NDAB-900 further exhibits a low pressure hysteresis (thin portion after p/po<0.4); an indication of micro-porosity within the catalyst. Its PSD reveals that most pores have a diameter of 5 nm with a small fraction of ca 16 nm. This

bimodal pore size distribution is similarly captured in the isotherm which shows two hysteresis, the smaller occurring at a higher p/po (P/Po=0.8 – 1.0) indicating that it comes from pores with larger diameters. The presence of pores with diameter of ca 16 nm shows that some pores in the template KIT-6 were unfilled (Wu *et al.*, 2012).

When the template was removed, these pores collapsed to produce larger ones in the carbon. DNOMC-900 is the nitrogen doped carbon catalyst synthesized directly from a soft-template as against NDAB-900. It has an H4 hysteresis loop. Its very broad PSD with most being in the macropore range is marked in **Figure 4-2**e,f. DNOMC-900 was synthesized with the hope of obtaining a facile procedure for nitrogen doped ordered mesoporous carbons. From the point of structure, we may say that this was not fully achieved. This indicates that this method may not be efficient for producing uniform highly ordered mesoporous nitrogen doped materials. **Table 4-4** presents a summary of the textural and structural properties of the three mesoporous materials. The total surface area is 612 m^2/g, 558 m^2/g and 404 m^2/g for KIT-6 mesoporous silica template, NDAB-900 and DNOMC-900 respectively. Values for the pore volume are DNOMC-900-0.19 cm^3/g , NDAB-900-0.38 cm^3/g and KIT-6 - 0.80 cm^3/g

Table 4-4 Textural and structural properties of KIT-6, NDAB-900 and DNOMC-900

	Total Surface area (m^2/g)	External Surface area (m^2/g)	Micropore Area (m^2/g)	Pore Volume (cm^3/g)	Pore Size (nm)
KIT-6	612	465	147	0.80	6.00
NDAB-900	558	245	313	0.38	4.86
DNOMC-900	404	127	278	0.19	5.58

4.2.3 **Transmission Electron Microscopy (TEM)**

Figure 4-3 shows the transmission electron microscopy micrographs for KIT-6, NDAB-900 and DNOMC-900. A unique and somewhat unexpected feature can be seen in the high resolution transmission electron microscope (HRTEM) micrograph of NDAB-900 Figure 4-3d, i.e the crystalline nature of the pore walls

(Bojdys *et al.*, 2008). This is a pointer that the material is highly graphitic (Wu *et al.*, 2012) while still maintaining the structural order. This is notable considering that conventionally, graphitized carbon materials are produced via high temperature treatment of up to 2200 ^{o}C (Chai *et al.*, 2012b). For ordered mesoporous materials, this could lead to a breakdown of the structural order (Gierszal *et al.*, 2008). A generality of the methods that preserve mesopore order and structure while producing a highly graphitized carbon are either complicated or costly (Wang *et al.*, 2011). Hence obtaining highly graphitic pore walls combined with extensive structural order at 900 ^{o}C is commendable. That NDAB-900 contains some measure of crystallinity is further confirmed by wide-angle XRD shown in **Figure 4-4**

This data shows two characteristic peaks occurring at around 25^{o} and 44^{o} 2 theta. These peaks are indexed to the (002) and (101) planes of graphitic carbon. The calculated d-spacing based on the 2 theta value of 25^{o} is 0.356 nm. This is close to the value for crystalline graphite i.e. 0.355 nm (Howe *et al.*, 2003).

The benefits of this are numerous. The highly graphitic pore walls enhances the attachment of metal catalysts like platinum, rhodium and titanium oxide, thus making them ideal carbon supports (Cui et al., 2009; Wang et al., 2011; Chai et al., 2012b). Contrary to what may be deduced from the nitrogen physisorption data for DNOMC-900, its TEM micrographs in Figure 4-3e, f reveal large areas of periodically ordered meso-channels.

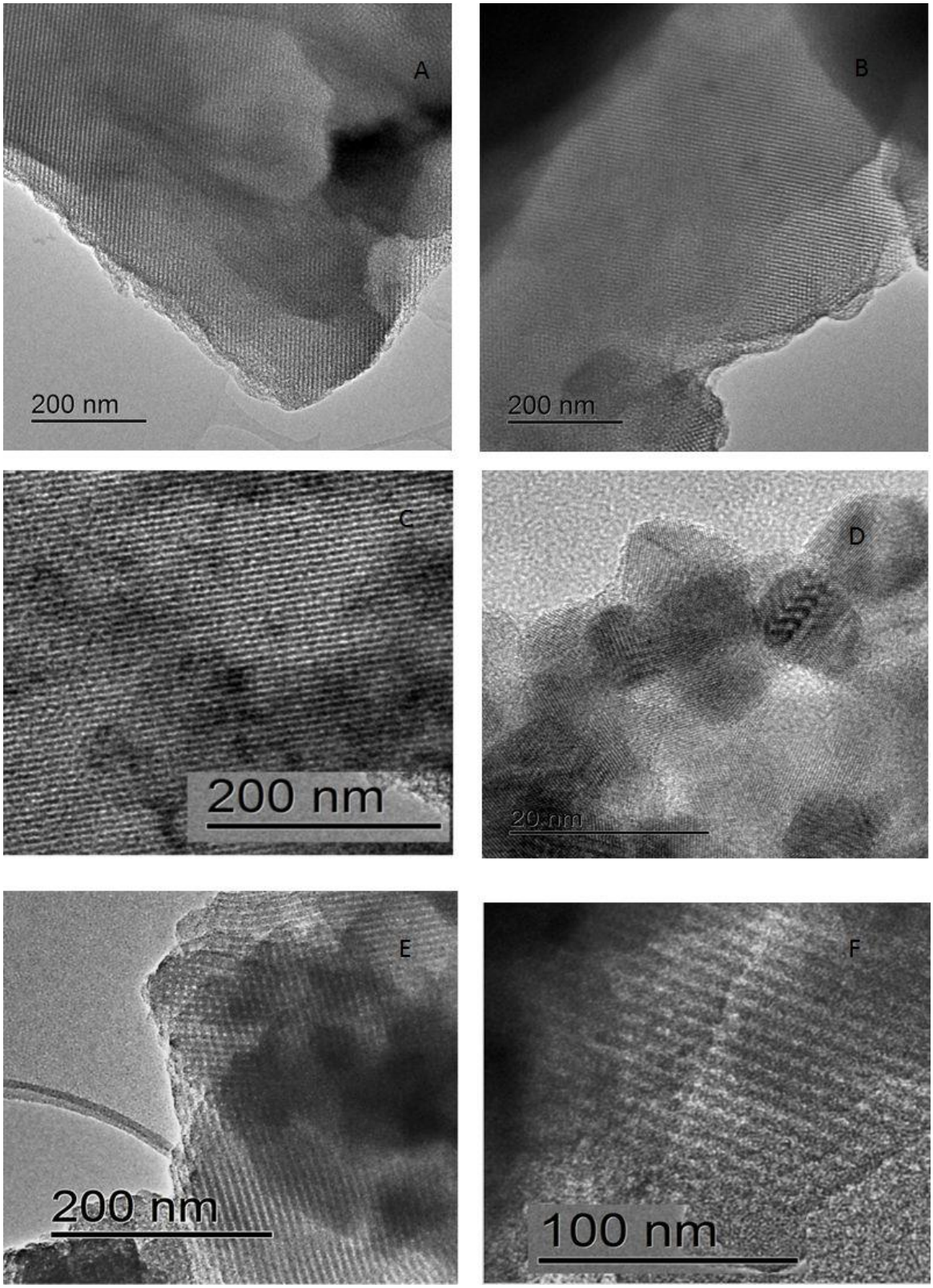

Figure 4-3 TEM of a, b KIT-6; c, d NDAB-900; e, f DNOMC-900

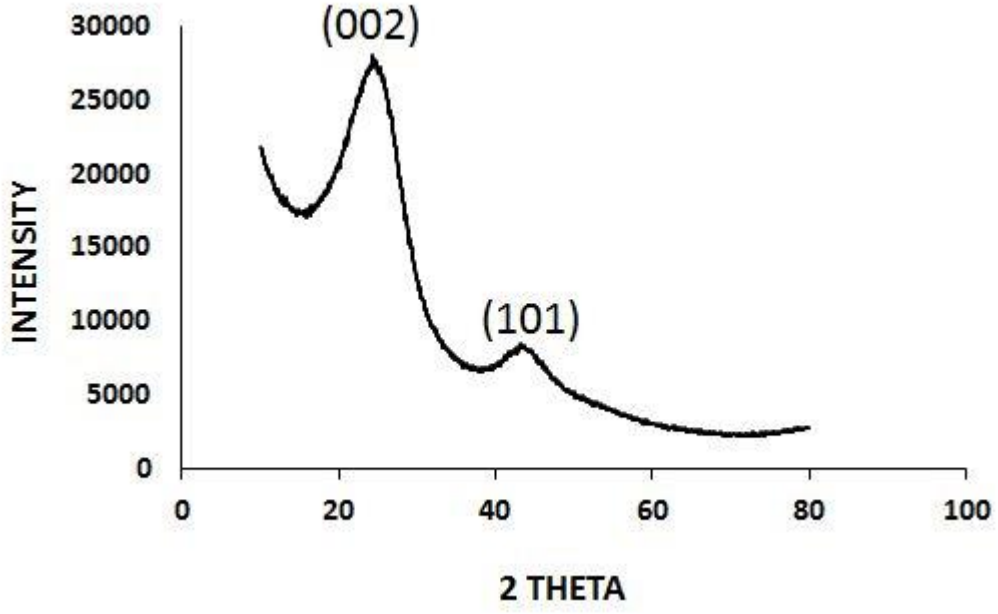

Figure 4-4 Low-angle XRD of NDAB-900

The uniform pores are also visible on the upper-centre of **Figure 4-3**e. This may mean that the direct synthesis procedure did succeed in producing some degree of order within the nitrogen doped carbon.

4.2.4 **Characterization of CMK-8 carbon and Vulcan XC-72**

For comparison, two other carbons were tested. One is highly ordered mesoporous carbon (CMK-8) which should highlight the effect of the presence or absence of nitrogen doping. This was prepared with the same ordered mesoporous silica (KIT-6) template used for the NDAB group but with sucrose as carbon source and no nitrogen. The other was commercial Vulcan, expected to highlight the effect of the absence of both nitrogen doping and an ordered structure. This could not be nitrogen doped due to the nature of the procedure used; carbon and nitrogen would need to be available in the same material. It would have been insightful to compare the ORR capacity of nitrogen doped non-mesoporous carbon but this was not possible due to time constraints. The XPS spectra for each of these carbon is shown in **Figure 4-5**. The data from the survey spectra is summarized in **Table 4-5**. From the survey spectra it is apparent that while Vulcan is made up of almost 100% carbon, CMK-8 has a

significant amount of oxygen functional groups as revealed by the ca 14 % oxygen in addition to the ca 80 % carbon by atomic weight. This is expected to contribute significantly to its oxygen reduction capability (Gilbertson *et al.*, 2014; Wu *et al.*, 2014). Comparing the deconvoluted spectra, it can be said that the two carbons contain similar carbon functional groups. However, the intensities reveal that the quantity in CMK-8 far exceed that in Vulcan.

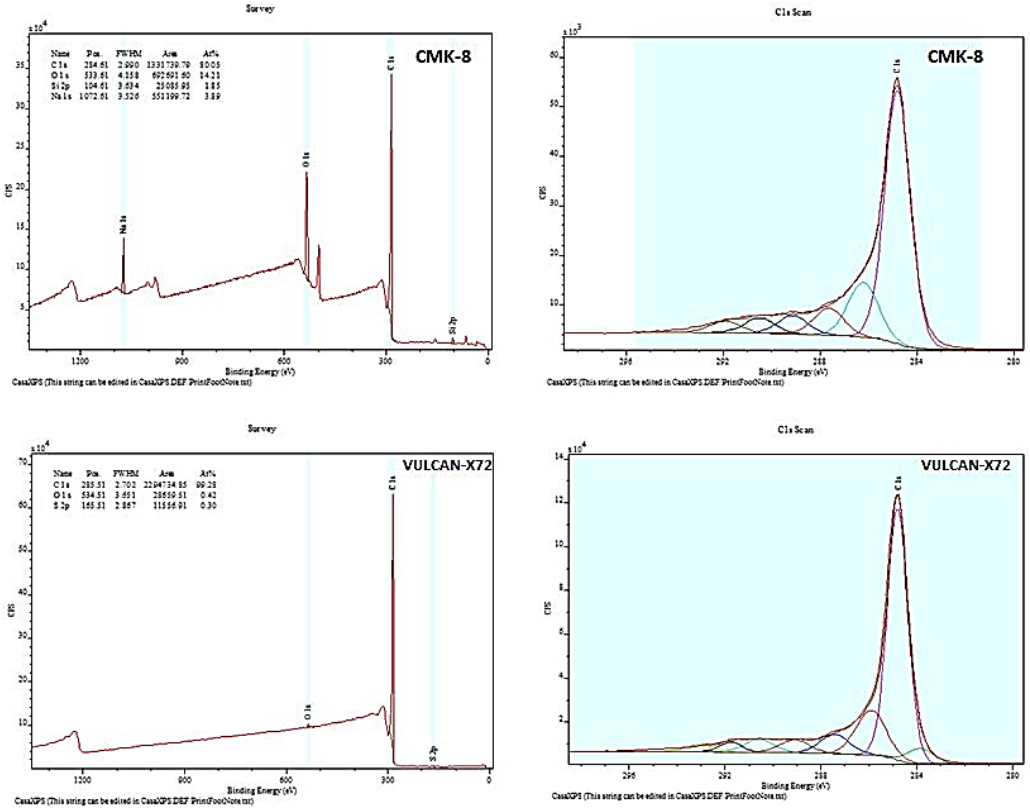

Figure 4-5 Survey and Deconvoluted Spectra of CMK-8 and Vulcan Carbon

Table 4-5 XPS identified elemental composition of CMK-8 and Vulcan carbons

Catalysts	CMK-8	VULCAN
Carbon	79.64	99.00
Oxygen	14.54	0.65
Nitrogen	0.00	0.00

Table 4-6 Identification of functional groups present in CMK-8

Name	Position	FWHM	% Concentration	Reference
C-C, C-H	284.8	1.24	62.96	(Bhattacharyya *et al.*, 1998)
C-O	286.2	1.45	15.96	(Delpeux *et al.*, 1998)
C=O	287.6	1.46	7.82	(Delpeux *et al.*, 1998)
carboxyl groups	289.1	1.46	5.46	(Gelius *et al.*, 1970; Buchwalter and Czornyj, 1990)
carbonate functional group	290.5	1.45	4.44	(Gardner *et al.*, 1995)
pi to pi* transition	291.9	1.46	3.36	(Gardella *et al.*, 1986; Doren *et al.*, 1994; Brena *et al.*, 2004)

TEM of CMK-8

The TEM micrograph of CMK-8 carbon (**Figure 4-6**) shows its ordered mesoporous structure. Figure 4.6a shows the pores as seen from the top with a pore size of ca 6nm. The narrow PSD and high degree of order is evident. Figure 4.6b gives a lateral view, showing uniformly arranged mesochannels. Such uniformly arranged channels are known to enhance mass transfer both of substrates and products within highly ordered mesoporous catalysts. This contributes to an overall better catalytic performance vis a vis porous but not highly ordered catalysts.

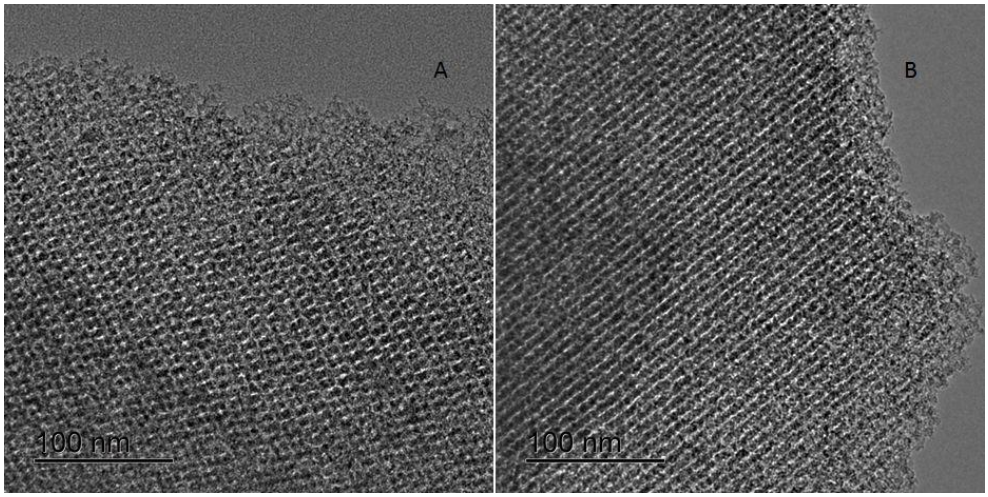

Figure 4-6 TEM micrographs of CMK-8

4.3 Electrochemical Analysis

4.3.1 **NDAB Carbon Catalysts**

The electrochemical analyses of the NDAB catalysts were performed using linear sweep voltammetry in combination with a rotating ring disc electrode (RRDE). This result is often presented in the form of plots of disc (and ring) currents versus voltage (Ag/AgCl). A typical plot is that of the NDAB-900 catalyst which was synthesized at a pyrolysis temperatures of 900 ^{o}C (**Figure 4-7**).

It is pertinent to know that during oxygen reduction reactions, electrons are consumed on a whole number, stoichiometric basis at the electrode. Hence the rate of reaction rate is exactly mirrored by the flow of electrons; the two being directly proportional (Faulkner, 1983)

The following regions can be observed on the plot

a) A region where the charge transfer kinetics is rate limiting. This region starts at the onset potential which here is -0.09 V (Ag/AgCl). Here the rate at which the reactant is being transferred from the bulk as a result of rotation is faster than the rate at which they are reacting at the electrode. Hence the intrinsic rate determines the overall reaction rate. The catalysts being the same (this plot is for the same catalysts i.e. NDAB-900 at different rotation rates) all have the same reaction rate and the lines coincide.

b) The second region is where the charge transfer rate begins to increase as the voltage becomes more negative. The rate of reaction rate competes with the rate of mass transfer and a region where both are limiting is observed. For the slower sweeps, the charge transfer rate quickly surpasses the rate at which the reactant is reaching the surface of the catalysts, making mass transfer rate limiting much earlier on. For the faster rotation rates, because of the more rapid sweep rates, the charge transfer rate does not catch up with the mass transfer rate early on, hence it continues to increase until such a point where it eventually surpasses the mass transfer rate; henceforth, the mass transfer rate becomes limiting and the curve hits a plateau.

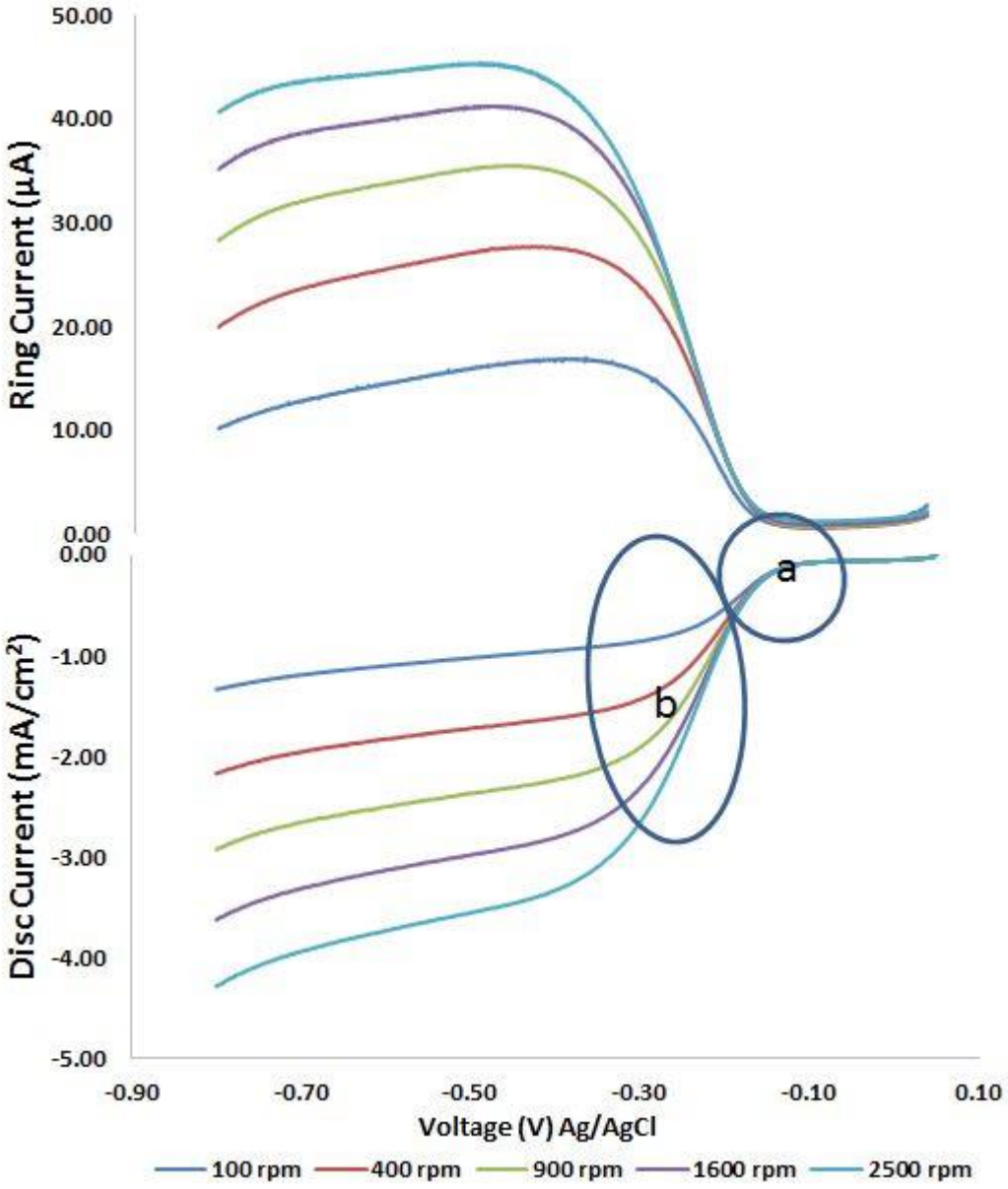

Figure 4-7 Disc and ring current plots for NDAB-900 in 0.1 M KOH from a scan rate of 5 mV/s and a ring potential of 0.35 V; pH 13 and RT

c) The third region is where the reaction is strictly limited by mass transfer and the polarisation plot forms a plateau. The fact that the plateau is inclined rather than flat could be an indication of low intrinsic rate (Jiang and Anson, 1991). It may also mean a change in the number of electrons for the ORR with potential in this region.

The theoretical background to this can be seen from the hydrodynamics of the rotating disc electrode. As the sweep rate increases, the diffusion layer

separating the surface of the electrode from the bulk solution becomes thinner, thus enhancing the rate of mass transfer to the electrode surface. The faster the sweep rate, the thinner the diffusion layer, the faster the mass transfer and longer it takes for the charge transfer rate to catch up.

Nitrogen doped carbon obtained by using o-phenylenediamine in a mesoporous silica template NDAB, was prepared at three different pyrolysis temperatures (700^{o}C, 800^{o}C and 900^{o}C). The investigation carried out helped to examine the relationship between ORR activity and pyrolysis temperature, total nitrogen content, nitrogen functional groups, oxygen functional groups and structural properties. **Figure 4-8** shows the disc and ring currents, number of electrons and Tafel slopes obtained from the electrochemical analysis. The variation of activity, specifically the activation controlled current, with physico-chemical properties is depicted in **Figure 4-9**.

Due to the low sweep rate of 5 mV/s, capacitive currents are not expected to have a significant impact on the polarisation plots (Gasteiger *et al.*, 2005).

The charge transfer region of the disc current plainly shows that the NDAB catalyst pyrolyzed at 900 ^{o}C has a better onset potential (-0.09V) and by inference superior catalytic activity. From visual inspection, the diffusion limited region is inclined. This is characteristic of most carbon based non-platinum group metal catalysts (Subramanian *et al.*, 2006; Liu *et al.*, 2007). From the concepts explained earlier, a likely reason is low ORR activity. As a result, when the voltage is being polarised in the negative direction, the rate of the charge transfer does not become large enough to surpass the mass transfer rate. Hence mass transfer does not becoming limiting and the flat plateau that characterizes it is not seen.

The ring current shown in the upper part of **Figure 4-8**a should be directly proportional to the amount of hydrogen peroxide generated by the catalysts. The amount of peroxide produced increases with the disc current, i.e. the catalysts with the higher disc current also have a higher ring current (this changes for NDAB-900 beyond -0.40 V (Ag/AgCl)). However, this is not sufficient to obliterate

the superior overall performance of NDAB-900 as captured in the plot of n-numbers, **Figure 4-8**b which shows the number of electrons transferred. This was calculated from the disc and ring currents (Equation 3.8) and ranges from approx. 3 – 3.4 within both the low and high polarization areas. Thus indicating that a mixed 2 and 4 electron mechanism is being followed. The values are in close agreement with those obtained using the Koutecky-Levich equation which ranges from 2.54 – 2.94.

Tafel slopes were obtained from the charge transfer region of the plots $-0.25 \leq V \geq -0.15$. Because the polarization plots did not exhibit a well-defined limiting current plateau, the value of the current at -0.8 V vs Ag/AgCl was used. The slopes are 86 mV/dec, 101 mV/dec and 103 mV/dec for NDAB-900, NDAB-800 and NDAB-700 respectively.

The history of Tafel slopes not falling within well-defined values of 60 mV/dec or 120 mV/dec started with Tafel. He obtained a slope of 107 mV/dec which was a departure from the expected value of 118 mV/dec. This he assumed to be a result of experimental errors or temperature variation. When the physical significance of ß, the symmetry factor was discovered, it was realised that the slopes are likely to vary when ß is not 0.5 (Conway *et al.*, 1989; Gabe, 2005). In line with this, the Tafel slopes of 101 mV/dec and 103 mV/dec obtained here can be said to indicate a slow first electron transfer step being rate determining. Other workers have also obtained Tafel slopes which cannot be readily classed in the well-defined range of 60 and 120 mV/dec. Tammeveski et al (1999) working with Pt–TiO_2 in alkaline solution obtained a Tafel slope of 80 mV/dec within the first Tafel region. In the second region, they obtained Tafel slopes from -260 to -490 mV/dec. The slopes were observed to increase with Pt film thickness. Also Banham and co-workers (2009) in a well-designed experiment, varied catalyst layer properties in order to see the effect on Tafel slopes. They increased the pore length, decreased the pore diameter and increased the catalyst layer resistance of 5 – 40 wt% Pt.

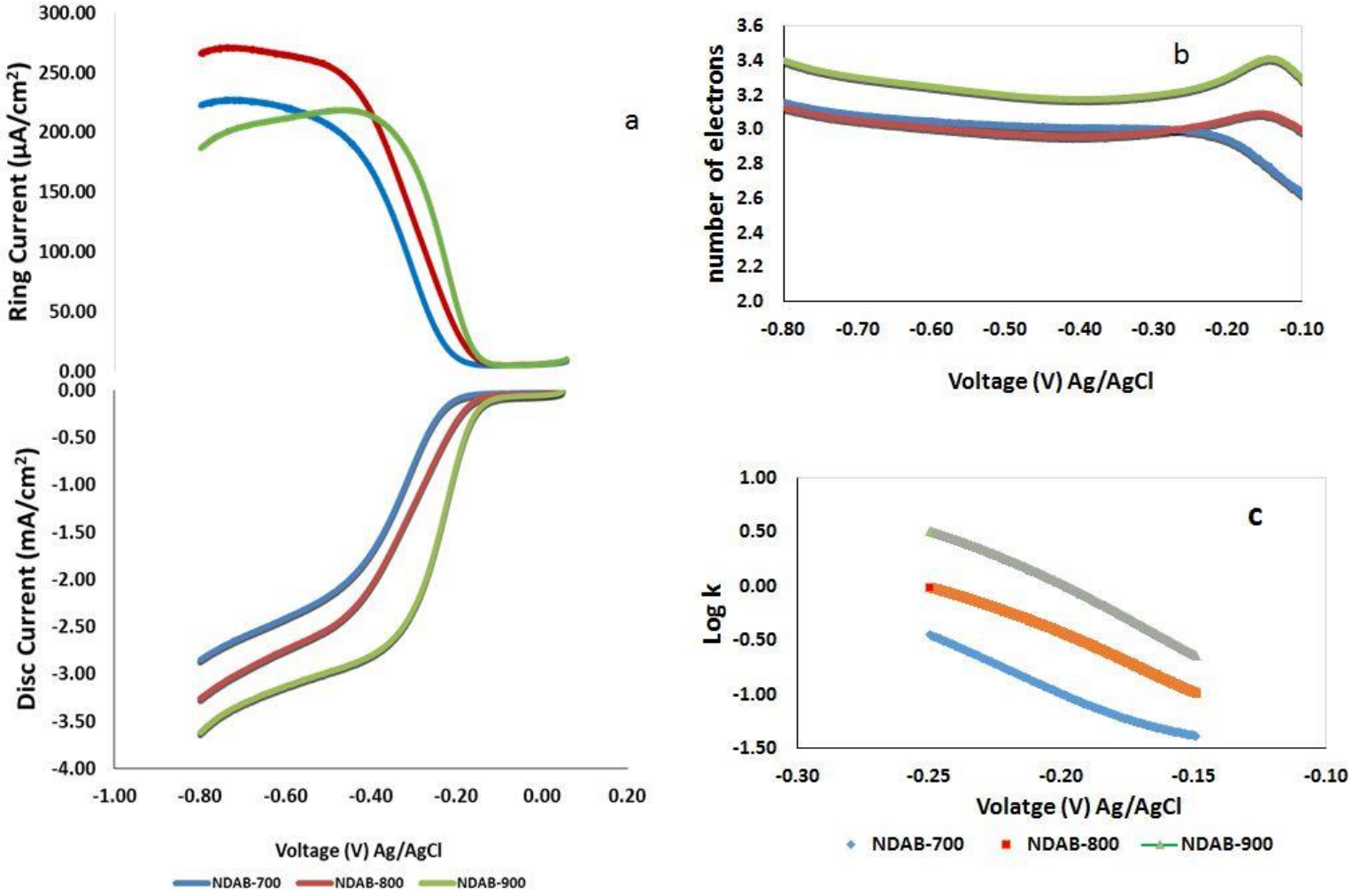

Figure 4-8 Electrochemical analysis of NDAB catalysts in 0.1 M KOH. a) Disc and ring currents at 1600 rpm and 5 mV/s b) number of electrons transferred and c) Tafel plots; all performed at pH 13 and RT

Typical Tafel slopes obtained in the work include 77±3, 84±3 and 97±3 mV/dec which were larger compared with the mechanistically expected values.

One other reason why the Tafel slopes do not fall into the defined regions may be because of the ill-defined limiting currents (Ye and Vijh, 2005).

Figure 4-9 captures how the physico-chemical properties vary with kinetic current. In **Figure 4-9**a, the total amount of nitrogen and atomic percentage of pyridinic nitrogen are observed to decrease as temperature of pyrolysis is increased from 700 ^{o}C to 900 ^{o}C.

Conversely, the atomic percentage of graphitic nitrogen present within the catalysts increases with increasing pyrolysis temperature showing a similar trend with the amount of nitrogen oxides present.

In Figure 4.9b, NDAB-700 displayed a slightly higher amount of total oxygen content and atomic percent of carbonyl functional group compared with NDAB-800. However, a significant decline in both properties is seen as the pyrolysis temperature is increased to 900 ^{o}C. For reasons not immediately clear, the surface area of the nitrogen doped carbons increases very significantly as pyrolysis temperature goes from 700 ^{o}Cto 900 ^{o}C. This is shown in **Figure 4-9**c. The trend in the I_D/I_G ratio which captures the relative amounts of disordered and graphitic carbon can be seen in **Figure 4-9**d. It reduces with increasing pyrolysis temperature.

From **Figure 4-9**a, kinetic current increases with the amount of graphitic nitrogen present albeit not at the same rate. Conversely, it increases even as the amount of pyridinic nitrogen is decreasing. Much has been said about which of pyridinic or graphitic (quaternary) nitrogen actually influences oxygen reduction (Liu *et al.*, 2010b; Wang *et al.*, 2010).

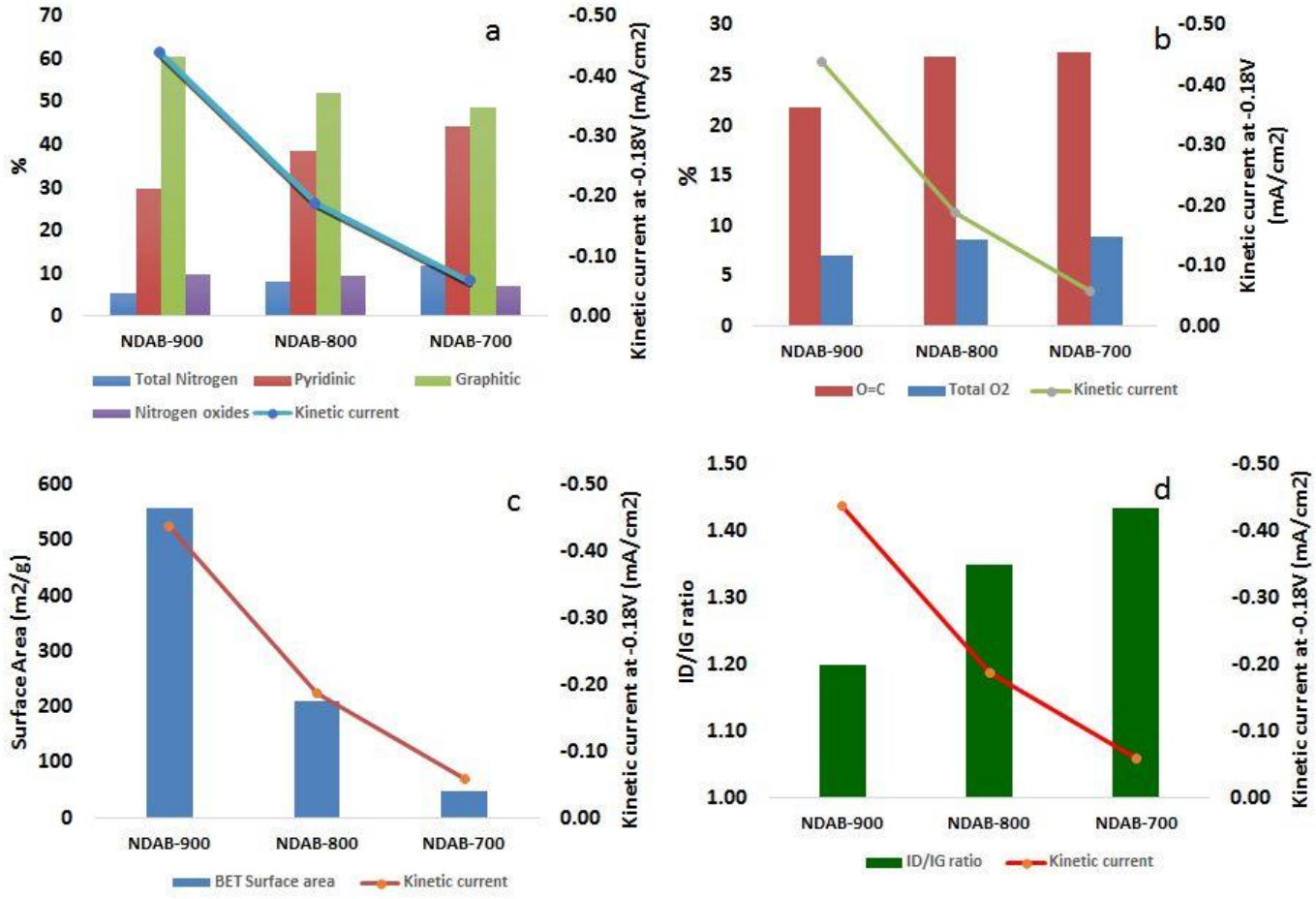

Figure 4-9 Variations in activity of NDAB catalysts with a) nitrogen and nitrogen functional groups, b) Oxygen and the carbonyl functional group, c) BET surface area and d) I_D/I_G ratio from Raman analysis

Based on the results here it is observed that quaternary nitrogen content increases with increasing activity while the converse is true for pyridinic. Hence it can be concluded that ORR activity is dependent on quaternary nitrogen content. This agrees with explanations drawn from first principles (Dommele, 2008). It is known that the nitrogen oxides do not contribute to oxygen reduction.

Though carbon materials have been used as catalyst supports over many years, they also possess some measure of catalytic activity (Su *et al.*, 2013). Depending on the carbonization or pyrolysis temperature, carbon materials often contain different total amount and varied composition of surface oxygen functional groups. While some like the carboxylic group are inimical to ORR, others like the carbonyl group enhance it (Gilbertson *et al.*, 2014; Wu *et al.*, 2014). This has been ascribed to their electron donating potential (Montes-Morán *et al.*, 2004). The total amount of oxygen reduces with increasing temperature. The percentage of carbonyl groups seems to be equal for NDAB-800 and NDAB-700 while it reduces in NDAB-900. This is not unexpected. Oxygen functional groups are known to break down easily as pyrolysis temperature increases. The order of their lability being carboxylic (ca 300 - 400^{o}C), hydroxides (ca 600 – 700 ^{o}C) and carbonyl (ca 700 - 900 ^{o}C) (Figueiredo *et al.*, 1999; Szymański *et al.*, 2002). Hence the results obtained are in line with literature values. It is interesting to note that the higher carbonyl content of NDAB-700 and NDAB-800 in **Figure 4-9**b was not sufficient to change the trend of catalytic activity. Hence it can be concluded that carbonyl functional groups in themselves are not critical factors in determining the ORR.

Catalysis is a surface phenomenon, hence the third parameter considered was BET surface area shown in **Figure 4-9**c. This increased very appreciably as pyrolysis temperature changed from 700 ^{o}C to 800 ^{o}C and then to 900 ^{o}C. Considering the relationship between the trend of changing surface area and that of ORR activity it can be safely said that within this context, the former plays a critical role in determining ORR activity. Wang

et al (2015b) in their work with nitrogen doped CNTs also showed that the ORR activity improved in direct proportion to the BET surface area.

Two key parameters obtained from Raman analysis are the intensity of the D-band (I_D) and the intensity of the G-band (I_G). While the former indicates the amount of disorder present within the structure, the latter gives an indication of the extent of graphitization of the material. Disorder within a carbon structure may be due to the presence of nitrogen within it or the existence of edge site defects (Banks *et al.*, 2005). The I_D/I_G ratio indicates the relative amount of these two present in any material. Raman analysis was performed to better understand how the graphitic structure of the NDAB catalysts impact on their ORR activity. The spectra are presented in **Figure 4-10**. The results are better appreciated when it is understood that there are two separate processes occurring with nitrogen doping. On the one hand, an extra electron is being introduced into the π system and on the other there is an accompanying disorder within the lattice of the graphite. Two bands are typical of the spectra of carbon based materials. First is the D or disorder band that appears at ca 1350 cm^{-1}. This indicates the presence of disorders and/or defects within the graphitic structure. The other band is known as the G or graphitic band which characterizes ordered graphitic carbon and appears at ca 1600 cm^{-1} (Dresselhaus *et al.*, 2005). Hence the ratio of the intensities of these bands referred to as the I_D/I_G gives an indication of the relative amount of graphitic order or crystallinity present or conversely the relative amount of defects and disorders existing within the structure.

In **Figure 4-9**d the I_D/I_G ratio decreases from 1.44 to 1.35 to 1.2 corresponding with NDAB-700, NDAB-800 and NDAB-900 respectively. This is not surprising given that the total amount of nitrogen also reduces in the same direction. The presence of nitrogen introduces disorder; the smaller the amount, the lesser the expected intensity of the D-band. How does this affect the ORR activity? It was noted with the XPS analysis that the total amount of nitrogen does not have a direct impact on activity. This is confirmed here.

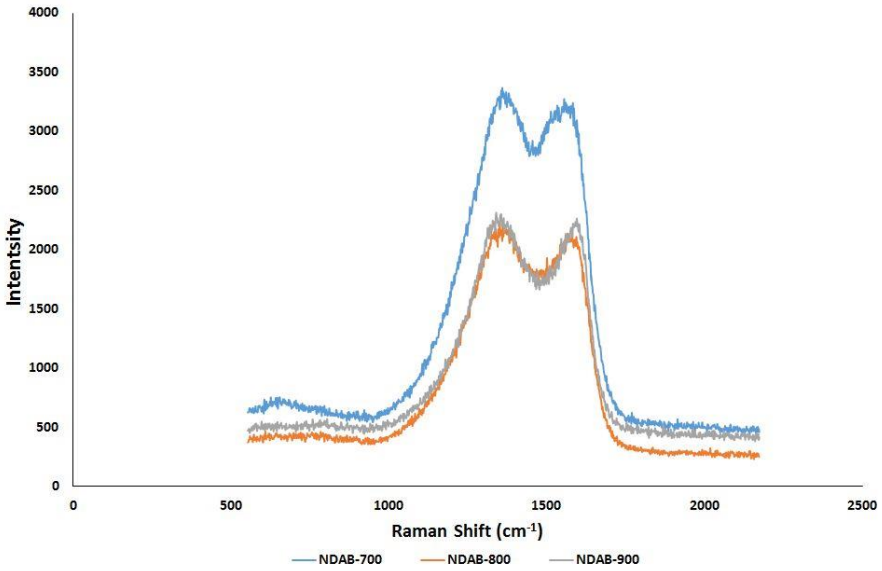

Figure 4-10 Raman spectra of NDAB 700, 800 and 900

A school of thought worth considering on this issue is that of Compton (Banks *et al.*, 2005). They argued that edge plane sites contribute significantly to catalytic activity in carbon materials. Edge planes, if abundant, would produce a high intensity of the defect band and a concomitant comparatively higher I_D/I_G ratio. If indeed they contribute to ORR, I_D/I_G ratio would increase with activity. This is not the case here. Hence it can be concluded that edge plane sites do not contribute to ORR in this scheme. A plausible inference from **Figure 4-9**d is that as the order of the graphitic structure increases, activity also increases.

A summary of the most important parameters for the NDAB prepared at different temperatures is presented in **Table 4-7**. Pragmatically, direct electrocatalytic parameters can be compared by two methods viz, a) comparing the value of the currents at a particular voltage given that for all the electrocatalysts in question this voltage falls within the kinetic region. b) comparing the onset potential. This ideally should be the voltage at which the departure from zero current is visually distinct (Gasteiger *et al.*, 2005; Thorum *et al.*, 2009). In some instances it might be possible to apply both.

Table 4-7 Summary of activity parameters for NDAB carbon catalysts

Catalysts	E_{onset}/V vs Ag/AgCl	Kinetic current at -0.18V (mA cm^{-2})	i_k/mA cm^{-2} Activation controlled current at infinite rotation -0.40 V	N-number (ring & disc) at -0.18 V	N-number (Koutecky-Levich) at -0.40 V	% peroxide	b(V dec^{-1})
NDAB-900	-0.09	-0.44	10.7	3.4	2.94	29	86
NDAB-800	-0.13	-0.19	4.64	3.1	2.82	46	101
NDAB-700	-0.19	-0.06	3.26	2.9	2.54	61	103

The onset potential in this context is defined as the voltage when the current gets to -80 μA; a visually distinct region on all the plots. It is evident that NDAB-900 showed the best ORR activity having the highest onset at -0.09 V.

4.3.2 **DNOMC carbon catalysts**

Because of the expensive materials or complicated procedures involved, most of the new methods for developing non PGM catalysts might best be described as pyrrhic**.** Hence the facile synthesis procedure for the Direct Nitrogen Doped Ordered Mesoporous Carbon (DNOMC) catalysts. The synthesis is unique because it does not require the use of ordered mesoporous silica as hard template. Hence it excludes the procedure and materials for synthesizing ordered mesoporous silica. Rather it uses Pluronic F127, a surfactant, as soft-template. This helps to guide the formation of the nitrogen doped mesoporous carbon. The results of the ORR activity of DNOMC catalysts in 0.1 M KOH are displayed in **Figure 4-11** and how their activity relates with physico-chemical properties in **Figure 4-12**.

In **Figure 4-11**a, the charge transfer controlled region shows that DNOMC-700 is the least active while DNOMC-800 and 900 have the same onset potential and likely the same activity.

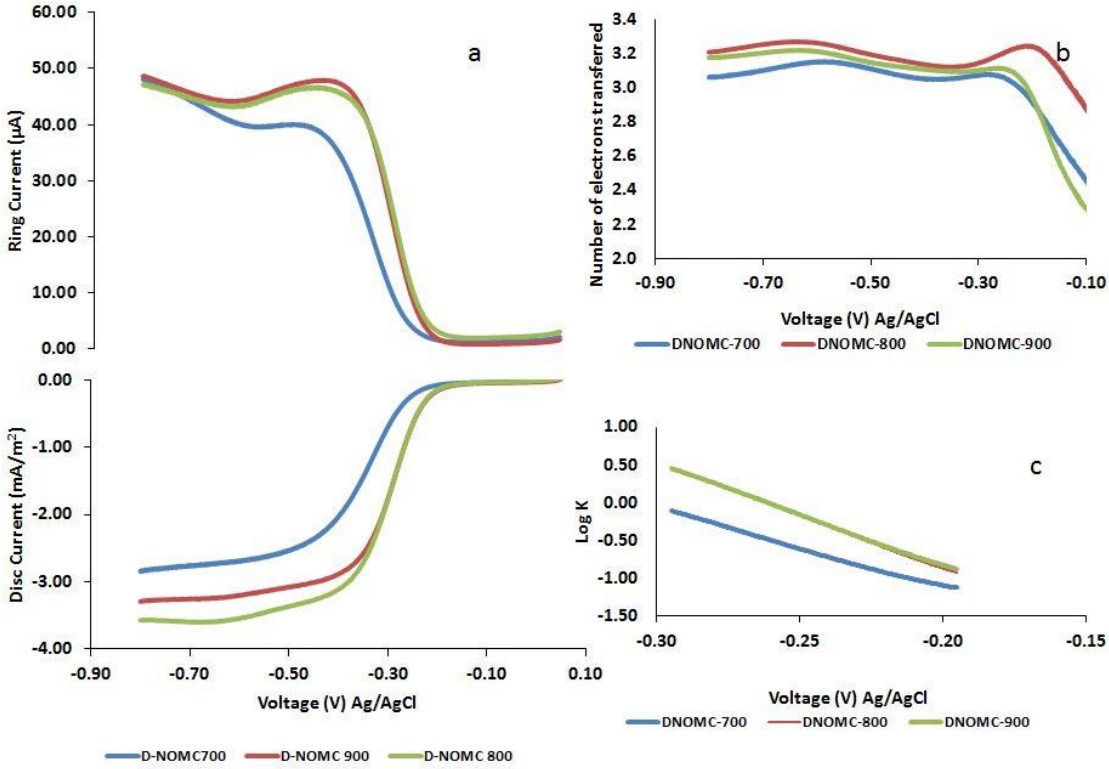

Figure 4-11 Electrochemical analysis of DNOMC catalysts in 0.1 M KOH. a) Disc and ring currents at 1600 rpm b) number of electrons transferred and c) Tafel plots; all performed at pH 13 and RT

This trend continues into the combined mass transfer and charge transfer controlled region. It is interesting to note that the three DNOMC catalysts tend to have a flat plateau within the mass transfer controlled region. This is rare among carbon based catalysts and is a pointer to a relatively good activity.

The same trend is repeated in the upper half Figure 4-11 , where the ring current (directly proportional to amount of H_2O_2) is shown. At approx. -0.6 V, the plots for the three catalysts exhibit an upward swing indicating a marked increase in the amount of H_2O_2 being produced.

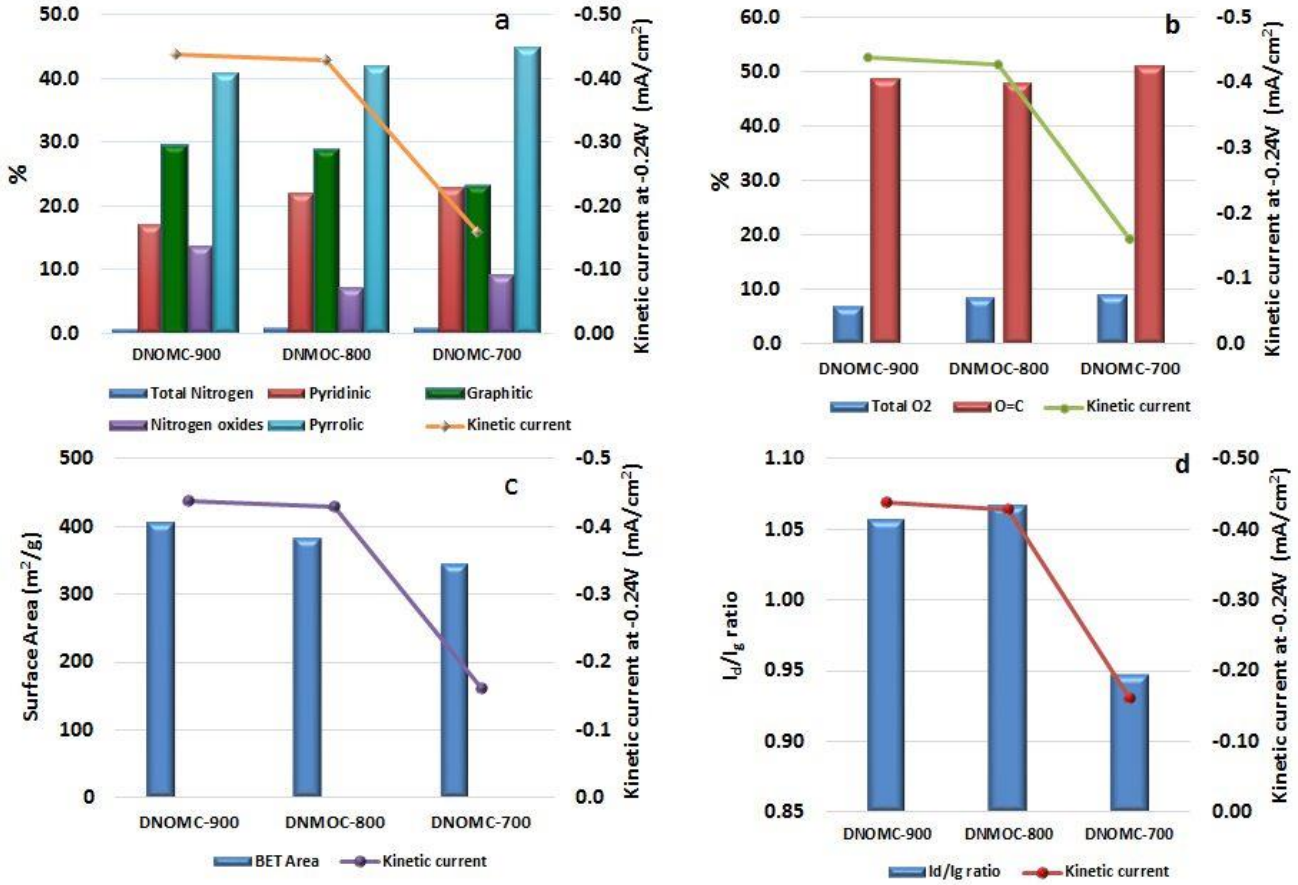

Figure 4-12 Variations in activity of DNOMC catalysts with a) nitrogen and nitrogen functional groups, b) Oxygen and the carbonyl functional group, c) BET surface area and d) ID/IG ratio from Raman analysis

A look at a possible mechanism would help to adduce a reason for this.

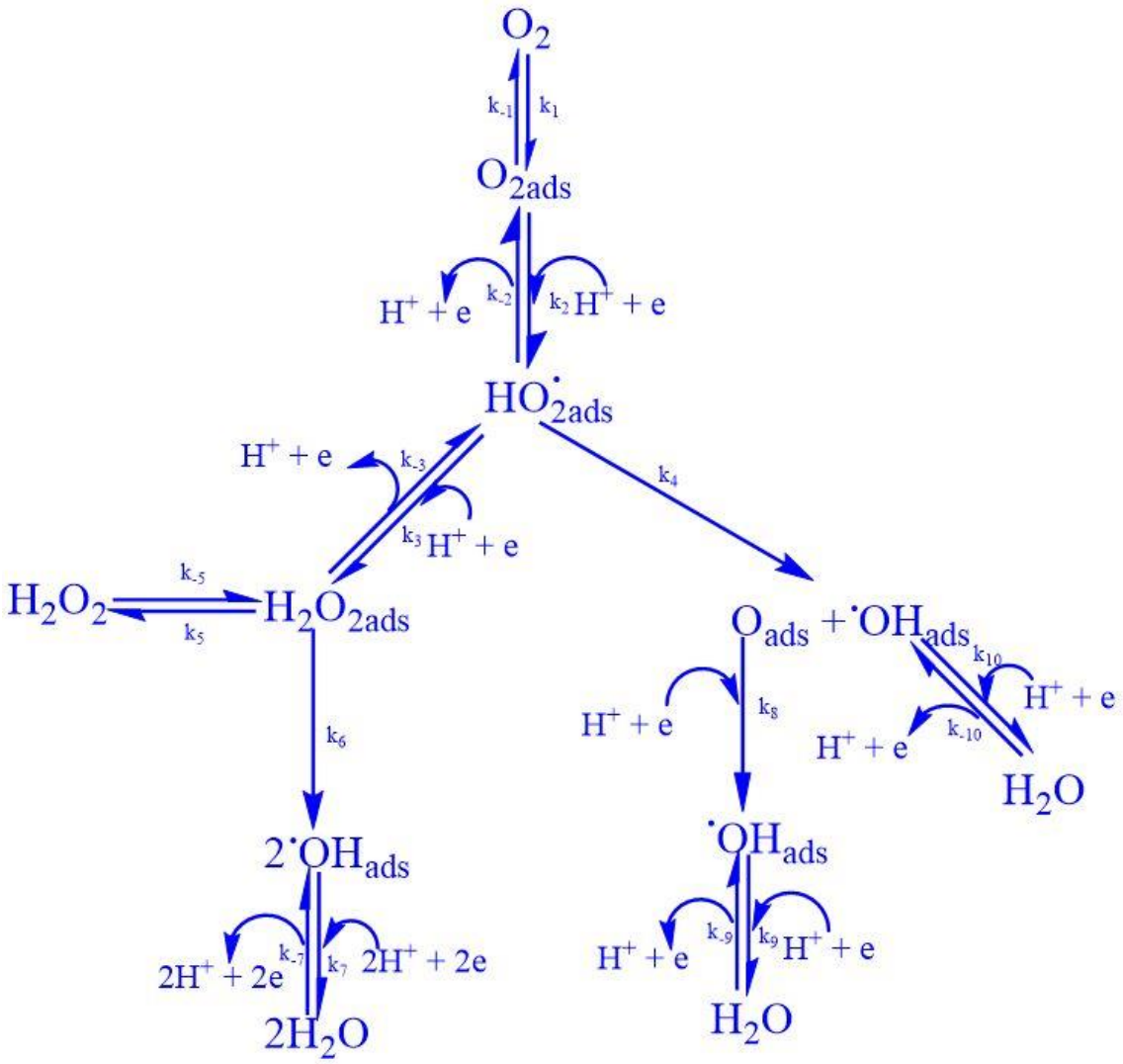

Figure 4-13 Possible mechanism for oxygen reduction (Ruvinskiy *et al.*, 2011)

Figure 4-13 shows the different pathway that could be followed for ORR. The path on the left (circled) would be more common for ORR on carbon based catalysts. In the case of DNOMC catalysts, as the voltage became more negative, it is likely that the amount of H_2O_2 increased greatly such that its previous rate of dissociation through path k_6 could not meet up and the excess was desorbed into the solution. This resulted in the increased ring current.

The variation of the number of electrons transferred, (also known as n-number) with increasing voltage is shown in **Figure 4-11**b. From the

voltage that corresponds to their onset potential, the catalysts have an n-number of approx. 3-3.2. This also confirms a combined 2 and 4 electron pathway, probably with the 2-electron pathway being dominant.

The current values used for the Tafel slopes were obtained from the charge transfer limiting region. The slopes are 73 and 95 mV/dec for DNOMC-900 (same as DNOMC-800) and DNOMC-700 respectively. Similar to what was obtained for the NDAB catalysts, this also does not fall within the well-defined values and would indicate a mixed mechanism for the rate determining step.

For nitrogen doped catalyst such as the DNOMC range, it is expected that the primary agent of oxygen reduction would be the nitrogen functional groups embedded within the carbon structure. **Figure 4-12**a displays the various percentages of nitrogen functional groups present and how they vary with the kinetic current at -0.24 V. The percentage of total nitrogen content in the catalysts is quite small with values of 0.62 for DNOMC-900 and 0.78 for DNOMC-700 and 800. The key nitrogen functional group responsible for ORR has been identified as the graphitic or substitutionary one (Niwa *et al.*, 2011). The percentage of graphitic nitrogen present in each sample increases as the pyrolysis temperature increases going from 23.04 % for DNOMC-700 to 28.8 % and 29.3 % for DNOMC-800 and 900 respectively. The activity also follows a similar trend leading to the conclusion that this factor indeed contributes to ORR activity. Another component known to influence ORR reaction is the carbonyl functional group. **Figure 4-12**b shows the variations in total oxygen and percentage carbonyl content with each catalyst. Carbonyl groups generally begin to decompose around 700 ^{o}C. Hence it is not surprising that DNOMC-700 has the highest percentage of carbonyl groups. But there does not seem to be a correlation between this and the ORR activity. Consequently it can be said that this is not a decisive factor in the determination of activity in DNOMC's.

The surface areas of each catalyst is depicted in **Figure 4-12**c. As these increase with temperature, the activity also increases, hence it can be

suggested that the surface area plays a key role in the determination of ORR activity.

Lastly is the nature of defect or disorder as well as the graphitic order within the materials synthesized. Aptly captured in the Id/Ig ratio derived from Raman analysis in **Figure 4-12**d. The Id/Ig ratios are 0.95, 1.07 and 1.06 for DNOMC-700, 800 and 900 respectively. Thus activity intensifies with the degree of graphitic order. The importance of the sp2 carbon network for oxygen reduction was emphasized by the work of Niwa *et al.*(2011). Considering that the Id/Ig ratio only increased by ca 10 % and the activity by ca 50 % it must be noted that this factor works with other parameters like the graphitic nitrogen content and the total surface area to determine the overall activity of each DNOMC catalyst.

A summary of the activity parameters of the DNOMC catalysts is given in **Table 4-8**. The n-values obtained are in agreement with what was calculated using the Koutecky-Levich equation.

Table 4-8 Summary of activity parameters for DNOMC carbon catalysts

Catalysts	E_{onset}/V vs Ag/AgCl	Kinetic current at -0.22V (mA cm^{-2})	i_k/mA cm^{-2} Activation controlled current at infinite rotation -0.40 V	Number of electrons at -0.22 V	Number of electrons at -0.40 V (Koutecky Levich)	% peroxide	b (V dec^{-1}
DNOMC-900	-0.16	-0.25	11.7	3.0	2.9	45	72.7
DNOMC-800	-0.17	-0.23	13.19	3.2	3.0	43	72.7
DNOMC-700	-0.20	-0.10	4.72	3.0	2.6	47	94.46

4.3.3 **Methanol Tolerance of NDAB-900**

The good activity of platinum catalysts becomes a set-back in the presence of methanol. This is due to its ability to catalyse oxygen reduction and methanol oxidation, hence both are in competition for the active site. This results in a mixed potential which degrades the ORR potential (Yang *et al.*, 2005). NDAB-900 was tested in the presence of methanol and its activity compared with that of 20 wt% Pt. **Figure 4-14**a and b show the LSV of 20

wt% Pt and NDAB-900 respectively in the presence of increasing concentrations of methanol. The onset potential of ORR on platinum is observed to shift towards more negative values. In addition, an oxidation hump is seen that gets bigger with increasing methanol concentration. This can be explained by the fact that in the competition for the active site, the increasing concentration of methanol upturns the contest in their favour. This results in the intensifying of the oxidation peak. On the contrary, the plot for NDAB-900 remains very consistent even with increasing amounts of methanol.

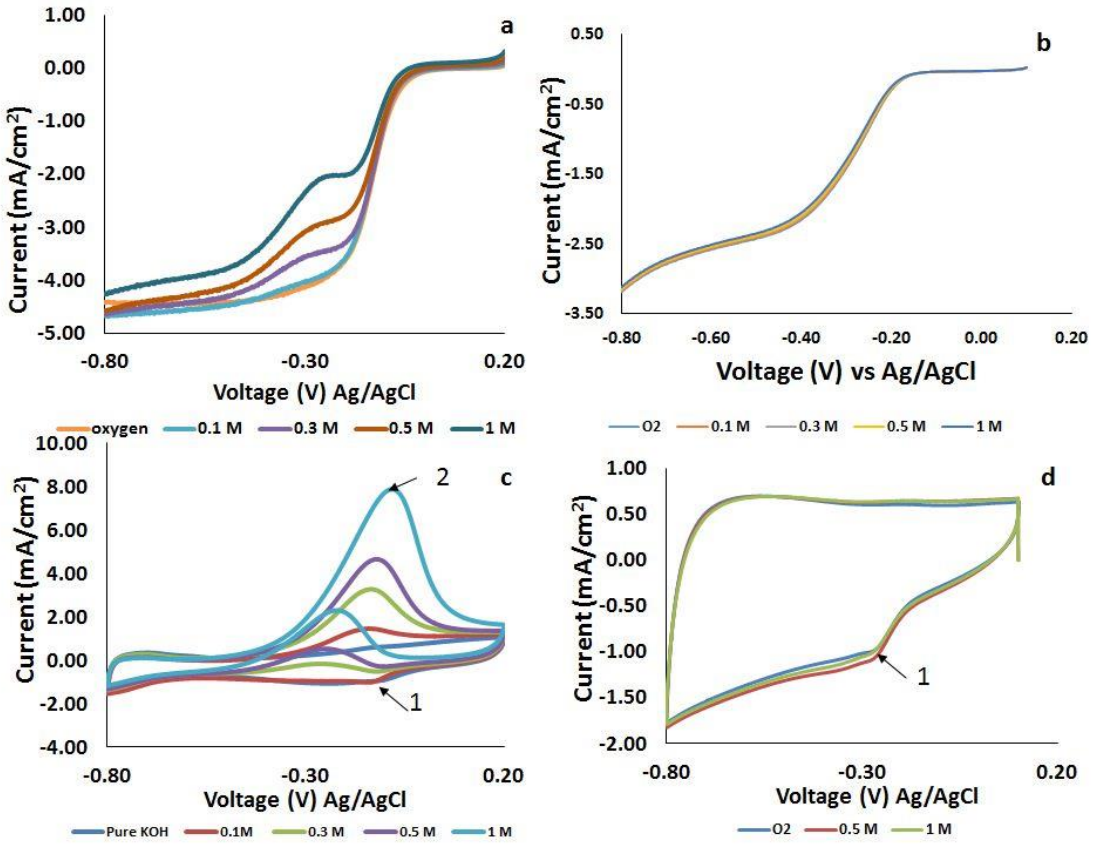

Figure 4-14 Methanol tolerance of NDAB-900 and 20 wt%Pt; a and b at RDE 1600 rpm and 5 mV/s for 20 wt%Pt and NDAB-900 respectively; c and d CV 100 mV/s for 20 wt%Pt and NDAB-900 respectively. 1-oxygen reduction peak; 2-methanol oxidation peak; all performed at RT

A similar trend is observed with the cyclic voltammograms in **Figure 4-14**c and d. The conclusion is that the active sites of NDAB-900 are not capable of

oxidizing methanol. Hence they would be ideal for ORR that would involve methanol cross-over.

4.3.4 **Stability**

The stability of NDAB-900 and DNOMC-900 were tested with chronoamperometry. **Figure 4-15** presents the results obtained. The two catalysts experienced a gradual decline in activity over time. NDAB-900 retained ca 88% of the initial activity while DNOMC-900 retained ca 90% after two hours.

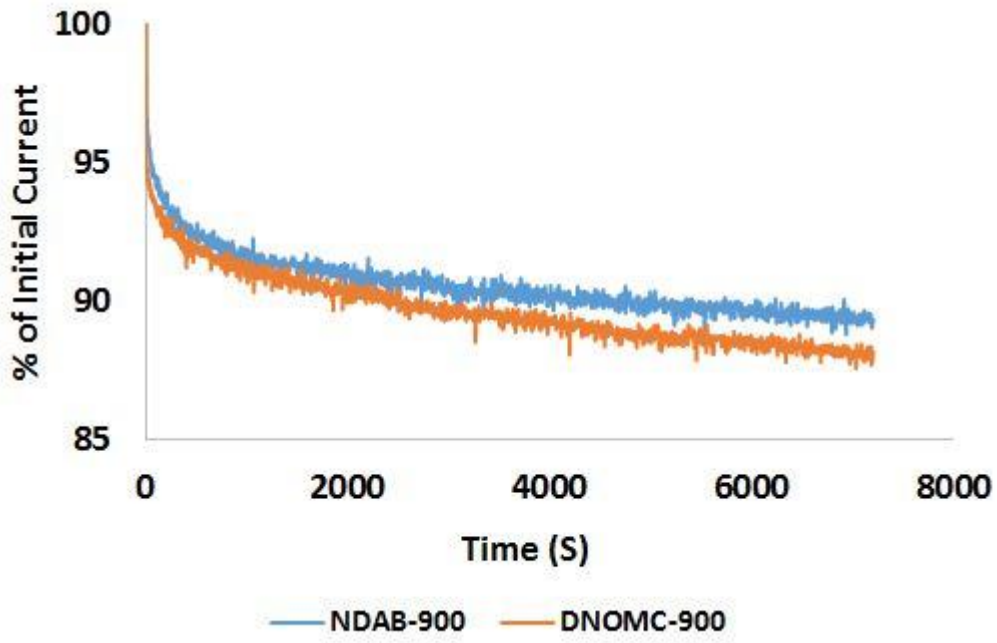

Figure 4-15 Chronoamperometry plots for NDAB-900 and DNOMC-900 at a rotation rate of 900 rpm while bubbling with a small quantity of oxygen; carried out at pH 13 and RT

The two catalysts showed a good stability. This can be ascribed to the fact that the nature of their active sites makes them less susceptible to carbon corrosion and degradation mechanisms that plague platinum/carbon.

4.4 Comparison of Electrochemical Properties of NDAB-900, DNOMC-800, CMK-8 AND Vulcan XC-72

For completeness, the activity of the best in the class of NDAB and DNOMC were compared with ordered mesoporous carbon (CMK-8) made from the

same template (KIT-6 mesoporous silica) but without any form of nitrogen doping. Another useful comparison was with commercial Vulcan XC-72 that was neither ordered nor nitrogen doped. These are shown in **Figure 4-16**.

Table 4-9 sets out the important electrochemical parameters that characterize the four carbon based catalysts being compared.

The onset potential is taken to be the voltage when ORR current gets to -80 μA. Surprisingly, NDAB-900 and CMK-8 had very similar values. The order of superiority was NDAB-900>CMK-8>DNOMC-800>Vulcan XC-72.

The number of electrons transferred at -0.25V were also compared. These was determined from the disc and ring currents of the rotating-ring-disc electrode. Here all the catalysts had a similar value of 3.2 with the exception of Vulcan-XC72 that had 2.9. The tafel slopes were also calculated by fitting the Tafel equation to a portion on the kinetic region of the catalysts. CMK-8 had the lowest with a value of 60 mV/dec implying that the rate determining step here was a chemical step following a fast one electron transfer. Vulcan carbon had the highest with 110 mV/dec an indicator that the first electron transfer step is probably rate determining here.

The activation controlled current density captures the actual value of the ORR current when there is no mass transfer limitation. It gives a good estimate of the inherent catalytic capability of any catalyst. Traditionally, it is determined from the intercept of the Koutecky-Levich at a particular voltage. However, due to the irregular trends of the i-V plots obtained from polarization in this experiment, the activation controlled current density obtained from Koutecky-Levich plots was misleading. Hence, a different approach was devised.

Considering Typical divisions on a polarization curve **Figure 4-17** (Gileadi and Gileadi, 2011). The first section is activation controlled. Here the rate of reaction is determined by the inherent kinetic activity of the catalyst. Curve **a** shows the likely path the current would have followed as the voltage is increased, if mass transport limitation does not set in.

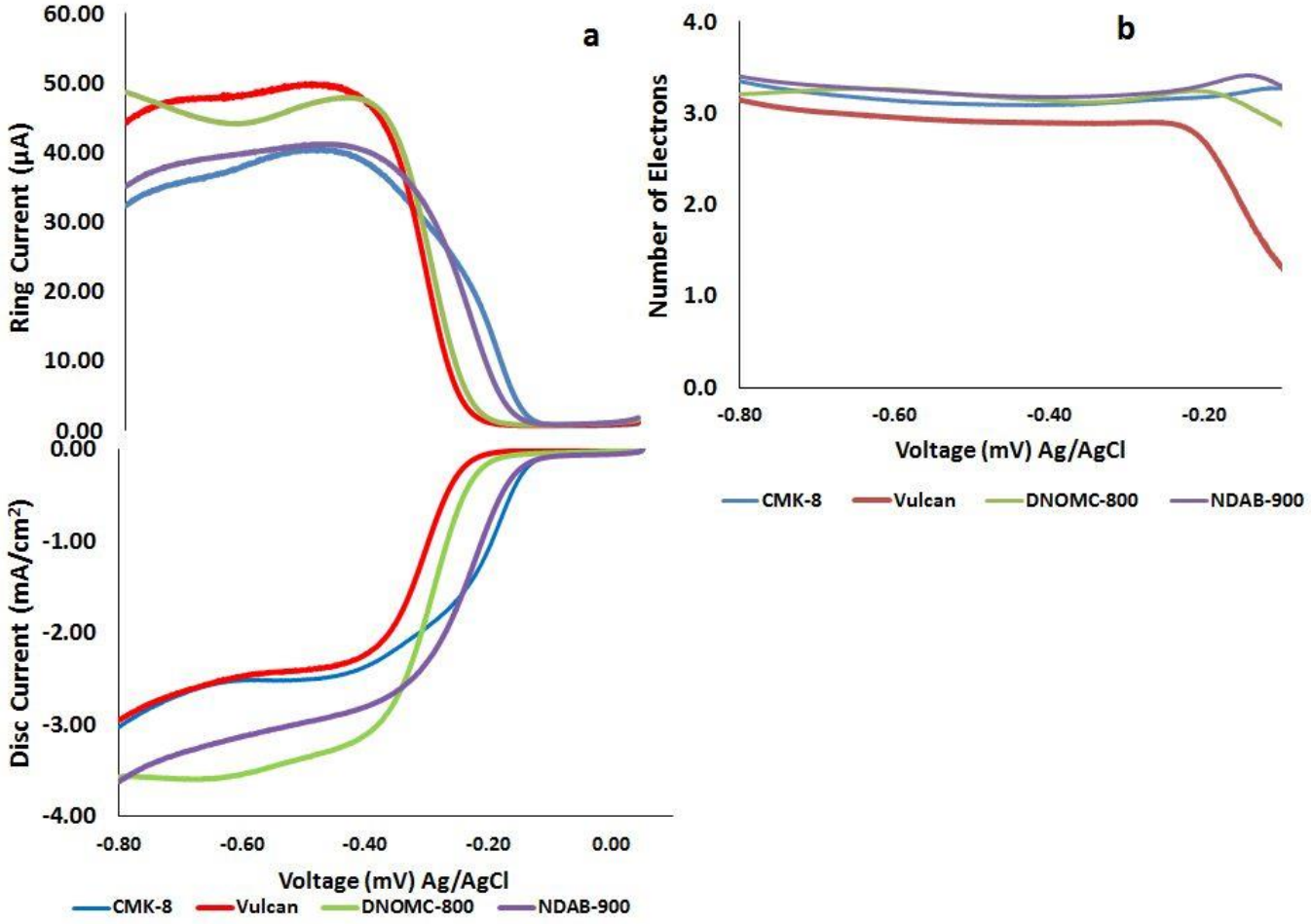

Figure 4-16 a) Disc and Ring Currents for NDAB-900, DNOMC-800, CMK-8 and Vulcan XC-72 in 0.1 M KOH at 1600 rpm and 5 mV/s; b) number of electrons transferred for each catalyst; all experiments were performed at pH 13 and RT

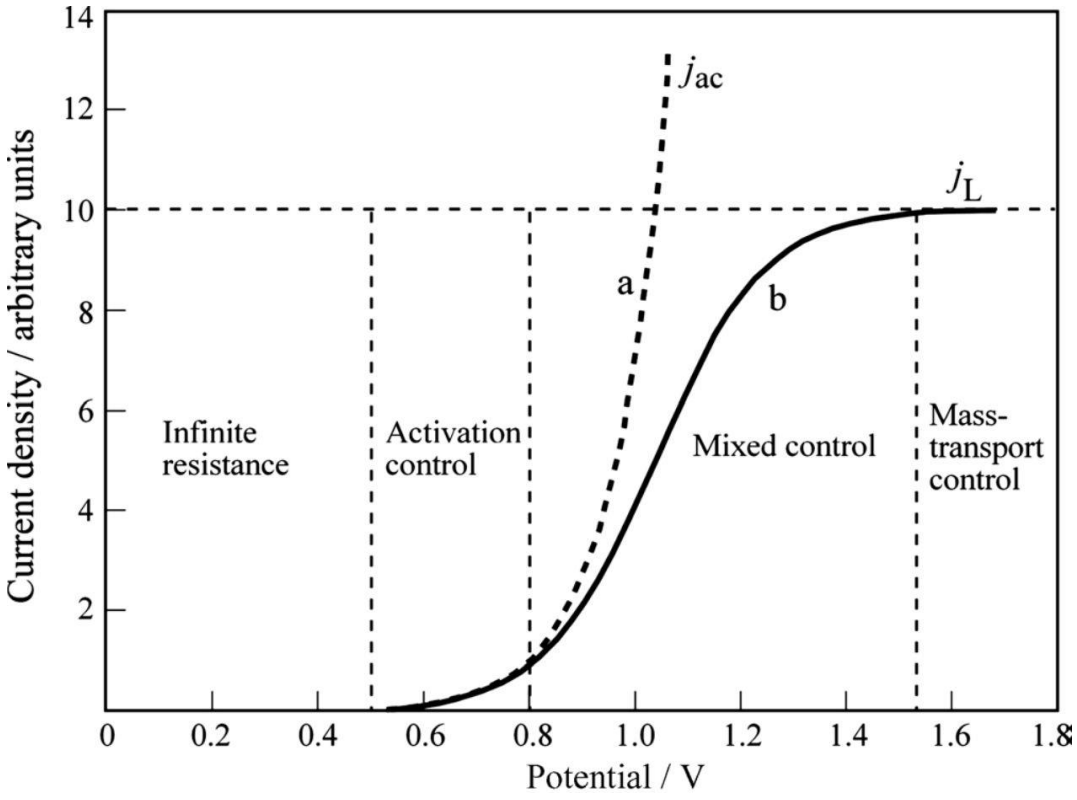

Figure 4-17 Typical divisions on a polarization curve

This mass transport free path can be predicted, if it was possible to develop a model that fits the activation controlled section. Using voltage as the independent variable, this can be extrapolated beyond the apparent activation controlled section. Hence the mass transport free current density can be determined at a given voltage. With aid of the MATLAB software, a model was developed to fit the activation controlled section of each of the catalyst. From this the activation controlled current was then determined at -0.25 V (a region that extends beyond the apparent activation controlled region).

Figure 4-18 shows a typical fitted plot for NDAB-900 MnO_2 20 wt% $KMnO_4$ with the model parameters. The model equation obtained and the constants are

$$i_k(x) = a * \exp(b * x) + c * \exp(d * x)$$

a= -0.01783; b = -28.25; c = -0.07893; d = 13.63 R^2 = 0.9997 and x is voltage

It is worth noting that the model equations obtained have two exponential terms. This has a resemblance with the Butler-Volmer equation which governs this region. Values obtained for each catalyst are stated in **Table 4-9**. Seeing that the activation controlled current is an intrinsic property, and that the values here are obtained using experimental data, this scan be said to be the best measure of the inherent capacity of any of the catalysts for ORR. Therefore the ORR activity of the catalysts compared here increase in the order Vulcan-XC72<DNOMC-800<NDAB-900<CMK-8.

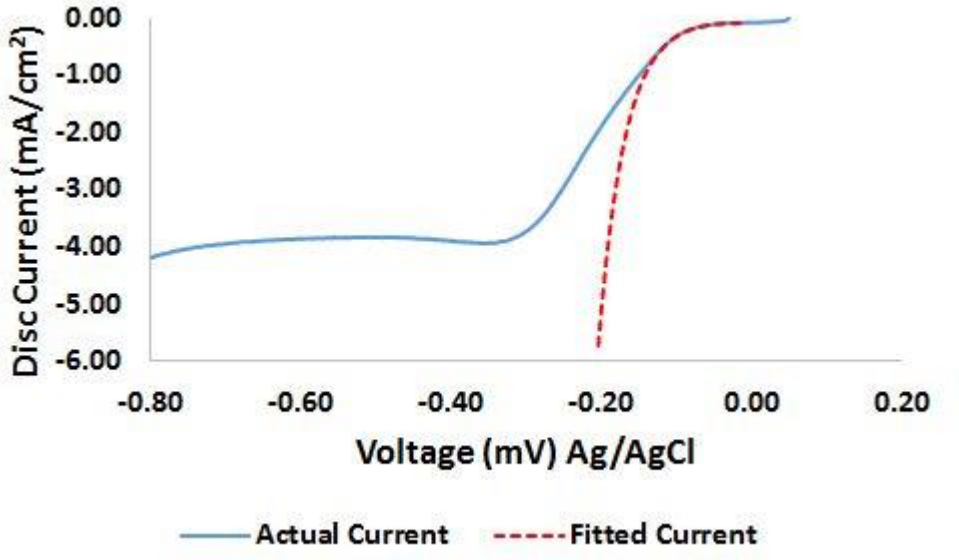

Figure 4-18 Fitted activation controlled current and actual Current for NDAB-900 MnO_2 20 wt% $KMnO_4$

Table 4-9 Electrochemical parameters that characterize NDAB-900, DNOMC-800, CMK-8 and Vulcan XC-72 as catalysts for ORR in 0.1 M KOH

Catalysts	E_{onset}/V vs Ag/AgCl	E_{onset}/V vs RHE	i_k/mA cm^{-2} Activation controlled current at -0.25V	Number of electrons at -0.25 V	b (V dec^{-1}
NDAB-900	-0.09	**0.93**	**-10.00**	3.2	86
DNOMC-800	-0.17	**0.85**	**-1.21**	3.2	73
CMK-8	-0.10	**0.92**	**-73.14**	3.2	61
Vulcan	-0.21	**0.81**	**-0.27**	2.9	110

Three factors that contribute to the activity of OMCs are a high concentration of edge plane defective sites, large amount of oxygen functional groups and high surface area (Ndamanisha and Guo, 2012)

According to Banks et al(2005) almost all the electron transfer and catalytic activity of graphitic carbon materials occurs at edge-plane like defect sites. Ordered mesoporous carbons are known to possess a significant amount of these (Inagaki *et al.*, 2013; Zhou *et al.*, 2014). The Id/Ig ratio obtained from Raman analysis also testifies to this. For CMK-8 it was 1.04 compared with Vulcan (which also consists of pure carbon) that had a value of 1.01. Carbonyl functional groups are known to play a significant role in ORR. **Figure 4-19** shows the carbonyl and oxygen composition for the carbon catalysts considered. CMK-8 had the highest total oxygen content and also a high carbonyl composition. Though the percentage of carbonyl in Vulcan is very high, it has a total oxygen of only 0.65%. Hence the carbonyl content pales into insignificance.

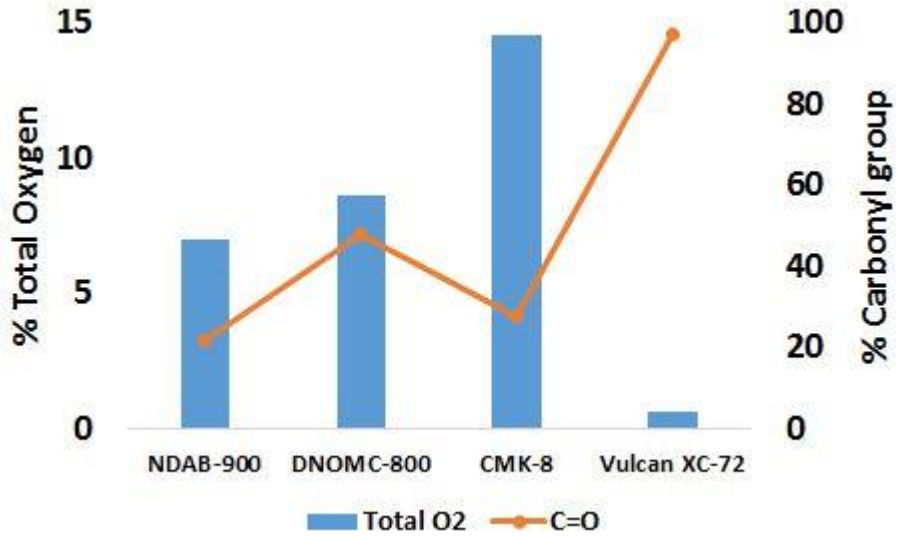

Figure 4-19 Total oxygen and carbonyl composition for NDAB-900, DNOMC-800, CMK-8 and Vulcan XC-72

The carbon source used to prepare a templated OMC adds a different perspective to why CMK-8 may also have a catalytic activity comparable to NDAB-900. You and co-workers (2011) in a well-designed experiment used CMK-8 from KIT-6 mesoporous silica to immobilize redox proteins. The

CMK-8 was derived from two carbon sources namely sucrose and phenyl formaldehyde and results obtained led to the conclusion that CMK-8 from sucrose had a higher electrical conductivity and electro-catalytic activity.

4.5 Comparison with other published works.

In **Table 4-10** an attempt is made to compare the activity obtained here with that of other researchers. However, there is the need to point out the blind spots in this. A parameter that is often compared is the onset potential. However there is no generally accepted standard for what constitutes this. For example Ma et al (2015) defined their onset potential as the point at which the current density goes below 0 mA/cm^2. Other researchers might choose -10 μA/cm2. In this work we have chosen -80 μA/cm^2 as the threshold for onset potential. The baseline for this being shrouded in secrecy or left to individual interpretations creates ambiguities.

Table 4-10 Comparison with other published works on nitrogen doped carbons and pure carbon catalysts used for ORR

Catalysts	Onset Potential in 0.1M KOH VS Ag/AgCl	Onset Potential in 0.1M KOH VS RHE	Reference
NDAB-900	-0.09	0.93	This work
CMK-8	-0.10	0.92	This work
Graphene Nanosheets	-0.13	0.89	(Benson *et al.*, 2014)
Ordered mesoporous carbon (OMC)	-0.195	0.83	(Momčilović *et al.*, 2014)
Phosphorus doped OMC	-0.125	0.90	(Pašti *et al.*, 2015)
Boron Doped OMC	-0.130	0.89	(Pašti *et al.*, 2015)
Nitrogen doped OMC	-0.165	0.86	(Pašti *et al.*, 2015)
Sulphur and nitrogen co-doped OMC	-0.11	0.91	(Song *et al.*, 2015)
Nitrogen doped OMC	-0.11	0.91	(Li *et al.*, 2015)
Nitrogen doped OMC	-0.10	0.92	(Sheng *et al.*, 2015)
OMC	-0.19	0.83	(Wang *et al.*, 2015a)
Sulfur and Nitrogen Dual-Doped Mesoporous Graphene, N-doped graphene	-0.06, -0.18	0.96, 0.84	(Liang *et al.*, 2012a)

If there is going to be any meaningful progress in this area, activity standards as well as their measurement methodologies need to be established and adhered to (Gasteiger *et al.*, 2005). This would ensure that all catalysts being developed can be compared with a common baseline.

Comparing with some other nitrogen doped catalysts reported in literature, the ORR activity obtained exceeds that of some that were synthesized with more expensive precursors e.g. (Song *et al.*, 2015). With regards to procedures, the method adopted here can be used for large scale production compared with processes like evaporation induced self-assembly (EISA) used by Pasti *et al*(Pašti et al., 2015)

4.6 Summary

N-doped carbons were synthesized using o-phenylenediamine as simultaneous nitrogen and carbon source and KIT-6 mesoporous silica as template. A template free method was also attempted with promising results that compared favourably with the templated method.

Looking at the correlation between the ORR activity and nitrogen functional groups, it is seen that quaternary nitrogen content increases with increasing activity while the converse is true for pyridinic. This was found to be true for the NDAB as well as the DNOMC catalysts. Hence it can be concluded that ORR activity is dependent on quaternary nitrogen content.

The surface area of the NDAB catalysts increase as pyrolysis temperature changed from 700 ^{o}C to 800 ^{o}C and then to 900 ^{o}C while ORR kinetic current (at -0.18 V) improved from -0.06 mA cm^{-2} to -0.19 mA cm^{-2} to -0.44 mA cm^{-2} respectively. Hence, it can be safely said that within this context, surface area plays a critical role in determining ORR activity. The same trend was observed with the DNOMC catalysts. Furthermore, from the Raman analysis, it was detected, that contrary to some schools of thought, edge plane defects do not have a direct bearing on the ORR activity of the NDAB catalysts.

CMK-8 carbon (no nitrogen doping) made from the same template as NDAB catalysts was used for ORR. Interestingly, its onset potential of 0.92 V vs RHE , was somewhat similar to that of NDAB-900 (0.93 V vs RHE) with nitrogen doping. Some factors that contribute to the activity of OMCs are a high concentration of edge plane defective sites, large amount of oxygen functional groups and high surface area.

While the NDAB catalysts did not measure up to platinum activity wise, their methanol tolerance and long term stability stands out as advantages. Another obvious advantage of this work compared with many before it, is that the procedures and materials used are such as can be easily scaled up.

Chapter 5. **Physical and Electrochemical Characterization of Manganese Oxides Supported on Nitrogen-Doped Ordered Mesoporous Carbons**

This chapter presents the results from investigation carried out to understand the physical and chemical characteristics of the nitrogen doped carbon-manganese oxide composite catalyst. It also contains detailed information on the oxygen reduction activity of the catalysts as demonstrated by results from electrochemical analysis in 0.1 M KOH. Finally, it presents the stability of the manganese oxide catalysts and their performance relative to platinum and similar catalysts synthesized prior to this time. Physical characterization was done with the aid of x-ray photoelectron spectroscopy (XPS), X-ray powder diffraction (XRD), nitrogen adsorption-desorption (BET analysis) and transmission electron microscopy (TEM). Linear sweep voltammetry using a rotating ring-disc electrode was used for electrochemical analysis.

5.1 Introduction

Metals like iron, nickel, manganese and cobalt are some of the most bountiful elements within the earth's crust; hence the name earth abundant metals. Their widespread availability helps to overcome a key drawback of the platinum group metals (PGM). Also, they are cheaper compared with elements like platinum and palladium. In addition, some, like manganese are biocompatible. Thus, any negative impact on health and environment would be minimal relative to the platinum group metals. Hence they have a lot of potential applications as catalyst.

Manganese oxides have been used as catalysts in a number of settings. Amongst many other applications, they have been used as anode and cathode materials in batteries (Oh *et al.*, 2015; Sumboja *et al.*, 2015) for supercapacitor applications (Ali *et al.*, 2015; Mendoza-Sánchez *et al.*, 2015) and as oxygen reduction reaction (ORR) catalysts (Kenko *et al.*, 2013; Gao *et al.*, 2014; Ma *et al.*, 2015). During ORR they are known to exhibit both 4 and 2 e^- reduction depending on the oxidation state (or its combination) of the

manganese (Stoerzinger *et al.*, 2015). The synergy derived from their combination with ORR active nitrogen doped carbon can be harnessed for practical applications.

Combining the activity of nitrogen doped carbon with that of manganese oxides by means of a facile synthesis route is one of the major benefits of the first synthesis route used in this chapter. The other is the possibility of preserving the highly ordered mesoporous nitrogen doped carbon nanostructure and combining this with high surface area MnO_2. Hence $KMnO_4$ was reduced through the sacrificial oxidation of the ordered nitrogen doped carbon and ordered mesoporous carbon without nitrogen doping separately. The second route used entails the deposition and heat treatment of $Mn(NO_3)_2$ on nitrogen doped carbon and ordered mesoporous carbon without nitrogen doping. The expected end was also MnO_2. Thermal decomposition was performed at 250°C, 350°C and 450°C with the aim of finding a treatment temperature that gives optimal ORR activity. It is pertinent to note, that the procedures adapted here do not require any high end technology and are also easily scalable.

5.2 Catalyst Characterization

5.2.1 **XPS analysis**

X-ray photoelectron spectroscopy was used to understand the chemical composition of the surface of the catalyst and support. **Figure 5-1Error! Reference source not found.** shows the XPS survey, manganese spectra and nitrogen spectra for NDAB-900/MnOx catalysts. These were obtained by reacting NDAB-900 with 10, 20 and 35 wt% $KMnO_4$ to give NDAB-900 (10 wt% KM), NDAB-900 (20 wt% KM) and NDAB-900 (35 wt% KM) respectively. **Table 5-1** gives an analysis of the chemical composition for all the manganese oxide catalysts. Catalyst obtained from 20 wt% $Mn(NO_3)_2$ (wet deposition followed by heat treating) have the prefix MN-250 and MN-350 to show the heat treatment temperature. Some important features of the variations in chemical composition can be noticed.

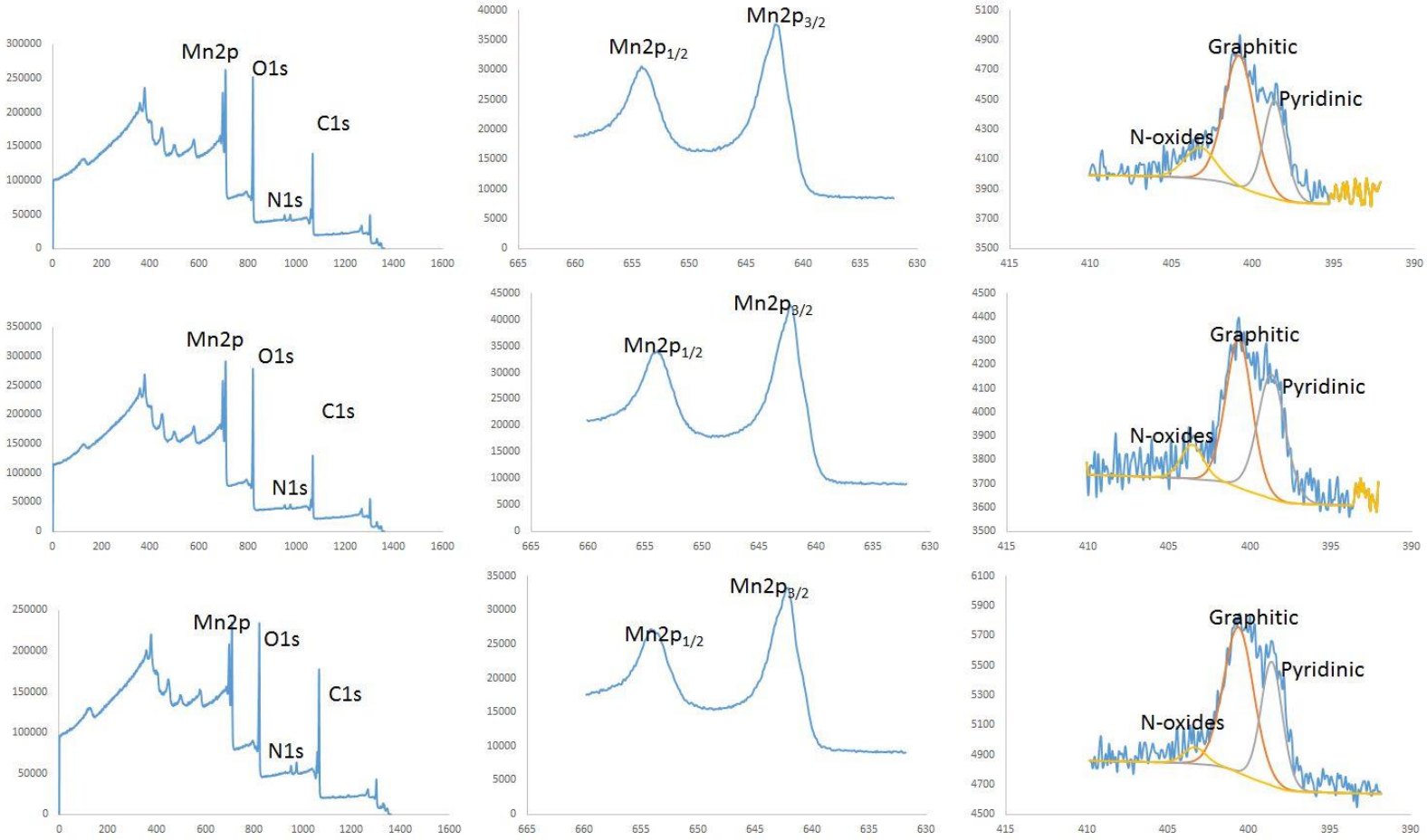

Figure 5-1 XPS survey, manganese spectra and nitrogen spectra for NDAB-MnO_2 obtained using - 10 wt% $KMnO_4$ (first row); 20 wt% $KMnO_4$(second row); 35 wt% $KMnO_4$(third row)

Table 5-1 Chemical composition of the catalysts obtained from XPS analysis

Catalysts	Carbon	Nitrogen	Oxygen	Manganese	Nitrogen		
					Graphitic	Pyridinic	N-oxides
NDAB-900	85.47	5.31	6.98	0.00	60.6	29.6	9.8
NDAB-900(10%KM)	55.63	1.96	30.59	11.22	56.16	30.18	13.65
NDAB-900(20%KM)	48.94	1.53	35.51	13.84	47.92	42.56	9.52
NDAB-900(35%KM)	64.37	2.35	24.93	7.71	59.18	35.93	4.89
NDAB-900(20 wt% MN-350)	49.33	1.92	33.89	14.69	63.53	29.88	6.58
NDAB-900(20 wt% MN-250)	42.47	1.50	40.39	14.96	39.79	26.1	0.00
CMK-8	79.64	0.00	14.54	0.00	0.00	0.00	0.00
CMK-8(20%KM)	70.61	0.00	22.36	6.73	0.00	0.00	0.00
CMK-8(20 wt% MN-350)	78.98	0.00	15.39	2.12	0.00	0.00	0.00
Vulcan	99.00	0.00	0.65	0.00	0.00	0.00	0.00
Vulcan (20%KM)	85.79	0.00	12.11	1.89	0.00	0.00	0.00

CMK-8 is the ordered mesoporous carbon prepared with sucrose as carbon precursor and having no nitrogen within it. Generally, the nitrogen doped carbons possessed a higher amount of manganese relative to the undoped CMK-8. This endorses what was mentioned in chapter 4 that the highly graphitic pore walls of NDAB-900 (confirmed through TEM and XRD analysis) would enhance the attachment of metal catalysts (Cui *et al.*, 2009; Chai *et al.*, 2012a). In addition, the nitrogen-doped active sites can also serve as anchoring points for metal deposition (Lee *et al.*, 2014). It would be

worthwhile to further exploit these property of NDAB-900 in other areas of catalysis.

For the catalysts obtained by reducing $KMnO_4$ with NDAB-900(first three rows **Table 5-1**), there is a correlation between the amount of carbon remaining and the amount of Mn deposited. As Mn increases, amount of carbon reduces. Thus confirming that the Mn deposited is as a result of carbon oxidation. Another useful observation here is that the amount of graphitic nitrogen is inversely proportional to the amount of manganese deposited. This shows that in addition to the pure carbon, the sites where nitrogen is doped in the substitutionary form are also likely to be reactive centres for $KMnO_4$ reduction. Theory wise (Dommele, 2008), it is the substitutionary nitrogen sites that contribute the electrons for oxygen reduction. Hence it follows that they are also active enough to donate electrons to $KMnO_4$.

In the second block of catalysts obtained from decomposing $Mn(NO_3)_2$ on NDAB-900, the compositions are close (14.69 and 14.96 at% of Mn). Thus it can be inferred, that heat treatment would be mainly responsible for any difference in ORR activity.

The third block contains the catalysts derived from CMK-8 carbon. Here, the Mn obtained from electroless deposition (6.73 at%) is much higher than that obtained from $Mn(NO_3)_2$ decomposition (2.12 at%). A first hand conclusion is that for ordered mesoporous materials a more effective way to obtain manganese oxides is the electroless deposition. This is justified given that the well-ordered channels in CMK-8 allow for easy diffusion of the $KMnO_4$ solution into the pores of the carbon. As opposed to the deposition of $Mn(NO_3)_2$ that would likely remain a surface phenomenon due to the large particles of the salt. Of note is the high amount of good quality carbon in the CMK-8 group relative to the others i.e. small particle size and excellent 3D morphology. These can also contribute to improved ORR activity. Lastly, much higher amount of Mn on CMK-8 relative to VC-72 can also be ascribed to its ordered mesoporous structure that enhances the diffusion of the permanganate solution into its pores

The valence of manganese within the oxides can be deduced from interpreting the XPS in the light of the XRD analysis. A characteristic feature of manganese in XPS analysis being the doublet separation between the $Mn2p_{1/2}$ and the $Mn2p_{3/2}$ peak. This can be used to differentiate between the various oxidation states. However, the challenge here is that the doublet separations for each valence state are very close and often overlap. An example can be taken from the work of Strohmeier et al. (1984). Here the separation for α-MnO_2 was 11.6 eV, same as that for MnO. Except some extra features such as the core level XPS peaks of K 2p are noticeable, further analysis with tools like XRD would be needed before a conclusion can be reached.

Table 5-2 shows the doublet separation for the manganese oxide catalysts. For the block of catalysts where NDAB-900 was reacted with different amount of $KMnO_4$, the doublet separation confirms that MnO_2 was deposited. Further information about the nature of the Mn in this group can be gained from their K 2p XPS spectra shown in **Figure 5-2**.

Table 5-2 Mn doublet separation and identification of type of oxide for all catalysts

Catalysts	Mn2p1/2 peak (eV)	Mn2p3/2 peak (eV)	Doublet Separation (eV)	Type of Oxide	Reference
NDAB-900 (10%KM)	653.98	642.29	11.69	MnO_2	(Strohmeier and Hercules, 1984)
NDAB-900 (20%KM)	653.87	642.28	11.59	MnO_2	(Strohmeier and Hercules, 1984)
NDAB-900 (35%KM)	654.09	642.61	11.71	MnO_2	(Strohmeier and Hercules, 1984)
NDAB-900 (20 wt% MN-350)	653.27	641.55	11.72	Mn_3O_4	(Oku *et al.*, 1975; Strohmeier and Hercules, 1984)
NDAB-900 (20 wt% MN-250)	653.56	641.96	11.6	γ-MnOOH Mn_3O_4	
CMK-8 (20%KM)	653.66	642.04	11.62	MnO_2	(Strohmeier and Hercules, 1984)
CMK-8 (20 wt% MN-350)	653.39	641.68	11.71	Mn_3O_4 MnO(XRD)	(Strohmeier and Hercules, 1984)
VC-72 (20%KM)	653.86	642.02	11.84	MnO_2 MnOOH	

When core electrons signal generate peaks at around 292.7 eV and 295.5 eV, it indicates the formation of K-birnessite, a type of MnO_2 (Zhang *et al.*, 2013). This is also confirmed by the XRD analysis of NDAB-900 (20%KM). Hence it can be said for certain that this group of catalysts contain K-birnessite Mn with an oxidation state of 4^+.

The other catalysts obtained from $KMnO_4$ are CMK-8 (20%KM) and VC-72 (20%KM). While the doublet separation from CMK-8 (20%KM) was 11.62 eV and correlates directly with the literature value, which of the latter was 11.84 eV, a bit distant from the literature value; however, the XRD analysis confirms the presence of MnO_2. Weak and broad K2p peaks can be observed for CMK-8 (20%KM). An indication that it also contains a small amount of K-birnessite Mn.

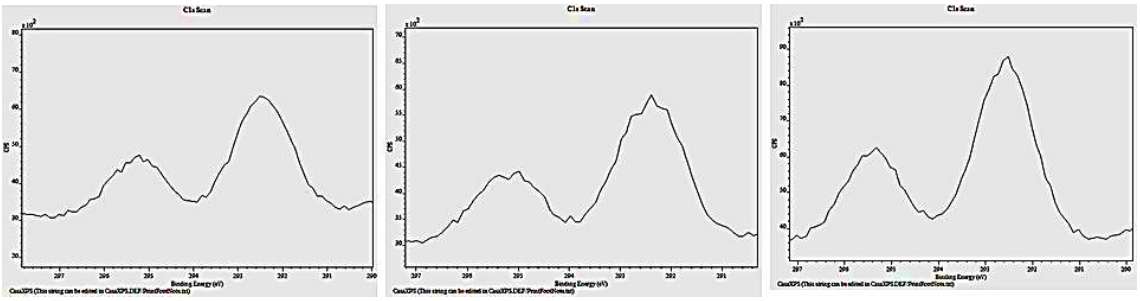

Figure 5-2 XPS K 2p peaks for NDAB-900 10, 20, 35 %KM respectively

When the decision was taken to decompose $Mn(NO_3)_2$ the expected outcome based on literature (De Bruijn *et al.*, 1981; Nohman *et al.*, 1995) was MnO_2.

$$Mn(NO_3)_2 solution \rightarrow Mn(NO_3)_2 \cdot H_2O_l \begin{cases} \xrightarrow{2nd\ step} MnO_2 \\ \rightarrow MnO_2 \end{cases}$$

However the doublet separation for manganese oxides supported on NDAB-900 and heated to 350 °C falls within the range obtained in literature for Mn_3O_4. A further confirmation of this are the very distinct tetragonal hausmannite Mn_3O_4 peaks seen in the XRD pattern (JDCDS: 04 004 864 **Figure 5-3**b. For that heated at 250 °C, the separation is a bit vague, notwithstanding the XRD patterns in **Figure 5-3**d confirm the presence of

Mn_3O_4 (JDCDS: 04 004 8640). The peaks here are however not as many and as sharp as those for the sample heat treated at 350 ^oC. Worthy of note is the presence of MnOOH –Manganite (JCPDS: 04-010-4788) in addition to Mn_3O_4.

The other carbons used as support were CMK-8 and VC-72. XPS analysis showed that Mn_3O_4 was formed on CMK-8 (based on doublet separation of 11.71 eV) this was confirmed by the XRD pattern in **Figure 5-3**. The XRD pattern also showed that cubic manganosite MnO was present (JCPDS: 04-004-3408). It was corroborated by the BE of oxygen at 530.0 eV (Tan *et al.*, 1991). This requires further investigation seeing that MnO should normally evolve from MnO_2 after two or three intermediates at ca 1300^oC (Liu *et al.*, 2004).

The answer to the question of why Mn_3O_4 instead of MnO_2 throws up some very useful observations. $Mn(NO_3)_2$ would normally decompose at temperatures above 200^oC to give MnO_2. Increasing the temperature further would result in the reduction of MnO_2 to Mn_2O_3 at a temperature of ca 550^oC. Mn_3O_4 would usually be produced around 900^oC (Nohman *et al.*, 1995; Liu *et al.*, 2004). As a result, researchers have developed various synthetic procedures for producing Mn_3O_4 at a low temperature. However with NDAB-900 as a support Mn_3O_4 was produced at ca 350 ^oC. A difference of around 600^oC. A first guess would be that the procedure was catalysed by the presence of nitrogen-doped active sites.

5.2.2 X-ray Diffraction Analysis

X-ray Diffraction was used to determine the bulk crystalline phase present in the samples. The results are presented in **Figure 5-3**. Much of these has already been discussed in line with the XPS analysis.

The pattern for the oxides obtained by reduction of $KMnO_4$ display a weak peak at ca 2θ of 37^o which according to JCPDS 00-053-0633 is tetragonal manganese oxide. The peaks at 37^o and 66^o are characteristic of amorphous manganese oxides (Lee *et al.*, 2011). Comparing the patterns for NDAB-900 (20 wt% MN-350) and NDAB-900 (20 wt% MN-250) as the heat treatment

temperature is increased there is an intensification of the peaks signifying better crystallization.

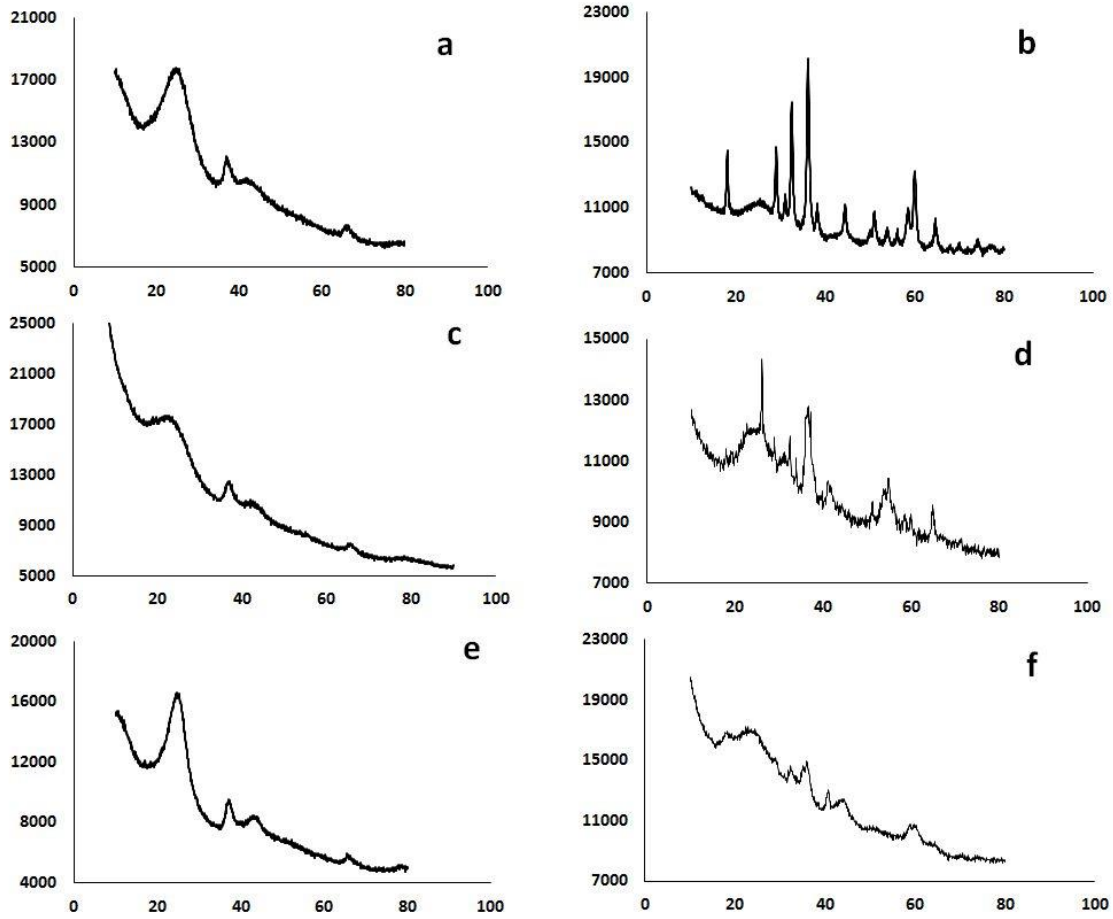

Figure 5-3 XRD Patterns for a) NDAB-900(20%KM) b) NDAB-900(20% MN-350) c) CMK-8(20%KM) d) NDAB-900(20% MN-250) e) VC-72(20% KM) f) CMK-8(20% MN-350)

5.2.3 **Transmission Electron Microscopy (TEM) Analysis**

The TEM micrographs in **Figure 5-4** show the morphologies of the manganese oxides deposited. **Figure 5-4**a, b show the lattice fringes of NDAB-900(20% MN-350). It is evident that a three dimensional high quality Mn_3O_4 was deposited on the nitrogen doped carbon. This is expected to be active not only for oxygen reduction but also for energy storage applications like the lithium-ion battery (Alfaruqi et al., 2016). **Figure 5-4** a, c captures the single crystals that make up the oxides deposited on NDAB-900 and heat treated at 250 ^{o}C. The rod like crystals have a diameter of ca 20 nm and length of ca 300 nm.

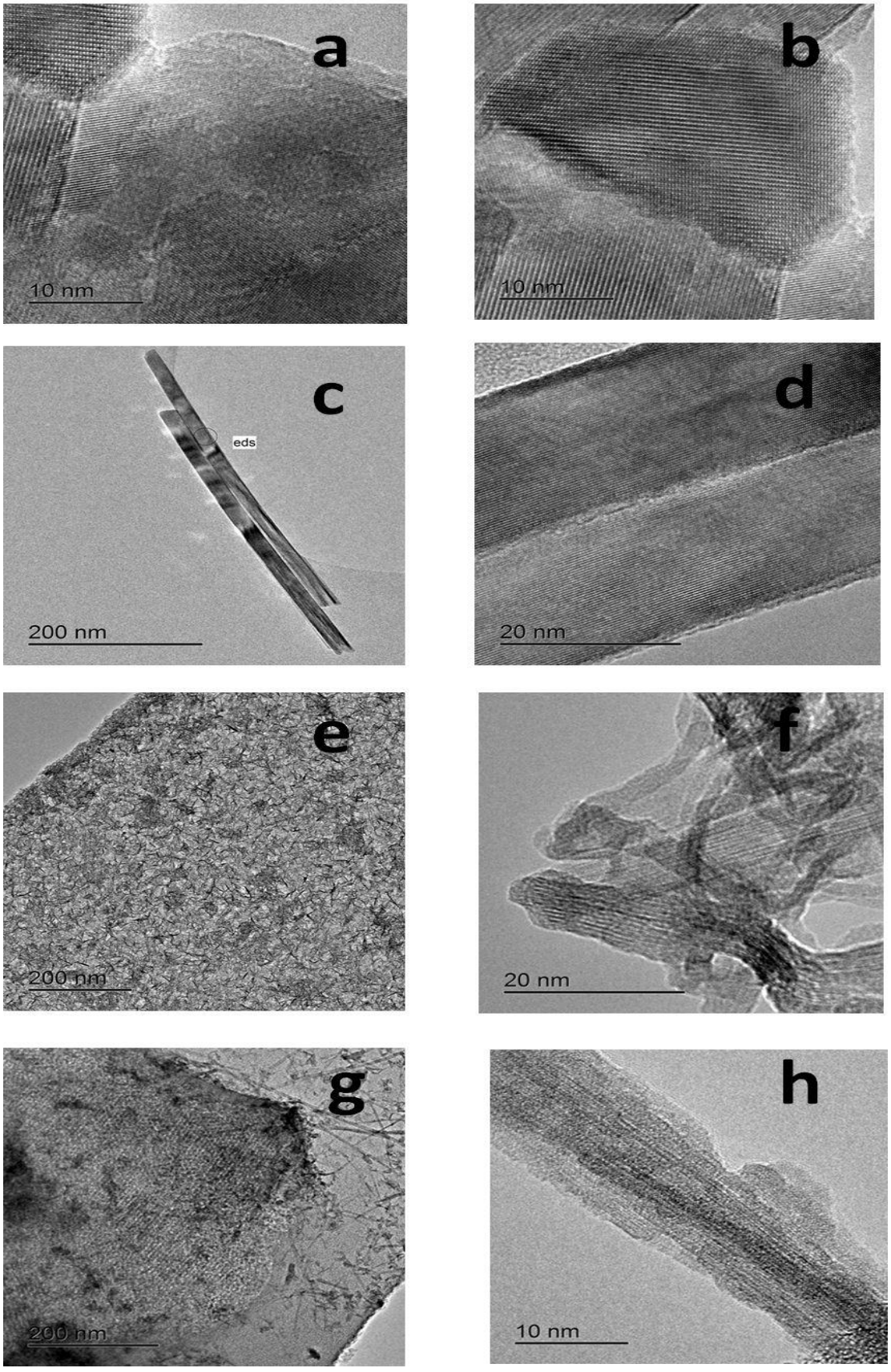

Figure 5-4 TEM of a,b) NDAB-900 (20 wt% MN-350); c,d) NDAB-900 (20 wt% MN-250); e,f) NDAB-900 (20%KM); g,h) CMK-8 (20%KM)

Figure 5-4 e,f and **Figure 5-4** g, h are for the oxides obtained by reducing 20 wt% $KMnO_4$ with NDAB-900 and CMK-8 respectively.

These were expected to be amorphous hence it not surprising that there are no distinct crystal structures observed. However, they still show a faint level of order, which indicates they could contain a small percentage of crystals. The diameter of the rod like structure for CMK-8 is ca 10 nm. It is worth noting that CMK-8 maintained its ordered mesoporous structure as can be seen in **Figure 5-4**g. The same can be said of NDAB-900 with Mn_3O_4 produced at 350 ^oC (not shown here).

5.2.4 **Surface area and pore size analysis**

The surface area analysis was performed using the nitrogen adsorption/desorption method. **Table 5-3** presents the data obtained and the trends are captured in **Figure 5-5**.

Table 5-3 Surface area and pore parameters for NDAB-900 and CMK-8 supported manganese oxide catalysts

	NDAB-900	**NDAB-900 (20wt% MN 250)**	**NDAB-900 (20wt% MN 350)**	**NDAB-900 20wt% $KMnO_4$**	**CMK-8 (20wt% MN 350)**
BET Surface area (m^2/g)	558	283	290	399	677
Cumulative volume of pores (cm^3/g)	0.38	0.10	0.09	0.22	0.72
Pore size (nm)	4.86	5.21	3.92	4.43	4.80
Micropore Volume: (cm^3/g)	0.13	0.08	0.08	0.09	0.07
Micropore Area (m^2/g)	313	163	175	223	276
External Surface Area (m^2/g)	245	119	116	176	401

It is worth noting how the catalysts were prepared. NDAB-900-250 and 350 were prepared by mixing NDAB-900 with 20 wt% aqueous $Mn(NO_3)_2$, drying and heat treating at 250 ^oC and 350 ^oC respectively. NDAB-900 20wt%

$KMnO_4$ was produced by oxidizing NDAB-900 in a neutral solution of $KMnO_4$ at ca 80 ^oC, centrifuging and drying.

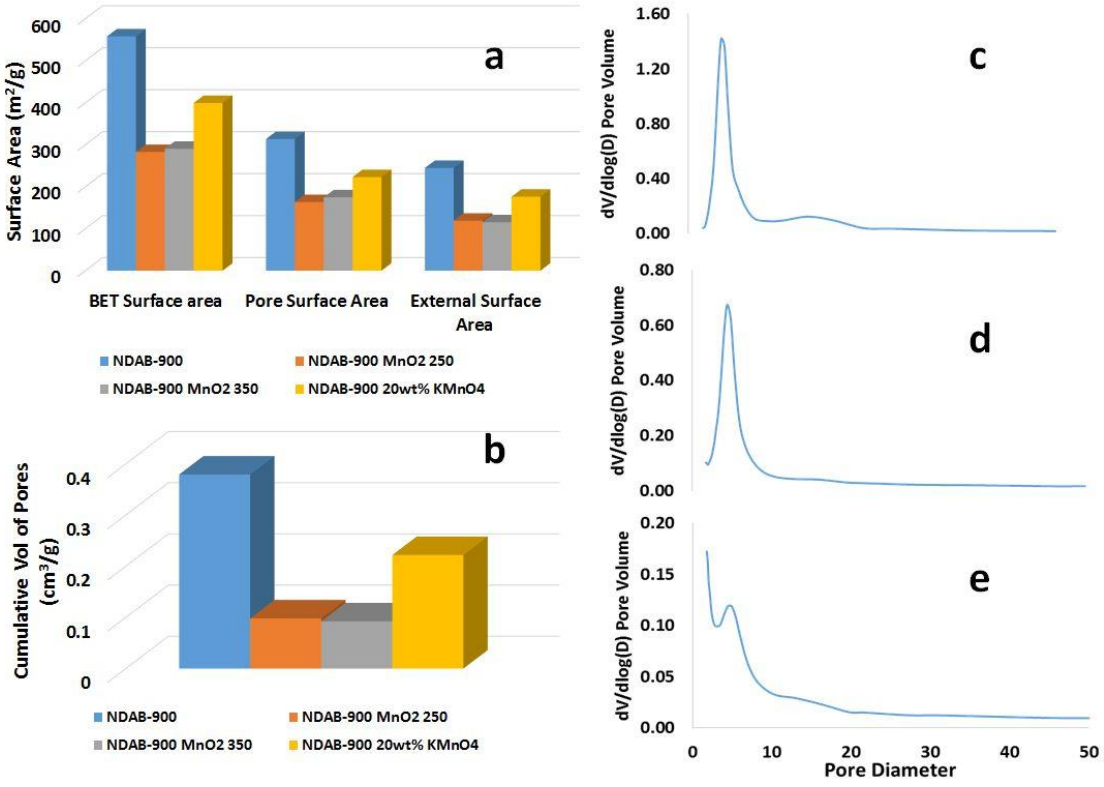

Figure 5-5 Comparison of surface and pore characteristics of NDAB-900 supported manganese oxide catalysts; c, d and e are pore size distribution of NDAB-900, NDAB-900 20wt%$KMnO_4$ and NDAB-900 MnO_2 350 respectively

It can be deduced from Figure 5-5a-e that the $KMnO_4$ process preserves the structural integrity of the ordered mesoporous carbon more than the $Mn(NO_3)_2$ process**.** Figure 5-5a shows that the nitrate derived catalysts lost almost half of the initial pore surface area while the ones from $KMnO_4$ lost about a third. A similar trend is seen with the external surface area. In Figure 5-5b change in pore volume after manganese oxide deposition is captured. There is a very significant reduction of the pore volume after deposition of $Mn(NO_3)_2$ and heat treating, with the oxide catalysts losing about 70% of the initial pore volume. The $KMnO_4$ process resulted in the loss of about 40% initial pore volume.

Considering **Figure 5-5**c, d and e, it is evident that the pore size distribution (PSD) of the catalysts from the $KMnO_4$ process i.e. **Figure 5-5**d

is almost the same as that of the starting NDAB-900 **Figure 5-5**c. Conversely, the PSD of the catalyst from $Mn(NO_3)_2$ is distorted.

A reasonable inference is that while the oxides from $Mn(NO_3)_2$ are deposited on the surface of the NDAB-900 and possibly block the pores, those from $KMnO_4$ are able to diffuse into the pores and get deposited on the pore walls, creating a thin layer of oxide catalyst. Thus, while the pore volume is reduced, the PSD remains much the same. This follows from the fact that the manganese oxides from $KMnO_4$ are amorphous and are easily spreadable within the pore network.

Interestingly and contrary to what was observed before, the catalyst formed by depositing manganese oxide on CMK-8 using $Mn(NO_3)_2$ had a narrow PSD. It may be deduced (**Table 5-3** row 2) from the large cumulative pore volume (almost seven times that of the NDAB catalysts from $Mn(NO_3)_2$) that the particles of the oxides could not block the pores.

5.3 Electrochemical Analysis

5.3.1 **Manganese Oxide Catalysts from $KMnO_4$**

These catalysts were prepared by reacting the carbon with a neutral solution of 10, 20 or 35 wt% $KMnO_4$. The ones with CMK-8 and Vulcan were prepared after it was determined that 20 wt% gave the optimal ORR activity. **Table 5-4** shows the summary of results from the rotating-ring-disk electrochemical analysis carried out in 0.1 M KOH at 1600 rpm.

NDAB-900 was the starting material for the first three catalysts with an onset potential of -0.09 V. Comparing with the best catalyst in this group i.e. NDAB-900 (20%KM), there was a 110 mV improvement in the onset potential after MnO_2 was deposited.

Table 5-4 Electrochemical Performance Indices for catalysts derived from reduction of $KMnO_4$

	onset potential (V) Ag/AgCl	onset potential (V) RHE	half-wave Potential (V)	Activation controlled current (mA/cm^2)	Tafel slope	Number of electrons
NDAB-900 (10%KM)	-0.08	0.94	-0.27	-3.55	100	3.5
NDAB-900 (20%KM)	0.02	1.04	-0.19	-20.8	86	3.4
NDAB-900 (35%KM)	-0.07	0.95	-0.25	-4.61	106	3.5
CMK-8 (20%KM)	0.03	1.05	-0.20	-19.71	88	3.5
Vulcan (20%KM)	-0.08	0.94	-0.26		73	3.8

Figure 5-6a shows the disc and ring current obtained by oxidizing NDAB-900 with different amounts of $KMnO_4$. NDAB-900(20 wt% KM) showed the best onset potential of 0.02 V (Ag/AgCl). The onset potential of NDAB-900(35 wt% KM) at -0.07 V was slightly better than that of NDAB-900(10 wt% KM) at -0.08 V. The order of superiority with respect to disc current was reversed when the amount of peroxide produced was considered. Hence, NDAB-900(20 wt% KM) with the highest disc current also seemed to produce the highest amount of peroxide going by the ring currents. However, it can be argued that within the voltage range that may be most relevant for practical applications viz. 0.00 - -0.20 V there was no significant difference in peroxide production. The limiting current density of the three catalyst were close. The chemical composition obtained from XPS analysis (**Table 5-1**), helps to explain some of the variations observed. The activity of manganese oxides is determined not only by the chemical composition but also by other factors like morphology, crystallographic phase and nature of support.

Based on XPS analysis the three catalyst (i.e. NDAB-900 reacted with 10, 20 and 35 wt% $KMnO_4$ respectively) contain MnO_2. In addition, from the presence of very strong K 2p peaks, they are known to exist in the birnessite phase also known as δ-MnO_2.

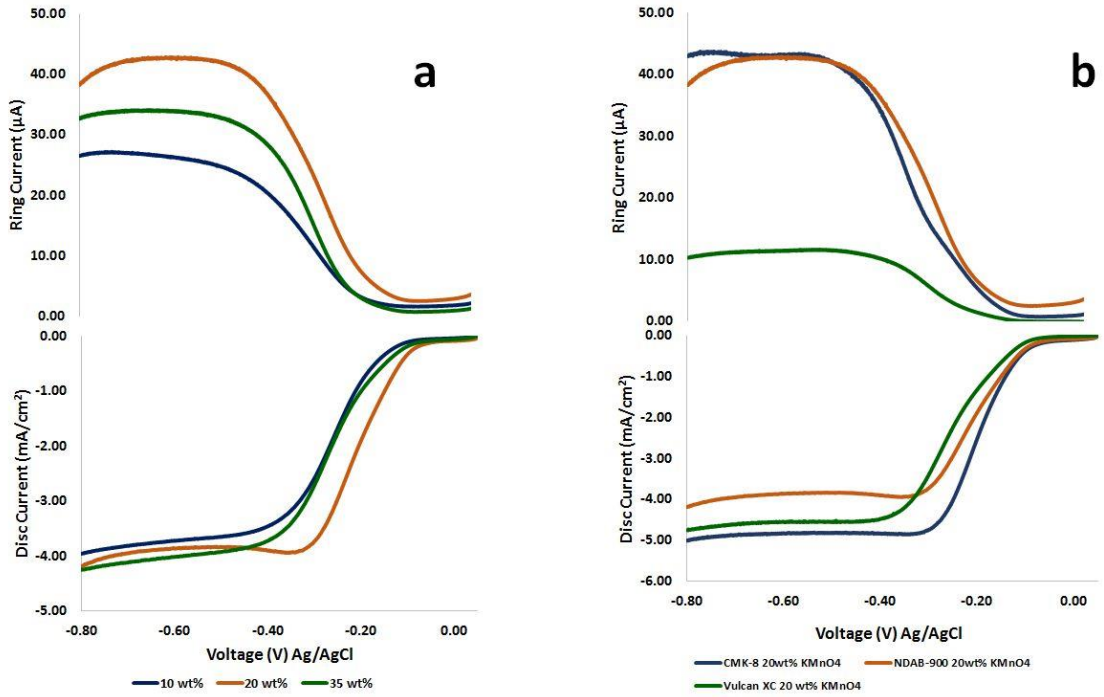

Figure 5-6 Disc and ring current for a) NDAB-900 oxidized with 10, 20, 35 wt% KMnO4 b) NDAB-900, CMK-8 and Vulcan all oxidized with 20 wt% $KMnO_4$; experiments were performed at pH 13 and RT

In δ-MnO_2, the edge-shared MnO_6 octahedra are disconnected as a result of the presence of guest cations in-between them. The guest cations are usually hydrated ions like K^+ and Na^+ (Zhang *et al.*, 2013). In this work, it can be inferred that the presence of potassium from $KMnO_4$ facilitated the formation of this birnessite phase. With respect to ORR activity, δ-MnO_2 on its own is not very active, with the number of electrons transferred close to two and a poor onset potential (Meng *et al.*, 2014). However the presence of N-doped nitrogen in the graphitic form and the mesoporous nature of the support creates a synergistic effect. This effect is similar to that obtained by Lee et al (2011) when they deposited amorphous manganese oxide on Ketjenblack.

NDAB-900 (20%KM) had the highest amount of manganese and the best activity. This is not surprising considering that all the other factors that could affect activity are common to all the three catalysts (i.e. NDAB-900 reacted with 10, 20 and 35 wt% $KMnO_4$) in this category. However, considering the trend of ring currents, it also produced the highest amount of peroxide. Having established that δ-MnO_2 produces peroxide on its own

and seeing NDAB-900 (20%KM) had the highest amount of manganese oxide, it may be inferred that this is a likely reason for the relatively higher amount of peroxide. In terms of onset potential and disc current, the best ORR activity is obtained when 20 wt% $KMnO_4$ is used. This much was confirmed by another experiment that was performed in the course of this work though not reported here.

In **Figure 5-6**b, disc and ring currents from manganese oxide supported on Vulcan XC-72, CMK-8 and NDAB-900 (i.e. by reacting each of these with 20 wt% $KMnO_4$) are shown. CMK-8 (20 wt% KM) showed the best onset potential of 0.03 V (Ag/AgCl) (1.05 V RHE) followed very closely by NDAB-900(20 wt% KM) with 0.02 V(Ag/AgCl) (1.04 V RHE). Not surprisingly Vulcan (20 wt% KM) displayed the worst onset of -0.08 V (Ag/AgCl) (0.94 RHE). The gain in onset potential after manganese oxide deposition is depicted in **Figure 5-7**.

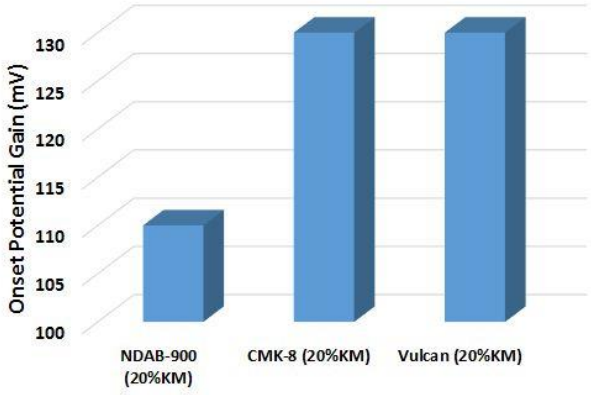

Figure 5-7 Gain in onset potential after manganese oxide deposition using 20 wt% $KMnO_4$

Vulcan-XC72 and CMK-8 (the ordered mesoporous carbon with sucrose as carbon source and no nitrogen doping) demonstrated the greatest improvement after deposition of MnOx using $KMnO_4$.

Considering the limiting current in **Figure 5-6**b, CMK-8 (20 wt% KM) maintained its superiority with a value of ca 5 mA/cm^2, however the limiting current of Vulcan (20 wt% KM), 4.7 mA/cm^2 surpassed that of NDAB-900

(20 wt% KM), 4.2 mA/cm^2. Analysing the ring currents, Vulcan-MnOx had a much lower value compared with CMK-8-MnOx and NDAB-900-MnOx. The pattern for the latter two being very close. It is evident that there is a synergy between the supports and manganese oxide. The amount of manganese deposited was 13.84, 6.73 and 1.89 at% for NDAB-900 (20 wt% KM), CMK-8 (20 wt% KM) and VC 72 (20 wt% KM) respectively and the onset potentials do not follow the same trend. Hence, it is clear that the catalyst with the best activity did not have the highest amount of manganese oxide. Thus confirming that the activity of the catalyst depends on the interplay between chemical composition, crystalline phase of the oxide, oxidation state of the oxide, morphology of oxide and nature of the support.

Two important features of **Figure 5-6**b cannot go unnoticed. One is that though the onset potential of VC 72 (20 wt% KM) was the lowest, it had an impressive limiting current. This may be ascribed to the fact that Vulcan-XC 72R is specially designed to have a very good conductivity. The second is the relatively very low peroxide production (evidenced by the low ring current). The answer to this can be found in the nature of the manganese oxide formed on it. XRD analysis shows a peak at 2θ of ca 65.7 that corresponds with that of tetragonal MnOOH in the vernadite phase (JCPDS 00-015-0604). According to Giovanoli (1980) the vernadite phase bears a similarity to the birnessite phase, in that it is a random stacking of the latter. In a well-designed experiment, Mao et al (2003), used Mn_2O_3, Mn_3O_4, Mn_5O_8 and MnOOH for oxygen reduction. They were able to conclude that while not being able to improve reduction potential, MnOOH had the greatest catalytic activity for disproportioning peroxide. This is replicated in **Figure 5-6**b. For future work, considering the widespread availability of Vulcan, it might be worth exploring the possibility of combining two supports. Vulcan XC72R and CMK-8 (that improves reduction potential) mixed as supports for manganese oxide may yet take us another step closer to the ideal alternative ORR catalyst.

One interesting finding is that the very strong K 2p peaks that were in the XPS plots of the manganese oxide supported on NDAB-900 (**Figure 5-2**) were very weak and broad in the XPS of CMK-8 (20 wt% KM). **Figure 5-8** shows the comparisons of the K 2p peaks. A safe inference is that other forms of MnO_2 likely the α-MnO_2 (considering the very good activity) may be present.

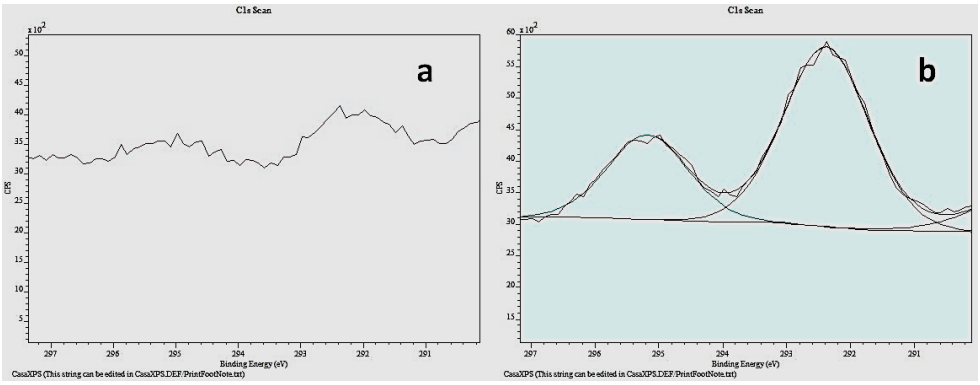

Figure 5-8 XPS K 2p peaks for a) CMK-8 (20 wt% KM) and b) NDAB-900 (20 wt% KM)

5.3.2 **Electrochemical analysis for manganese oxide catalysts from heat treated $Mn(NO_3)_2$**

These set of catalysts were prepared by stirring the carbon in a solution of 20 wt% $Mn(NO_3)_2$, drying and heat treating at 250 °C or 350 °C.

The catalysts were tested in 0.1 M KOH using a rotating ring-disc electrode (RRDE). The most important results are shown in Figure 5.9. The trend of the ring current shows that around the charge transfer limiting region, CMK-8 (20% MN350) and NDAB-900 (20% MN250) had the same ring current and by inference generated the same amount of peroxide. In the mass transfer limiting region the order of increasing peroxide generation was CMK-8 (20% MN350) < NDAB-900 (20% MN250) < NDAB-900 (20% MN350). Looking at Figure 5 9b it may be concluded that there is no significant difference in the amount of peroxide produced by each of the catalsyts.The onset potential can be defined as the potential when a catalysts starts to produce Faradaic current arising from oxygen reduction (here -80μA was used). From **Figure 5-9a,** the manganese oxide supported

on CMK-8 and heat treated at 350oC had the best onset potential (1.05 V RHE) closely followed by that on NDAB-900 treated at 250oC (1.03 V RHE) and lastly that deposited on NDAB-900 and heat treated at 350oC (1.02 V RHE). NDAB-900 (20% MN350) had the highest limiting current of 4.47mA/cm2, closely followed by that of CMK-8 (20% MN350) with 4.35 mA/cm2, NDAB-900 (20% MN250) displayed the least limiting current of 3.93 mA/cm2.

The trend of the ring current shows that around the charge transfer limiting region, CMK-8 (20% MN350) and NDAB-900 (20% MN250) had the same ring current and by inference generated the same amount of peroxide. In the mass transfer limiting region the order of increasing peroxide generation was CMK-8 (20% MN350) < NDAB-900 (20% MN250) < NDAB-900 (20% MN350). Looking at the **Figure 5-9b** it may be concluded that there is no significant difference in the amount of peroxide produced by each of the catalsyts.

Table 5-5 shows how important parameters compare**Error! Reference source not found.** while **Figure 5-9** displays the trend of these parameters with changing voltage.

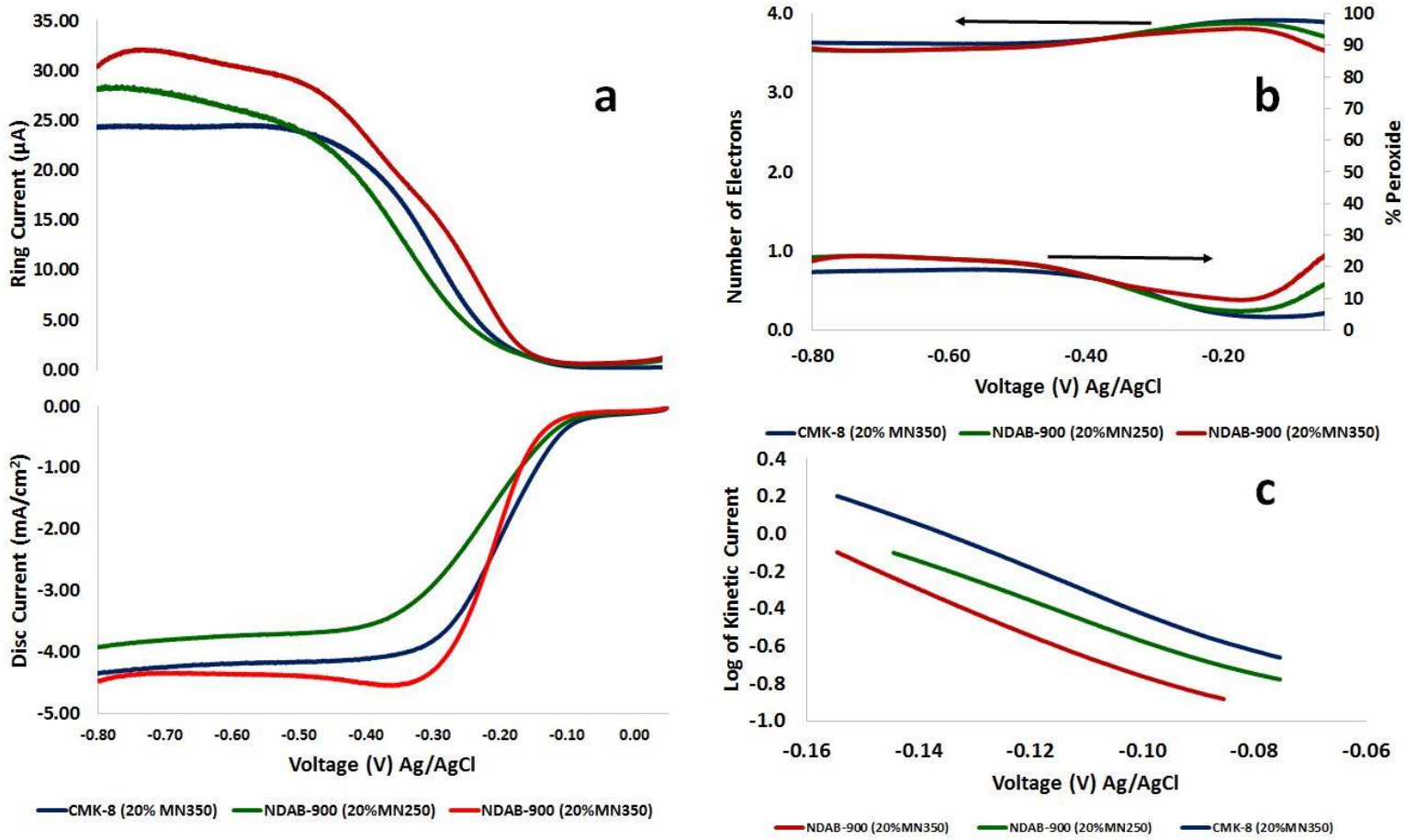

Figure 5-9 Results obtained from electrochemical characterization of catalysts made by depositing Mn(NO3)2 and heat treating a) Disc and ring currents, b)number of electrons transferred and percentage of peroxide produced and c) Tafel slopes. The data were obtained in 0.1 M KOH at a rotation rate of 1600 rpm, pH 13 and RT

The onset potential can be defined as the potential when a catalysts starts to produce Faradaic current arising from oxygen reduction (here -80μA was used). From **Figure 5-9**a, the manganese oxide supported on CMK-8 and heat treated at 350°C had the best onset potential (1.05 V RHE) closely followed by that on NDAB-900 treated at 250°C (1.03 V RHE) and lastly that deposited on NDAB-900 and heat treated at 350°C (1.02 V RHE). NDAB-900 (20% MN350) had the highest limiting current of 4.47mA/cm^2, closely followed by that of CMK-8 (20% MN350) with 4.35 mA/cm^2, NDAB-900 (20% MN250) displayed the least limiting current of 3.93 mA/cm^2.

The trend of the ring current shows that around the charge transfer limiting region, CMK-8 (20% MN350) and NDAB-900 (20% MN250) had the same ring current and by inference generated the same amount of peroxide. In the mass transfer limiting region the order of increasing peroxide generation was CMK-8 (20% MN350) < NDAB-900 (20% MN250) < NDAB-900 (20% MN350). Looking at the **Figure 5-9**b it may be concluded that there is no significant difference in the amount of peroxide produced by each of the catalsyts.

Table 5-5 Electrochemical activity indices for catalysts obtained by depositing $Mn(NO_3)_2$ followed by heat treatment

	onset potential (V) RHE	onset potential (V) 100μA Ag/AgCl	half-wave Potential (V) RHE	Activation controlled current (mA/cm2)	Tafel slope (mV/dec I)	Number of electrons
NDAB-900 (20% MN 350)	1.02	-0.06	0.81	-12.41	82	3.7
NDAB-900 (20% MN 250	1.03	0.00	0.79	-13.89	98	3.7
CMK-8 (20% MN 350)	1.05	0.02	0.82		90	3.7

However, the half-wave potential, does not follow a similar trend. The order of increase is NDAB-900 (20%MN250)<NDAB-900 (20%MN350)<CMK-8 (20 %MN350). It can be said that the foregoing results are a product of the chemical composition of the oxide, morphology, oxidation state and more importantly the synergy between the support and oxide. It is surprising

though, that CMK-8 (20 wt%MN350) with only 2.12 at% of manganese performed better than NDAB-900 (20 wt%MN350) with 14.69 at% and NDAB-900 (20 wt%MN250) having 14.96 at%. This strongly emphasizes the critical role that supports play.

When the onset potential of the supports are considered it is apparent that the improved activity is an outcome of the synergy between the support and manganese oxide. It can be seen from **Figure 5-10** that CMK-8 (20 wt%MN 350) had the greatest improvement of 140 mV having moved from 920 mV (RHE) to 1060 mV (RHE). The onset potential of NDAB-900 (20 wt% MN 350) and NDAB-900 (20% MN 250) increased by 90 and 100 mV respectively both of them having an initial onset of 930 mV (RHE). The onset potential of the two catalysts from NDAB-900 are very close. A similar trend was reported by El-sawy et al (2014) when they pyrolyzed amorphous manganese oxide at 400, 500, 700 ^{o}C and obtained onset potentials of 0.12, 0.10 and 0.11 V (RHE) respectively.

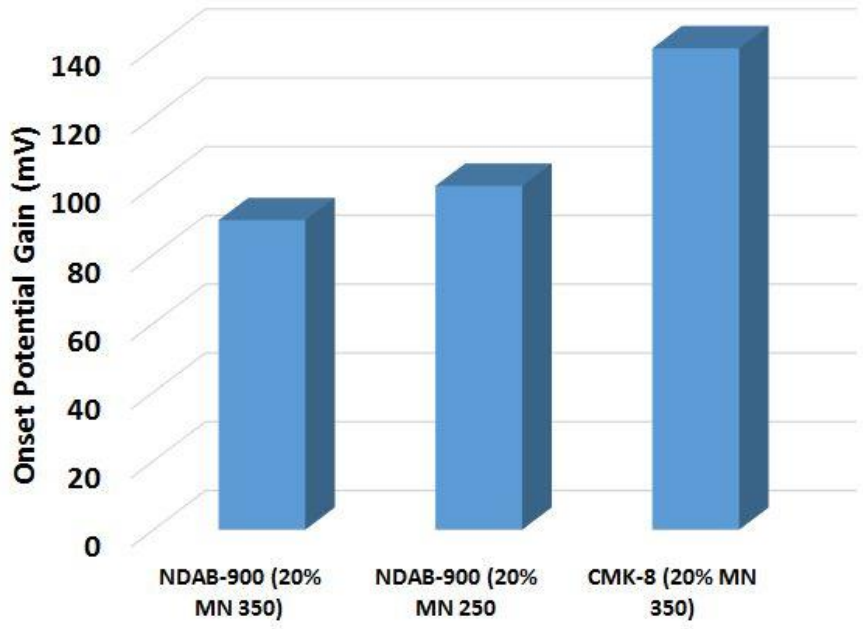

Figure 5-10 Gain in onset potential after deposition of manganese oxide using $Mn(NO_3)_2$

Mn_3O_4 is an oxide with a regular spinel construction. At room temperature, the stable phase is the hausmannite having a tetragonal structure. This has trivalent Mn_3^+ and divalent Mn_2^+ ions occupying the two octahedral and one

tetrahedral positions of the spinel structure, respectively. (Lee and Jung, 2012). The three catalysts made by depositing $Mn(NO_3)_2$ contain Mn_3O_4 as confirmed from XRD analysis (JCPDS 04-004-8640). Generally they have not been known to be very active for ORR i.e. in terms of good onset potential. Research carried out with Mn_3O_4 (Gorlin and Jaramillo, 2010; Gorlin *et al.*, 2012) obtained catalysts that had limiting current densities almost equal to that of platinum, but with onset potentials of ca 0.8 V RHE. This seems to explain why NDAB-900 (20 wt%MN350) that has only Mn_3O_4 displayed a low onset potential and high limiting current relative to the other two catalysts. One reason for the high limiting current might be the fact that it is usually produced at temperatures of around 350 – 500^{o}C thus obtaining a crystalline structure that may enhance conductivity. From XRD analysis, NDAB-900 (20 wt%MN250) also contains MnOOH while CMK-8 (20 wt%MN350) has some amount of MnO. Considering that MnO only shows moderate activity compared with MnOOH (Chen *et al.*, 2015; Liu *et al.*, 2015a) and that CMK-8 had earlier in this work demonstrated very good ORR activity, it is highly probable that much of the good activity showed by CMK-8 (20 wt%MN350) is a function of the interaction between the oxide and highly ordered mesoporous carbon support (CMK-8).

A good reason why the support might play a defining role is the relatively large surface area it bestowed on the final CMK-8 (20 wt%MN350) i.e. 676.51 m^2/g. This is more than twice that of NDAB-900 (20 wt%MN250) at 282.62 m^2/g and NDAB-900 (20 wt%MN350) at 290.28 m^2/g. This may explain why despite the small amount deposited i.e. 2.12 at% CMK-8 (20 wt%MN350) yet showed comparatively better activity in terms of onset potential.

The upper region of **Figure 5-9**a shows the ring current for each of the three catalysts. This can be better appreciated when explained along with the percent peroxide production shown in **Figure 5-9**b. Within the kinetic region ca -0.05< V > -0.2, CMK-8 (20 wt%MN350) produced the least amount of peroxide specifically ca 5 % peroxide. It is followed by NDAB-900

(20 wt%MN250), while NDAB-900 (20 wt%MN350) produced the highest amount (between 10 and 20%) within this region.

The values of Tafel slope obtained here were 82 mV/dec, 98m V/dec and 90 mV/dec for NDAB-900 (20 wt%MN350), CMK-8 (20 wt%MN350) and NDAB-900 (20 wt%MN250) respectively. These do not fall within the range of what can be interpreted as specific rate determining steps i.e. the 60 and 120 mV/dec. Tafel slopes not being 60 or 120 mV/dec are not unusual. Gao and co-workers (2015) found that the Tafel slope of sulphur doped managanese oxide and sulphur doped manganese oxide-graphitized carbon composite in 0.1 M KOH were 81 and 112 mV/dec respectively.

5.3.3 **Comparison with 20 wt% platinum.**

20 wt% platinum remains the benchmark catalyst for oxygen reduction. Hence the best of the manganese oxide catalysts obtained in this work were compared with it. The summary of results is presented in **Figure 5-11**. The manganese oxide catalysts compare well with platinum in terms of disc current. The best of them, CMK-8 (20 wt% KM) with amorphous manganese oxide has a limiting current of 5.0 mA/cm^2 compared with platinum's 5.7 mA/cm^2. The ring current in **Figure 5-11**a is explained along with the amount of peroxide produced **Figure 5-11**b.

Within the kinetic region -0.20<V>-0.05, the peroxide of the manganese oxide catalysts also comes close to that of platinum. CMK-8 (20 wt%MN350) for example produced peroxide of only ca 5% while CMK-8 (20 wt% KM) has peroxide values between 10 and 15%.

The difference in onset potential is not pronounced. However, the half-wave potential of platinum is only about half that of the manganese oxides. This affirms the kinetic superiority of the 20 wt% platinum catalyst.

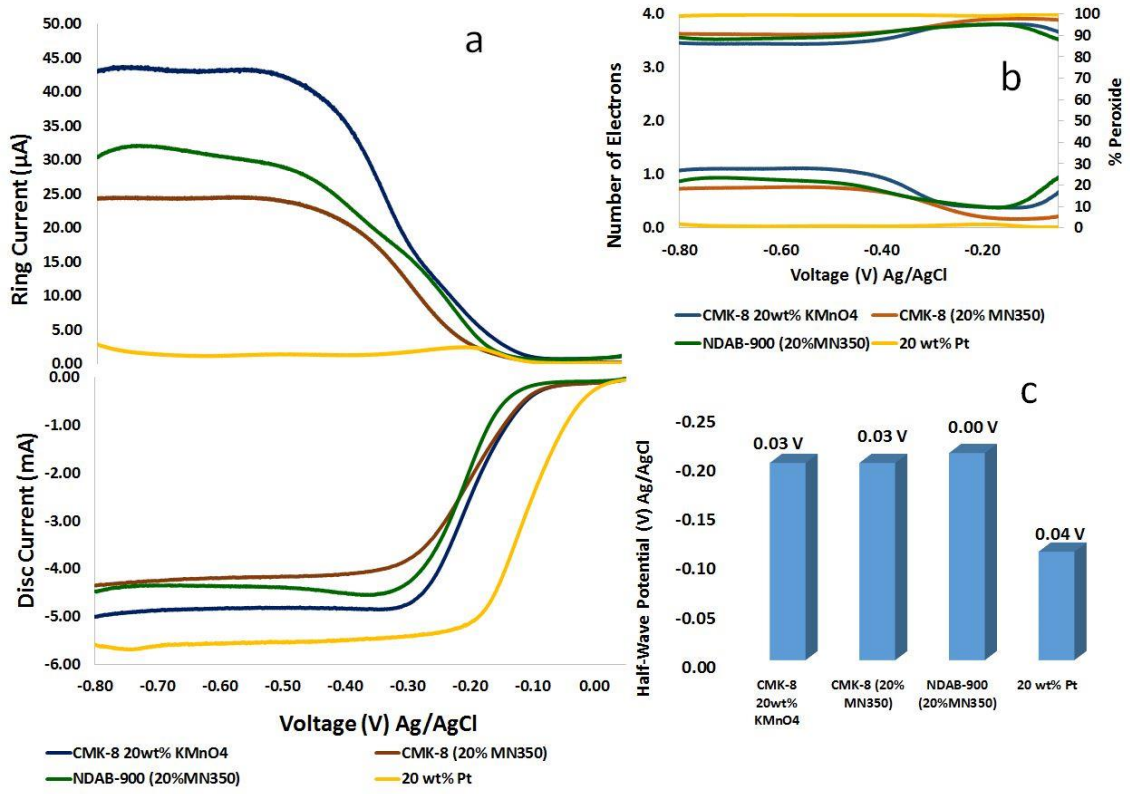

Figure 5-11 Comparison of results from electrochemical analysis performed for 20 wt% platinum, CMK-8 (20% KM), CMK-8 (20% MN350) and NDAB-900 (20% MN350); a) Disc and ring current b) percent peroxide produced and n-number c) half-wave potential with onset potential; analysis were carried out at pH 13 and RT

Amongst all the manganese oxide catalysts, CMK-8 (20 wt% KM) with amorphous MnO_2 has the best activity even when compared with the crystalline ones. Chemical composition aside, amorphous manganese oxide catalysts have been proved to have superior ORR activity compared with their crystalline companions. In a study involving an amorphous MnOx catalyst and crystalline Mn_3O_4 for ORR, Lee et al (2011) discovered that the amorphous catalyst performed better. They postulated that the amorphous catalyst had a higher concentration of surface defects and thus made available more active sites for adsorbing oxygen. Xu and co-workers (Yang and Xu, 2003) also argued that a distorted structure is advantageous for catalysis since it comprises of more active sites. They therefore inferred that because amorphous manganese oxides contain a greater amount of

structural distortion relative to the crystalline ones, they would be more active.

In furtherance of this line of argument, Sumboja et al (2015) grew manganese oxide on carbon paper with an accompanying excellent performance in a rechargeable zinc-air battery. One reason they gave was the very even distribution of amorphous manganese oxide within the pores. They claimed this enhances the three phase interaction between oxygen, electrolyte and catalysts. As a further evidence that this principle of amorphous catalysts doing better than crystalline ones is a general phenomenon, Indra et al (2014) prepared amorphous and crystalline cobalt iron oxides which were used for water oxidation and ORR. The amorphous one had a superior catalytic activity in both areas of application especially within the kinetic region.

5.3.4 **Stability**

The stability of the catalysts were tested using chronoamperometry and accelerated degradation tests (ADT). The results are presented in **Figure 5-12**. Fig. 5.12a shows the Chronoamperometry plots of NDAB-900(20 wt% MN)350 and NDAB-900(20 wt% KM). They both exhibit a gradual decline in current relative to the initial current. However, after ca 10 mins, NDAB-900 (20wt% KM) showed a greater level of depreciation in its current. It ended with a final current that was 82% of the initial while NDAB-900(20 wt%MN) maintained 84% of the initial current after about 2 hours.

Looking at the before ADT and after ADT plots, the three catalysts display a moderate negative displacement after the degradation tests.

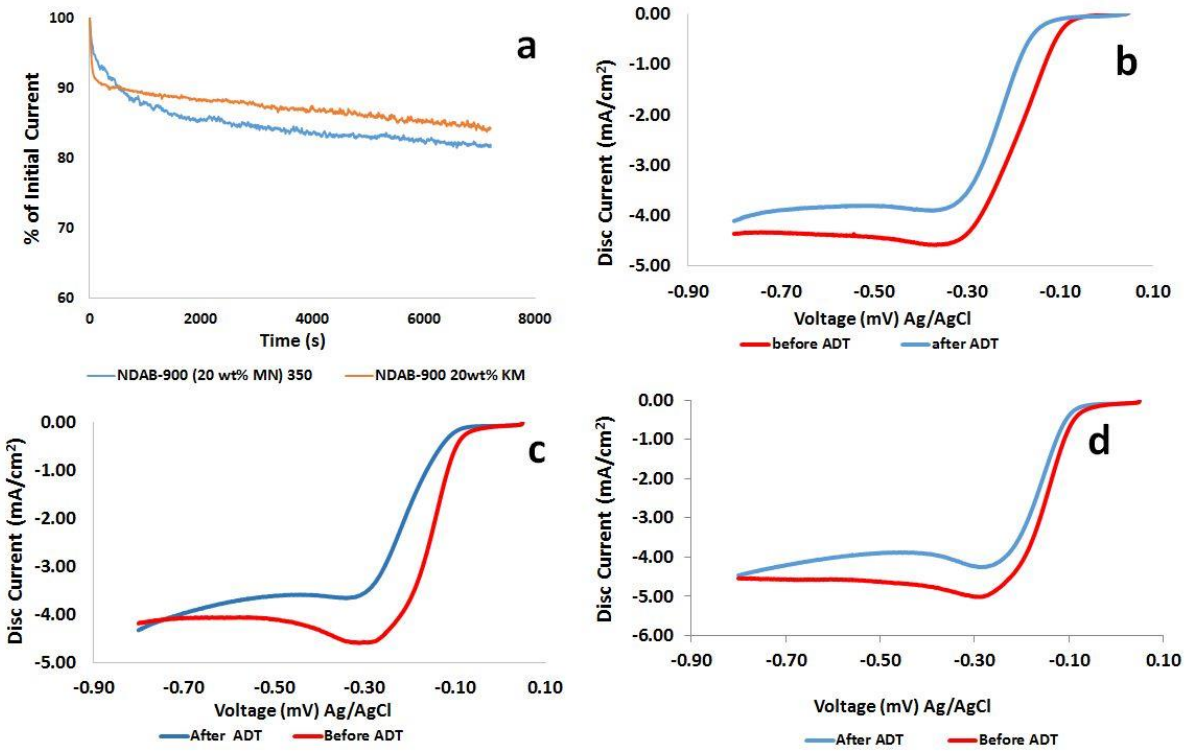

Figure 5-12 a) Chronoamperometry b, c, and d accelerated degradation tests (ADT) for NDAB-900 (20%MN 350), NDAB-900 (20% KM) and CMK-8 (20% KM) respectively; these were done at ph 13 and RT

5.4 Comparison with other works in Literature

This is most prominent in NDAB-900 (20 wt% KM) and least in CMK-8 (20 wt% KM). When the accelerated degradation tests are considered, CMK-8 (20 wt% KM) seems to be the most stable. Its onset potential remained the same, while that of NDAB-900 (20 wt% MN 350) shifted negatively by 20 mV and that of NDAB-900 (20 wt% KM) by 70 mV after degradation.

Looking at **Table 5-6** it is evident that the synergy between the MnOx catalysts and the support used resulted in ORR catalysts with very good activity relative to other catalyst of similar composition.

Table 5-6 Comparison with other reports that used manganese oxides in alkaline media

Catalyst	Support	Onset potential (V) Ag/AgCl	Half-wave potential (V) Ag/AgCl	Reference
CMK-8 20wt% KMnO4 (MnO_2)	CMK-8 OMC	0.03	-0.20	This work
CMK-8 (20% MN350) (Mn_3O_4)	N-doped OMC	0.03	-0.20	This work
NDAB-900 (20%MN350) (Mn_3O_4 & MnO)	N-doped OMC	0.00	-0.21	This work
3D-Mn_3O_4	nitrogenated graphene	NS	-0.20	**(Bikkarolla *et al.*, 2014)**
mesoporous manganese oxide/sulfur	graphitized carbon	-0.08	-0.20	(Gao *et al.*, 2015)
Manganese Oxide Molecular Sieve	Mixed with activated carbon	-0.07	NS	(El-Sawy *et al.*, 2014)
MnOx nanowires	nitrogen-doped graphene	-0.09	NS	(Lee *et al.*, 2014)
Ag on MnOx	Graphene	-0.12	-0.30	(Shypunov *et al.*, 2015)
Ag on MnO_2	Reduced graphene oxide	-0.12	NS	(Lee *et al.*, 2015)
Shewanella-mediated biosynthesis of Mn_2O_3	No support	0.07	-0.24	(Jiang *et al.*, 2015)
$CaMnO_3$	No Support	-0.06	-0.26	(Han *et al.*, 2013)
MnO containing mesoporous nitrogen doped carbon	No Support	NS	-0.21	(Tan *et al.*, 2012)
Spinel Manganese–Cobalt Oxide	Nitrogen-doped reduced graphene oxide	-0.07	NS	(Liang *et al.*, 2012b)

The onset potential from the catalysts in this work is the best with the exception of the oxide made from *shawanella* (Jiang *et al.*, 2015)which may not be classed in the same group with others listed. Considering scalability, it is obvious that the shawanella process would be hindered with many obstacles. Despite the complexity of some of the procedures listed, the very simple approach adopted in this work still produced better catalysts. This lends weight to the drive for easy commercialization of the catalysts that would serve as alternative to platinum.

5.5 Summary

In the course of depositing manganese oxides on NDAB-900 and CMK-8, the N-doped catalysts were found to be capable of retaining a higher amount of the oxides. This was ascribed to the highly graphitic pore walls of NDAB-900 as well as to the presence of N-doped active sites which can serve as anchoring points for metals. It was also discovered, that for undoped ordered mesoporous carbon, the electroless deposition proved to be more effective with a greater amount of manganese (6.73 at%) compared with that obtained from the deposition method (2.12 at%). With respect to the pore structure after deposition, the BET analysis showed that physical deposition followed by heat treatment leads to a loss of up to 70 % of pore volume. This is very high compared with the loss of up to 40 % which occurred when the electroless deposition was used.

Significant improvements in ORR activity were achieved by depositing manganese oxide on NDAB-900 and ordered mesoporous carbon (CMK-8) respectively. This is reflected in an enhancement of up to ca 0.13 V in the onset potential. Thus, this justifies the adoption of this approach and presents it as one that can help bridge the activity gap between non-platinum-group-metal catalysts and Pt/C.

Most importantly, very active manganese oxide catalysts that compare with the very best reported in literature have been prepared. The value of these synthesis procedures lie in their simplicity and scalability. For the first time, the exceptional activity of amorphous manganese oxide and the excellent structural capabilities of highly ordered mesoporous carbon have been harnessed to produce catalysts with good onset potential of 1.05 V vs RHE (compared with platinum/carbon with onset of 1.06 V vs RHE) and high limiting currents.

Considering the very good Mn_3O_4 synthesized, it would be worthwhile to use them in other areas, especially those involving metal deposition.

Chapter 6. **Nitrogen doped carbon as catalyst and catalyst support in neutral media and their application in microbial fuel cells**

In this chapter a nitrogen doped carbon (NDAB-900) synthesized in the course of this work was tested as an oxygen reduction catalyst in 50 mM phosphate buffer solution of pH 7. Electrochemical activity was investigated with the aid of linear sweep voltammetry (LSV) in a rotating ring-disc electrode system. An attempt was also made to expound the mechanism by which the oxygen reduction reaction (ORR) occurs. Thereafter, three of the catalysts synthesized earlier, were used along with 20 wt% platinum for ORR catalyst in the cathode of a microbial fuel cell. The catalysts used were nitrogen doped carbon pyrolyzed at 900^{o}C (NDAB-900), highly ordered mesoporous carbon (CMK-8) and highly ordered mesoporous carbon-manganese oxide composite, obtained by reacting CMK-8 with 20 wt% KMnO4 (CMK-8 (20 wt% KM))

6.1 Introduction

Over the years, platinum has carved a niche as the best ORR catalysts even in microbial fuel cells. However, as with other applications, issues of cost and availability continued to cast doubts on its economic as well as long term sustainability. Feng et al (2012) reasoned that due to the benefits of low cost, relatively good electrical conductivity and strong oxidation resistance, nitrogen-doped carbons are likely substitutes for noble metals in microbial fuel cells (MFCs) for wastewater treatment. Surprisingly, Liu and co-workers (2013) claimed to have synthesized nitrogen doped carbon that outperformed platinum in a microbial fuel cell. The nitrogen doped carbon cathode had a power output of 776 ± 12 mW/m^2 compared with platinum's 750 ± 19 mW/m^2. In the same vein, Gnana Kumar et al (2014) anchored α-MnO_2 on graphene oxide and used it in a microbial fuel cell. They reported a maximum power density of 3359 mW/m^2 which according to them was comparable to that of platinum. Thus this work seeks to improve on what is

already obtainable in the area of carbon based catalysts for ORR in microbial fuel cells.

6.2 Electrochemical Analysis

The electrochemical activity of nitrogen doped carbon (NDAB) pyrolyzed at 900 ^{o}C, NDAB-900 was tested in 50 mM solution of pH 7 phosphate buffer. **Figure 6-1** displays the most important results obtained. **Figure 6-1**a combines the disc and ring current obtained from the oxygen reduction reaction. Expectedly, the highest values of disc and ring currents occur at the highest rotation rate. Though the disc current increases as potential becomes more negative, it does not attain the plateau that signifies mass transfer limitation has been reached. The ring currents get to a peak at a voltage which varies with rotation rate, after which they experience a slight dip that continues until the end of the scan. **Figure 6-1**b presents the number of electrons transferred and the percentage of peroxide produced. **Figure 6-1**c is the Koutecky-Levich plot showing the variation of the inverse of current density with the inverse square root of the rotation rate expressed in radians. The plots are parallel which is said to be an indication of first order kinetics (Ye and Vijh, 2005).

The onset potential taken to be the voltage when the current gets to 80μA was -0.01 V. This is quite distant from that of platinum which was 0.35 V. The number of electrons transferred calculated using the ring and disc currents was 3.4 at -0.4 V and is the same as that calculated from the Koutecky-Levich equation i.e. 3.4. The heterogeneous rate constant showing the intrinsic rate capability of the catalyst was 0.10 cms^{-1}about a fifth of the value for platinum i.e. 0.56 cms^{-1}. **Table 6-1** gives a summary of these parameters.

6.3 Mechanism of Oxygen Reduction on Templated N-Doped Carbon from O-phenylenediamine

An attempt was made to clarify the mechanism by which NDAB-900 performs ORR in neutral media..

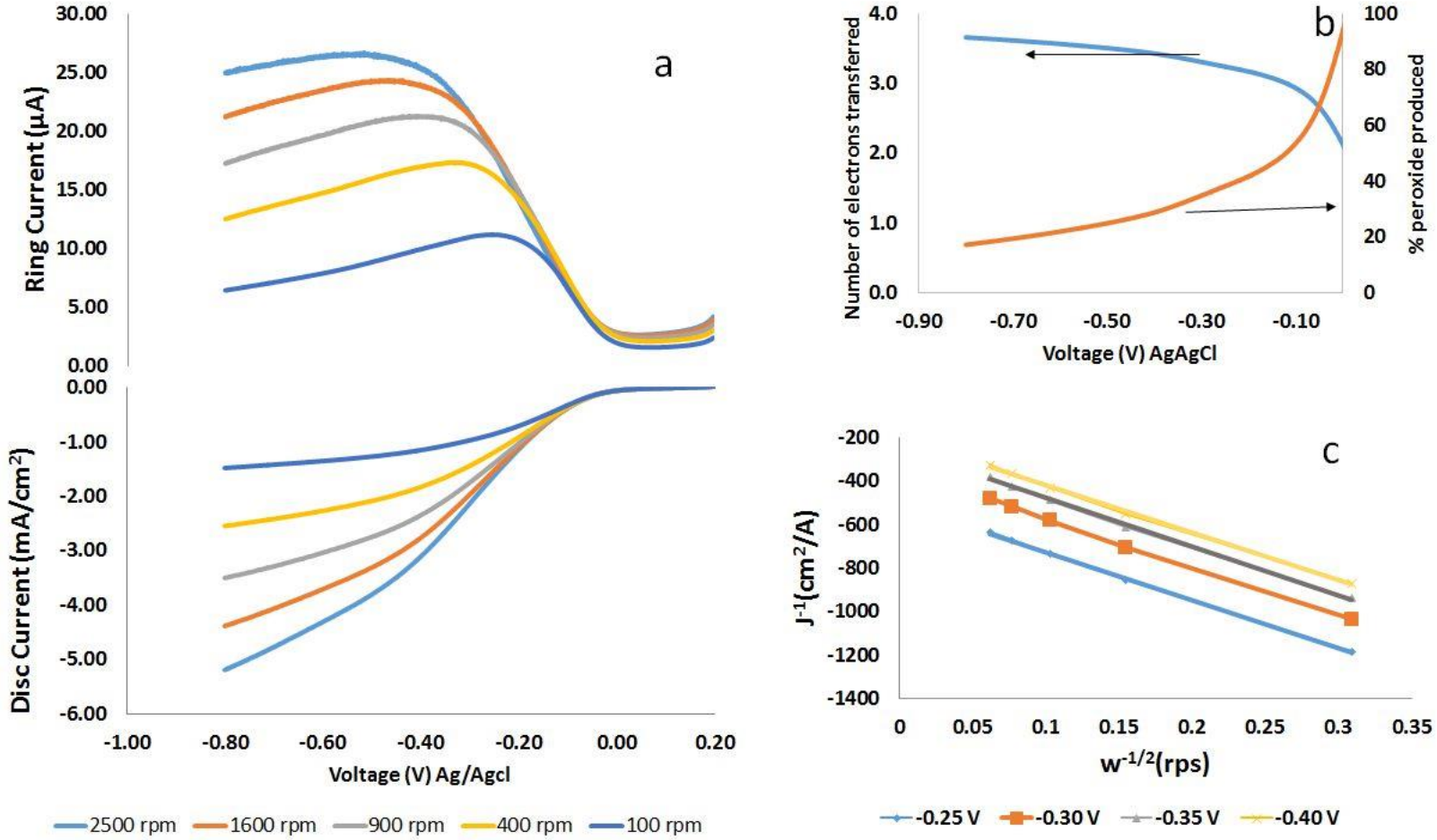

Figure 6-1 Electrochemical analysis of NDAB-900 in 50 mM PBS, pH 7 and RT. a) Disc and ring current b) number of electrons transferred and peroxide produced in percentage (obtained at 1600 rpm) c) Koutecky levich plots

Table 6-1 Electrochemical activity parameters for NDAB-900 in 50 mM PBS of pH 7

	Onset potential (V) Vs Ag/AgCl	k_h heterogenous rate constant (cms^{-1})	N-number	N-number Koutecky Levich
NDAB-900	-0.01	0.10	3.4	3.4
20 wt% Pt	0.35	0.56	4.0	4.0

To this end, the intrinsic changes in catalysis were tracked by analysing the ring current, disc current and combining these with theoretical/computational studies on the ORR activity of platinum.

Figure 6-2 shows how the ring current, disc current and the number of electrons transferred changed with voltage.

At potentials more negative than -100 mV, the disc current intensifies showing that the catalyst is enhancing the transfer of electrons to oxygen. The simultaneous rapid increase in ring current (with increase in disc current) indicates that the dominant pathway here is that of hydrogen peroxide. For some carbon catalysts, the trend at this point is that the number of electrons would remain at 2 as the voltage is increased, shifting to 3 or greater at higher voltage. However the variation of number of electrons with voltage shows that while the ring current was yet increasing at ca -100 mV, the number of electrons was approximately 3. This is a pointer to the fact that this is not strictly a two electron transfer. Hence it is more likely that a direct 4 electron transfer is also happening simultaneously, albeit on a smaller scale. In summary it is a combined two and four electrons transfer with the two electron transfer being dominant.

The justification for this lies in the fact that, it is sometimes assumed that catalysts with a high amount of peroxide follow the 4-electron pathway only after a considerable increase in voltage. By combining RRDE plots with that of number of electrons, it has been shown that the four electron pathway can be combined with the peroxide pathway from the onset of the ORR reaction.

An attempt was also made to propose a mechanism at the molecular level. The knowledge of this mechanism would be very useful if a mathematical model of the oxygen reduction process on this catalyst were to be developed. According to Feng et al (Feng *et al.*, 2011b) the first step is the adsorption of molecular oxygen which preferentially occurs in a **chemisorbed non-dissociated form** as confirmed by simulations of the ORR on carbon catalysts.

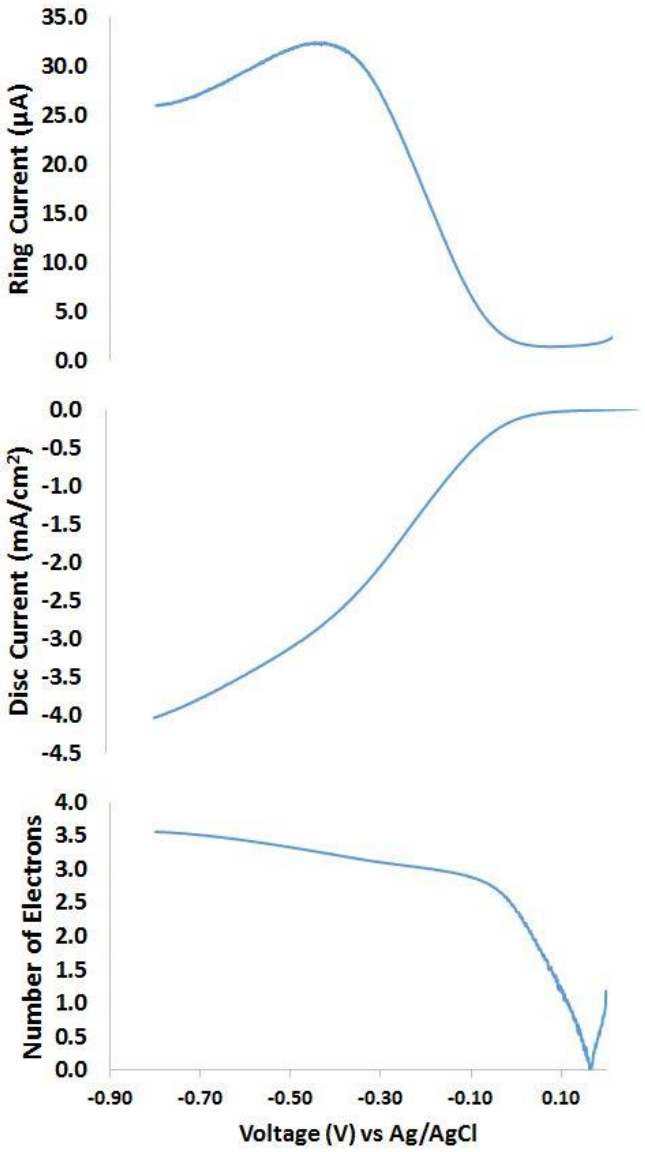

Figure 6-2 Ring current (top), Disc current at 1600 rpm (middle) and number of electrons transferred (bottom) for the ORR activity of NDAB-900 in 50 mM, PBS of pH 7 carried out at RT

Furthermore, there seems to be a consensus (Ikeda et al., 2008; Okamoto, 2009) that peroxide production proceeds from OOH hence the O_{2ads} accepts

an electron and a proton to form OOH_{ads}. This can either accept an electron and a proton to form hydrogen peroxide or dissociate into oxygen and a hydroxide. The oxygen and hydroxide go to form a molecule of water each by different pathways (**Figure 6-3**).

From the plot of number of electrons transferred in **Figure 6-2**, it follows that both the path leading to peroxide and that leading to oxygen and hydroxide occur simultaneously. This agrees with literature (Su, 2012). One possible reason why the peroxide pathway could be dominant here is that the conversion of HO_{2ads} to H_2O_2 is potential-driven as opposed to its dissociation into O + OH. Hence as we increase the voltage, the formation of peroxide proceeds more rapidly than the dissociation of HO_{2ads}.

A debatable aspect of this mechanism is whether the peroxide formed proceeds to water via a direct reduction (**Figure 6-3** scheme 2-step7) or first dissociates into two OH molecules which are then reduced to water (**Figure 6-3** scheme 1-step 6 and 7). An examination of the disc current plot in conjunction with the ring current and comparing with computational studies helps to explain this.

Were it to be that peroxide was being reduced directly; the ring current curve would have experienced a rapid downward slope(Ruvinskiy *et al.*, 2011). This is because according to **Figure 6-3** scheme 2, while diffusion of peroxide to the ring remains constant (step 5), due to a constant rotation rate, its reduction would be accelerated as the voltage is swept in the negative direction. Within a short time, the rate of reduction will likely surpass the diffusion rate and the ring current should become negligible. The ring current curve does not depict this.

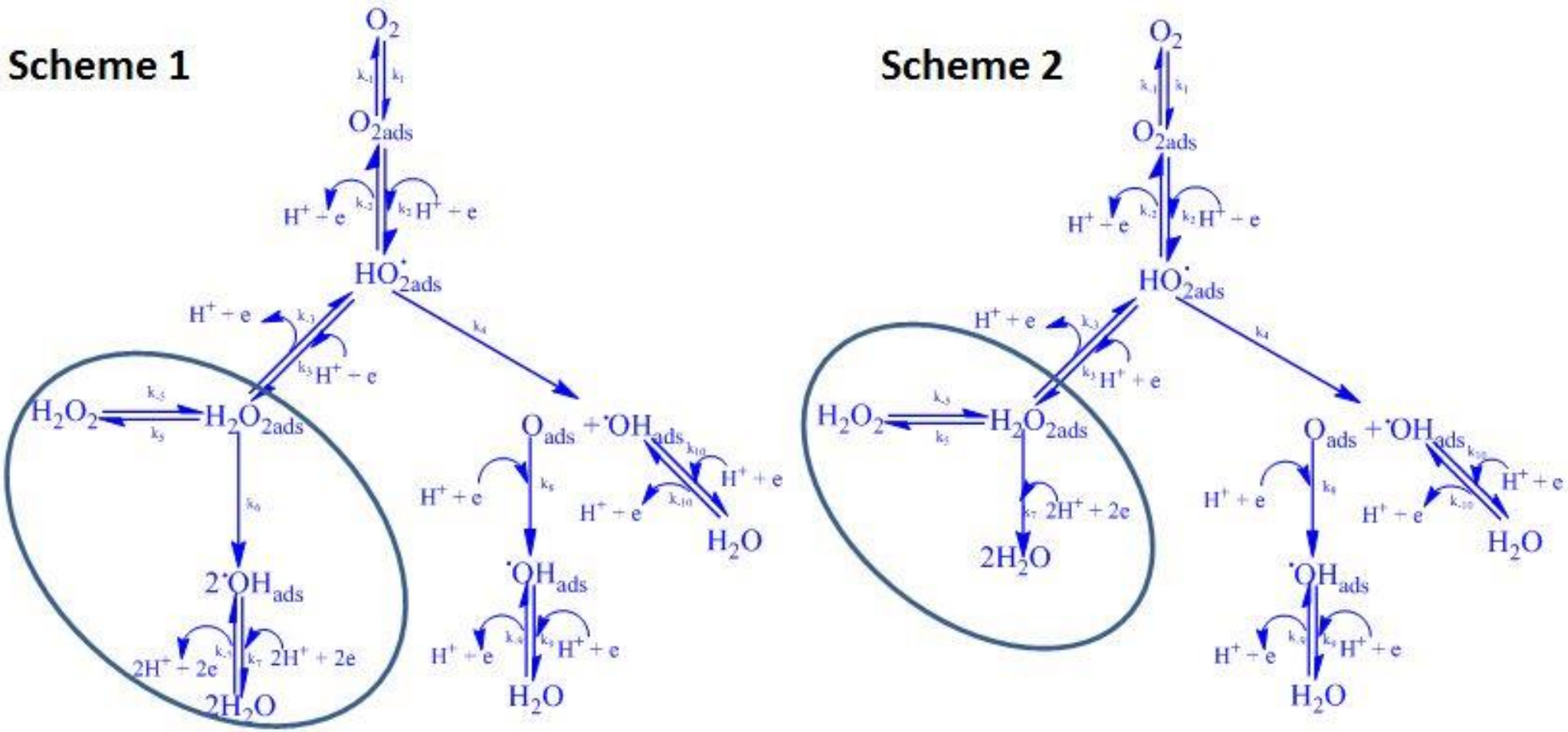

Figure 6-3 Oxygen reduction pathway on nitrogen doped carbon catalysts (in scheme 1 along the 2x2 pathway, water is being formed from the reduction of hydroxides produced after the dissociation of H_2O_2 i.e. steps 6 and 7; in scheme 2 along the 2x2 pathway, water is formed directly from the reduction of H_2O_2

Allowing for the peroxide to undergo dissociation implies that while the rate at which the peroxide is being formed (step 3, Scheme 1) is accelerating with the sweeping voltage, the rate at which dissociation occurs is likely to remain relatively the same. This gives room for peroxide to accumulate and diffuse towards the ring (scheme 1, step 5). Step 7 however is also potential driven and the rate goes faster with increasing voltage. Normally, this would speed up step 6 (the dissociation of peroxide) moderately. This is reflected in the gradual downslope of the ring current, depicting the slow increase in the reduction of peroxide via the hydroxide intermediate.

Yet another plausible reason for the decrease of the peroxide detection current on the forward scan could be that the peroxide was undergoing a catalytic rather than a chemical decomposition to form oxygen and hydroxide. However nitrogen doped carbons have not been known to be active for peroxide decomposition.

The summary of the mechanism of ORR on our nitrogen doped carbon catalyst can thus be described as a dominant two electron transfer accompanied by a minor direct four electron transport at the onset. The peroxide produced here is later converted to hydroxide and then to water which results in a further increase in the number of electrons transferred. This is scheme 1 in Figure 6.3

6.4 Microbial Fuel Cells

Three of the catalysts synthesized were tested in microbial fuel cells. These are nitrogen doped carbon NDAB-900; highly ordered mesoporous carbon, CMK-8 and CMK-8 with manganese oxide deposited by reaction with 20 wt% $KMnO_4$ i.e. CMK-8 (20 wt% $KMnO_4$). To put their performance in perspective 20 wt% platinum was also used. The experiments were performed in duplicates one after another; however, at the first run the cell with 20 wt% Pt did not produce current. Hence while the average for the three synthesized catalysts were obtained, only a set of values was obtained for 20 wt% Pt. This may likely skew the overall data. Hence the plots

presented in Figure 6.4 are for the three catalysts, the value for platinum would be stated for comparison.

Figure 6.4 shows the polarization curves. The x-axis is common to both **Figure 6-4** a and b i.e. current density in mA/m^2. The primary axis also compares the same parameter i.e. power density in mW/m^2. However the secondary axis for **Figure 6-4**a has the cell potential such that it depicts how the power output is changing with cell potential. On the other hand the secondary axis of Figure 6.4b captures the change in anode potential of each cell. Hence, Figure 6.4b seeks to clarify the relationship between power output and anode potential.

From Figure 6.4a and b, it is evident that power output from all the cells are almost equal within the low current region 43 mA/m^2 <I>480 mA/m^2, though the cell with NDAB-900 is slightly superior. Within the higher current region 506 mA/m^2 <I>1146 mA/m^2, the air-cathode microbial fuel cell with CMK-8(20 wt% $KMnO_4$) has the best power output followed by that of CMK-8 while that of NDAB-900 was least. From past experiments, it is known that very high resistances in the range of 5000 Ω to 52000 Ω (used here) tend to supress the difference in ORR activity of catalysts in the microbial fuel cell. Hence it can be concluded that CMK-8(20 wt% $KMnO_4$) that displayed the best performance at lower resistances is actually the best at all current range.

With respect to the cell potential, **Figure 6-4**a shows that the cell with NDAB-900 had a slightly higher potential within the low current region compared with the other two. However, this trend seems to be reversed as current increased such that at the high current region, it now had the least cell potential, while the cell with CMK-8(20wt% $KMnO_4$) displayed the best.

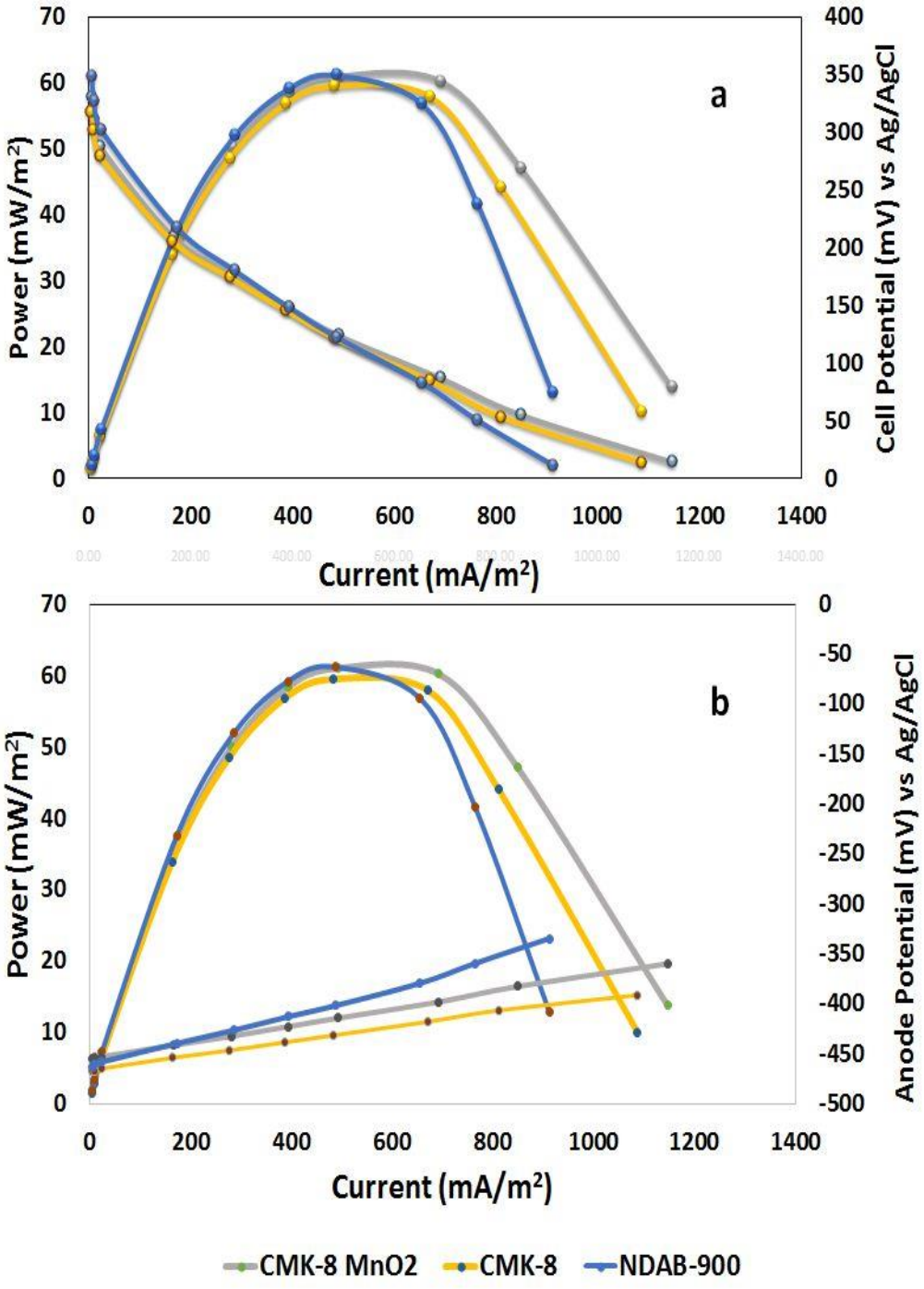

Figure 6-4 Polarization curves obtained from the air-cathode microbial fuel cells a) Power density and cell Potential b) Power density and anode potential. Anode medium was Acetate laden secondary inoculum. Experiments were carried out at pH 7 and RT.

According to **Figure 6-4**b, the best anode potential was shown by the cell with highly ordered mesoporous carbon CMK-8 as the cathode catalyst. Its superiority lasting through the entire current range. The other two catalysts had equal anode potentials within the current range 43 mA/m^2 <I>281 mA/cm^2. Beyond this, the cell with CMK-8(20wt% $KMnO_4$) had the better anode potential.

Expectedly, the trend of changing power output corresponds with that of cell potential in **Figure 6-4**a. The fact that the cells showed very similar cell voltage and power output within the region controlled by activation overpotential, typically V>150 mV (Lepage *et al.*, 2012) might indicate that in this setting the catalysts have the same inherent activity. The superiority of CMK-8(20wt% $KMnO_4$) is displayed only within the ohmic resistance controlled region. The possibilities are that either its superiority was previously supressed by the high resistors used or this may not be ascribed to its greater catalytic activity. On a positive note, CMK-8(20wt% $KMnO_4$) with the best performance in the high current region might be suited for applications that require significant current output. An example is the desalination of sea water using a microbial desalination cell (Jacobson *et al.*, 2011).

From **Figure 6-4**b the correlation between the anode potential and power output is a bit equivocal. Within the ohmic resistance controlled region CMK-8 with the best anode potential, did not have the best power output but NDAB-900 with the worst anode potential also had the worst power output. Considering that the differences in the anode potential is very small, ca 50 mV at most, it may be that the anode potential does not in any way limit the power output of the cell.

For comparison, the maximum power output obtained from the single experimental run with 20 wt% platinum was 205 mW/m^2 compared with the average maximum of 61 mW/m^2 obtained for CMK-8 and CMK-8(20wt% $KMnO_4$).

That the CMK-8 with MnO_2 deposited on it turned out to be the best is not surprising seeing that it was also the best within the alkaline system. This can be ascribed to the presence of manganese oxide combined with the excellent structural properties of highly ordered mesoporous carbon.

Chemical composition aside, amorphous manganese oxide catalysts have been proved to have very good ORR activity (Yang and Xu, 2003); Lee *et al.* (2011). One reason is that they are able to form a thin layer of manganese oxide on pores. This not only preserves the integrity of the structure to permit easy diffusion of substrate and product, but also allows for a fast three phase reaction and excellent catalyst utilization.

The possibility of increasing power density with increase in loading holds promise. Because the catalyst produced here are very cheap compared with platinum, a much higher loading can be used. This would have to be optimized though because of mass transfer limitations. Yuan et al (2010) used polypyrrole/carbon black composite for ORR in a microbial fuel with increasing catalysts loading and concluded that this led to an improved power output.

6.4.1 **Coulombic Efficiency**

One factor that can help advance the use of microbial fuel cells for waste water treatment and energy recovery is the coulombic efficiency (CE) of the cell (Fan *et al.*, 2007). This is defined as the amount of electrons that goes to produce current divided by the theoretical amount of electrons available for producing current (Logan *et al.*, 2006), expressed in percentage. CE was calculated for each of the cells and the results are presented along with the power density in **Figure 6-5**.

The MFC with CMK-8 carbon as cathode catalysts had the highest CE of 53%. The cell with NDAB-900 was next with 39%, closely followed by that with CMK-MnO_2 (20 wt% $KMnO_4$) 35%. CMK-8 had a slightly lower maximum power density of 59 mW/m^2. The other two cells had the same value of 61 mW/m^2.

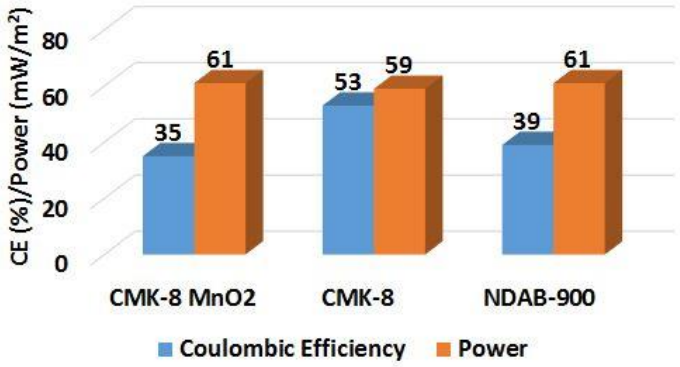

Figure 6-5 Coulombic efficiency and maximum power density of MFC's

That the CE is not directly proportional to maximum power density is not strange. Devasahayam and Masih (2012) carried out research using first *E. coli* and then water from a river (the substrate being glucose or sucrose) in a MFC. In both instances the CE and power density were calculated and there cell with the best power density also did not have the highest coulombic efficiency (CE).

It is observed in **Figure 6-4** that the cell with CMK-8 as cathode catalyst had an anode potential that was slightly higher than the other two. This might be a first-hand cause for the improved CE. Otherwise, all the cells had the same design and substrate and it might be possible that the difference in CE was a function of the cathode catalysts. The specifics of this cannot be explained at the moment.

It is encouraging however, that the cells here, especially that with CMK-8 carbon displayed a relatively high capability to recover electrons from substrates. This evidently puts them forward as candidates for use in waste water treatment and energy recovery. Of note is also the fact that this was achieved without any special treatment of the electrode materials or cell.

6.4.2 **Comparison with other MFCs**

Because of lack of common characteristics, making comparisons between microbial fuel cell from different sources is very difficult. This characteristics include exposed electrode surface area, type of electrolyte, nature of waste water, temperature and the gap between anode and cathode ((Roche *et al.*, 2010). However a comparison has been presented in Table 6.2. For a better perspective, the power densities obtained with platinum from the different sources are also included. This helps to emphasize the point that the performance shown might be due to other factors like cell architecture and not necessarily the cathode catalyst.

6.5 Summary

The nitrogen doped carbon catalysts synthesized in this work were tested in neutral media with a view to their application in microbial fuel cells. The onset potential was 0.60 V vs RHE as compared with platinum/carbon that had 0.96 V vs RHE. This would need to be improved on if the catalysts are to replace platinum in neutral media.

The synthesized catalysts namely NDAB-900, CMK-8 and CMK-8/MnO_2, were tested as cathode catalysts in a dissolved oxygen microbial fuel cell. The maximum power output of 61 mW/m^2 was generated by NDAB-900 and CMK-8/MnO_2. However, CMK-8 had the highest coulombic efficiency of 53%. Though the coulombic efficiency ranked very high, same cannot be said of the power density. This may be as a result of the architecture of the MFC, hence an improved architecture that maximises power output should be adopted for future work.

Catalyst and Ref	Nitrogen doped carbon powders (NDCP) (Feng *et al.*, 2012)	Mesoporous graphitic carbon nitride implanted with N_2 active sites (I-NG) (Feng *et al.*, 2013)	Activated nitrogen doped carbon nanofiber (ANCNF) (Yang *et al.*, 2014)	Nitrogen doped carbon derived from rice straw (NC). (Liu *et al.*, 2015b)	Manganese oxide functionalized CNT (Liew *et al.*, 2015)
Max power density in a MFC	In presence of sulfide 222.5 ± 8 mW/m^2 Pt-C 199.7± 4 mW /m^2	1618 ± 50 mW /m^2 Pt-C 1423 ± 25 mW/m^2	ANCNF-900 1377 ± 46 mW/m^2 Pt-C 1307 ± 43 mW/m^2	H-NC-900 2300 mW/m^2 Pt-C 1634 mW/m^2	520 mW/m^2
Catalyst and Ref	MnO_2-graphene hybrid (Wen *et al.*, 2012)	Nitrogen doped carbon (NDAB-900) This work	Ordered mesoporous carbon (CMK-8) This work	Manganese oxide functionalized Ordered mesoporous carbon (CMK-8) This work	Platinum/carbon This work
Max power density in a MFC	2084 mW/m^2 Pt/C 1714 mW/m^2	59 mW/m^2	61 mW/m^2	61 mW/m^2	205 mW/m2

Table 6-2 Comparison of the MFC power density from this work, with those from literature

Chapter 7. **Conclusion**

Using highly ordered mesoporous silica as template and o-phenylenediamine as carbon and nitrogen source, ordered mesoporous nitrogen doped carbon (NDAB) was prepared at pyrolysis temperatures of 700 °C, 800 °C and 900 °C. NDAB-900 showed the best activity. From physical and chemical analysis this can be ascribed to its superior surface area, higher proportion of graphitic nitrogen and the fact that it retained its ordered mesoporous structure. NDAB-900 had an onset potential of 0.93 RHE in 0.1 M KOH. The number of electrons transferred (calculated from disc and ring current) at 0.84 V RHE was 3.4. Though not better than platinum, the onset potential for this nitrogen doped carbon is one of the best compared with those reported in literature.

One of the most interesting findings of this work was the relatively good ORR activity of undoped highly ordered mesoporous carbon (OMC) CMK-8. This was not an objective at the onset. Synthesized using a surfactant as soft-template, it had an onset potential of 0.92 V RHE in 0.1 M KOH. This is the best ORR activity reported in literature for OMC in alkaline solution. It opens a new vista for the use of highly ordered mesoporous carbons as catalysts and catalyst supports for ORR in alkaline media.

Manganese oxides are known to be very abundant and environmentally benign. The synergy between them and the previously synthesized carbon catalysts namely nitrogen doped carbon and highly ordered mesoporous carbon was investigated. Two methods were used to deposit manganese oxide, namely the reduction of $KMnO_4$ in a neutral solution and the deposition followed by heat treatment of $Mn(NO_3)_2$ at 250 °C and 350 °C. The best onset potential of 1.05 V RHE in 0.1 M KOH was demonstrated by CMK-8/MnO_2 prepared by chemical oxidation using 20 wt% $KMnO_4$. To the best of our knowledge, this is the best onset potential amongst all credible sources cited in literature for inorganically synthesized manganese oxide catalysts.

This work has further strengthened the existing understanding that amorphous oxides when deposited or grown on porous structures yield very good activity (Yang and Xu, 2003; Lee *et al.*, 2011). Secondly, it is opening up the hitherto unexploited area of using the very simple procedure of chemical oxidation to produce highly active manganese oxide-ordered mesoporous carbon composites for ORR in alkaline media. This would further the objective of developing ORR catalysts that are easily produced on a large scale. The ease of the production process and availability of the materials would also drive down the final cost of the catalyst, while ensuring that it can be produced wherever it is needed.

The mechanism by which NDAB-900 carries out ORR in neutral media was studied. NDAB-900 reduces oxygen via a two and four electron pathway with the two electron reaction dominating. On a molecular level, along the four electron series pathway (as opposed to the direct four electron pathway), the peroxide is first converted to hydroxide which is then reduced to form water.

The use of these catalyst for waste water treatment and energy recovery was also explored. Though the power output was low with a maximum density of 61 mW/m^2, the coulombic efficiency (CE) of 53% for CMK-8 was impressive. Losses of coulombic can arise from secondary reactions. The high CE offers hope of future applications in waste water treatment given that the catalytic activity can be improved upon.

No doubt much still needs to be done if these catalysts must be developed to the point where they can be commercialised. Hence for future work the following are recommended,

I. Testing the catalysts in complete alkaline fuel cells.
II. Durability is critical to the commercialization of catalysts. Hence tests need to be conducted on how to improve the stability of the best catalysts obtained. Mild heat treatment readily comes to mind for this, other options would also be explored.

III. Investigation of the surface chemistry of the supports and how they interact with the manganese oxide precursors to yield the final oxide. Techniques like X-ray photoelectron spectroscopy and Fourier transform infra-red (FTIR) would be employed. This would lead to a directional design of specific manganese oxide catalysts.

IV. There still exists some gap between the best catalyst in this work and platinum. Thus there is the need to investigate what can be done to shrink this gap. Possible options would be combining the OMC support with more conductive ones and investigating the possibility of depositing other forms of manganese oxide.

V. The cost analysis should be done both on a cost of reactant basis as well as on an overall process cost basis. This may help to discover intrinsic costs attached to each catalyst.

VI. At present, most researchers report that they have synthesized exceptional catalysts without a common benchmark with which it can be assessed independently. Also, it is difficult to compare the work done by different researchers, because of cogent differences in their approach. Yet this is necessary in order to clearly identify the existing boundaries and what still needs to be done. There is therefore an urgent need for uniformity of standards of testing that will make factual progress obvious to all players in the field and not only to the researcher in question.

Without widely available and affordable oxygen reduction catalysts, market ready fuel cells may continue to be elusive; the promises the fuel cells hold for widespread and efficient use of environment friendly fuels like hydrogen may also not materialize and lastly the dream of saving our world from the environmental threat of fossil fuels. This work has brought us yet another step closer to the actualization of these dreams. ORR catalysts have been developed that have an activity much better than most already known and close to that of platinum in an alkaline system. This was achieved using highly ordered mesoporous carbon and manganese oxides that were synthesized from cheap and very widely available materials. Many complex procedures have been used previously in pursuant of this same goal but with lesser results. In contrast with

these, simple scalable processes which do not require high-end technology have been employed. This gives opportunity for widespread reproduction, even in countries with not too advanced technology. Hence, the days of expensive and scarcely available platinum as the only option for oxygen reduction in fuel cells are numbered.

References

Ackeret, M. and Ratner, B.D. (1992) 'Spin Cast Poly (vinyl isobutyl ether) Film on Glass Substrate by XPS', *Surface Science Spectra*, 1(1), pp. 96-99.

Ali, G.A.M., Yusoff, M.M., Ng, Y.H., Lim, H.N. and Chong, K.F. (2015) 'Potentiostatic and galvanostatic electrodeposition of manganese oxide for supercapacitor application: A comparison study', *Current Applied Physics*, 15(10), pp. 1143-1147.

Almar, L., Colldeforns, B., Yedra, L., Estrade, S., Peiro, F., Morata, A., Andreu, T. and Tarancon, A. (2013) 'High-temperature long-term stable ordered mesoporous Ni-CGO as an anode for solid oxide fuel cells', *Journal of Materials Chemistry A*, 1(14), pp. 4531-4538.

Artyushkova, K., Levendosky, S., Atanassov, P. and Fulghum, J. (2007) 'XPS Structural studies of nano-composite non-platinum electrocatalysts for polymer electrolyte fuel cells', *Topics in Catalysis*, 46(3-4), pp. 263-275.

Banham, D.W., Soderberg, J.N. and Birss, V.I. (2009) 'Pt/Carbon Catalyst Layer Microstructural Effects on Measured and Predicted Tafel Slopes for the Oxygen Reduction Reaction', *The Journal of Physical Chemistry C*, 113(23), pp. 10103-10111.

Banks, C.E., Davies, T.J., Wildgoose, G.G. and Compton, R.G. (2005) 'Electrocatalysis at graphite and carbon nanotube modified electrodes: Edge-plane sites and tube ends are the reactive sites', *Chemical Communications*, (7), pp. 829-841.

Bashyam, R. and Zelenay, P. (2006) 'A class of non-precious metal composite catalysts for fuel cells', *Nature*, 443(7107), pp. 63-66.

Benson, J., Xu, Q., Wang, P., Shen, Y., Sun, L., Wang, T., Li, M. and Papakonstantinou, P. (2014) 'Tuning the catalytic activity of graphene nanosheets for oxygen reduction reaction via size and thickness reduction', *ACS Applied Materials and Interfaces*, 6(22), pp. 19726-19736.

Bhattacharyya, S., Cardinaud, C. and Turban, G. (1998) 'Spectroscopic determination of the structure of amorphous nitrogenated carbon films', *Journal of Applied Physics*, 83(8), pp. 4491-4500.

Biesinger, M.C., Lau, L.W.M., Gerson, A.R. and Smart, R.S.C. (2010) 'Resolving surface chemical states in XPS analysis of first row transition metals, oxides and hydroxides: Sc, Ti, V, Cu and Zn', *Applied Surface Science*, 257(3), pp. 887-898.

Bikkarolla, S.K., Yu, F., Zhou, W., Joseph, P., Cumpson, P. and Papakonstantinou, P. (2014) 'A three-dimensional Mn3O4 network supported on a nitrogenated graphene electrocatalyst for efficient oxygen reduction reaction in alkaline media', *Journal of Materials Chemistry A*, 2(35), pp. 14493-14501.

Bojdys, M.J., Müller, J.O., Antonietti, M. and Thomas, A. (2008) 'Ionothermal synthesis of crystalline, condensed, graphitic carbon nitride', *Chemistry - A European Journal*, 14(27), pp. 8177-8182.

Boyd, K.J., Marton, D., Todorov, S.S., Al-Bayati, A.H., Kulik, J., Zuhr, R.A. and Rabalais, J.W. (1995) 'Formation of C–N thin films by ion beam deposition', *Journal of Vacuum Science & Technology A*, 13(4), pp. 2110-2122.

Brena, B., Luo, Y., Nyberg, M., Carniato, S., Nilson, K., Alfredsson, Y., Åhlund, J., Mårtensson, N., Siegbahn, H. and Puglia, C. (2004) 'Equivalent core-hole time-dependent density functional theory calculations of carbon $1s$ shake-up states of phthalocyanine', *Physical Review B*, 70(19), p. 195214.

Buchwalter, L.P. and Czornyj, G. (1990) 'Poly (methyl methacrylate) degradation during x-ray photoelectron spectroscopy analysis', *Journal of Vacuum Science & Technology A*, 8(2), pp. 781-784.

Bunazawa, H. and Yamazaki, Y. (2009) 'Ultrasonic synthesis and evaluation of non-platinum catalysts for alkaline direct methanol fuel cells', *Journal of Power Sources*, 190(2), pp. 210-215.

Calvillo, L., Celorrio, V., Moliner, R. and Lázaro, M.J. (2011) 'Influence of the support on the physicochemical properties of Pt electrocatalysts: Comparison of catalysts supported on different carbon materials', *Materials Chemistry and Physics*, 127(1-2), pp. 335-341.

Carvalho, A.C.M. and Dos Santos, M.C. (2006) 'Nitrogen-substituted nanotubes and nanojunctions: Conformation and electronic properties', *Journal of Applied Physics*, 100(8).

Chai, S.-H., Howe, J.Y., Wang, X., Kidder, M., Schwartz, V., Golden, M.L., Overbury, S.H., Dai, S. and Jiang, D.-e. (2012a) 'Graphitic mesoporous carbon as a support of promoted Rh catalysts for hydrogenation of carbon monoxide to ethanol', *Carbon*, 50(4), pp. 1574-1582.

Chai, S.H., Howe, J.Y., Wang, X., Kidder, M., Schwartz, V., Golden, M.L., Overbury, S.H., Dai, S. and Jiang, D.E. (2012b) 'Graphitic mesoporous carbon as a support of promoted Rh catalysts for hydrogenation of carbon monoxide to ethanol', *Carbon*, 50(4), pp. 1574-1582.

Charreteur, F., Jaouen, F., Ruggeri, S. and Dodelet, J.P. (2008) 'Fe/N/C non-precious catalysts for PEM fuel cells: Influence of the structural parameters of pristine commercial carbon blacks on their activity for oxygen reduction', *Electrochimica Acta*, 53(6), pp. 2925-2938.

Chen, R., Li, H., Chu, D. and Wang, G. (2009) 'Unraveling Oxygen Reduction Reaction Mechanisms on Carbon-Supported Fe-Phthalocyanine and Co-Phthalocyanine Catalysts in Alkaline Solutions', *The Journal of Physical Chemistry C*, 113(48), pp. 20689-20697.

Chen, R., Yan, J., Liu, Y. and Li, J. (2015) 'Three-dimensional nitrogen-doped graphene/MnO nanoparticle hybrids as a high-performance catalyst for oxygen reduction reaction', *Journal of Physical Chemistry C*, 119(15), pp. 8032-8037.

Chen, S., Chen, Y., He, G., He, S., Schröder, U. and Hou, H. (2012) 'Stainless steel mesh supported nitrogen-doped carbon nanofibers for binder-free cathode in microbial fuel cells', *Biosensors and Bioelectronics*, 34(1), pp. 282-285.

Ci, S., Wu, Y., Zou, J., Tang, L., Luo, S., Li, J. and Wen, Z. (2012) 'Nitrogen-doped graphene nanosheets as high efficient catalysts for oxygen reduction reaction', *Chinese Science Bulletin*, 57(23), pp. 3065-3070.

Conway, B.E., Tessier, D.F. and Wilkinson, D.P. (1989) 'Temperature dependence of the Tafel slope and electrochemical barrier symmetry factor, ß, in electrode kinetics', *Journal of the Electrochemical Society*, 136(9), pp. 2486-2493.

Cui, X., Shi, J., Zhang, L., Ruan, M. and Gao, J. (2009) 'PtCo supported on ordered mesoporous carbon as an electrode catalyst for methanol oxidation', *Carbon*, 47(1), pp. 186-194.

Czerw, R., Terrones, M., Charlier, J.C., Blase, X., Foley, B., Kamalakaran, R., Grobert, N., Terrones, H., Tekleab, D., Ajayan, P.M., Blau, W., Rühle, M. and Carroll, D.L. (2001) 'Identification of Electron Donor States in N-Doped Carbon Nanotubes', *Nano Letters*, 1(9), pp. 457-460.

De Bruijn, T.J.W., De Jong, W.A. and Van Den Berg, P.J. (1981) 'Thermal decomposition of aqueous manganese nitrate solutions and anhydrous manganese nitrate. Part 1. Mechanism', *Thermochimica Acta*, 45(3), pp. 265-278.

Delpeux, S., Beguin, F., Benoit, R., Erre, R., Manolova, N. and Rashkov, I. (1998) 'Fullerene core star-like polymers—1. Preparation from fullerenes and monoazidopolyethers', *European Polymer Journal*, 34(7), pp. 905-915.

Devasahayam, M. and Masih, S.A. (2012) 'Microbial fuel cells demonstrate high coulombic efficiency applicable for water remediation', *Indian Journal of Experimental Biology*, 50(6), pp. 430-438.

Dolhun, J.J. (2014) 'Observations on Manganese Dioxide As a Catalyst in the Decomposition of Hydrogen Peroxide: A Safer Demonstration', *Journal of Chemical Education*, 91(5), pp. 760-762.

Dommele, S.v. (2008) *Nitrogen Doped Carbon Nanotubes: synthesis, characterization and catalysis*. Utrecht University, Sorbonnelaan 16, Utrecht, The Netherlands.

Doren, A., Genet, M.J. and Rouxhet, P.G. (1994) 'Analysis of Poly(Ethylene Terephthalate) (PET) by XPS', *Surface Science Spectra*, 3(4), pp. 337-341.

Dresselhaus, M.S., Dresselhaus, G., Saito, R. and Jorio, A. (2005) 'Raman spectroscopy of carbon nanotubes', *Physics Reports*, 409(2), pp. 47-99.

El-Sawy, A.M., King'ondu, C.K., Kuo, C.H., Kriz, D.A., Guild, C.J., Meng, Y., Frueh, S.J., Dharmarathna, S., Ehrlich, S.N. and Suib, S.L. (2014) 'X-ray absorption spectroscopic study of a highly thermally stable manganese oxide octahedral molecular sieve (OMS-2) with high oxygen reduction reaction activity', *Chemistry of Materials*, 26(19), pp. 5752-5760.

Fabianowski, W., Coyle, L.C., Weber, B.A., Granata, R.D., Castner, D.G., Sadownik, A. and Regen, S.L. (1989) 'Spontaneous assembly of phosphatidylcholine monolayers via chemisorption onto gold', *Langmuir*, 5(1), pp. 35-41.

Fan, Y., Hu, H. and Liu, H. (2007) 'Enhanced Coulombic efficiency and power density of air-cathode microbial fuel cells with an improved cell configuration', *Journal of Power Sources*, 171(2), pp. 348-354.

Faubert, G., Lalande, G., Côté, R., Guay, D., Dodelet, J.P., Weng, L.T., Bertrand, P. and Dénès, G. (1996) 'Heat-treated iron and cobalt tetraphenylporphyrins adsorbed on carbon black: Physical characterization and catalytic properties of these materials for the reduction of oxygen in polymer electrolyte fuel cells', *Electrochimica Acta*, 41(10), pp. 1689-1701.

Faulkner, L.R. (1983) 'Understanding electrochemistry: Some distinctive concepts', *Journal of Chemical Education*, 60(4), pp. 262-264.

Feng, L., Chen, Y. and Chen, L. (2011a) 'Easy-to-operate and low-temperature synthesis of gram-scale nitrogen-doped graphene and its application as cathode catalyst in microbial fuel cells', *ACS Nano*, 5(12), pp. 9611-9618.

Feng, L., Yan, Y., Chen, Y. and Wang, L. (2011b) 'Nitrogen-doped carbon nanotubes as efficient and durable metal-free cathodic catalysts for oxygen reduction in microbial fuel cells', *Energy and Environmental Science*, 4(5), pp. 1892-1899.

Feng, L., Yang, L., Huang, Z., Luo, J., Li, M., Wang, D. and Chen, Y. (2013) 'Enhancing Electrocatalytic Oxygen Reduction on Nitrogen-Doped Graphene by Active Sites Implantation', *Scientific Reports*, 3, p. 3306.

Feng, Y. and Alonso-Vante, N. (2008) 'Nonprecious metal catalysts for the molecular oxygen-reduction reaction', *Physica Status Solidi (B) Basic Research*, 245(9), pp. 1792-1806.

Feng, Y., Shi, X., Wang, X., Lee, H., Liu, J., Qu, Y., He, W., Kumar, S.M.S., Kim, B.H. and Ren, N. (2012) 'Effects of sulfide on microbial fuel cells with platinum

and nitrogen-doped carbon powder cathodes', *Biosensors and Bioelectronics*, 35(1), pp. 413-415.

Figueiredo, J.L., Pereira, M.F.R., Freitas, M.M.A. and Órfão, J.J.M. (1999) 'Modification of the surface chemistry of activated carbons', *Carbon*, 37(9), pp. 1379-1389.

Fischer, A.E., Pettigrew, K.A., Rolison, D.R., Stroud, R.M. and Long, J.W. (2007) 'Incorporation of homogeneous, nanoscale MnO2 within ultraporous carbon structures via self-limiting electroless deposition: Implications for electrochemical capacitors', *Nano Letters*, 7(2), pp. 281-286.

Gabe, D.R. (2005) 'The centenary of Tafel's equation', *Transactions of the Institute of Metal Finishing*, 83(3), pp. 121-124.

Gao, H., Li, Z. and Qin, X. (2014) 'Synthesis of carbon microspheres loaded with manganese oxide as air cathode in alkaline media', *Journal of Power Sources*, 248, pp. 565-569.

Gao, X., Chen, Z., Yao, Y., Zhou, M., Liu, Y., Wang, J., Wu, W.D., Chen, X.D., Wu, Z. and Zhao, D. (2016) 'Direct Heating Amino Acids with Silica: A Universal Solvent-Free Assembly Approach to Highly Nitrogen-Doped Mesoporous Carbon Materials', *Advanced Functional Materials*, 26(36), pp. 6649-6661.

Gao, Y., Zhao, H., Chen, D., Chen, C. and Ciucci, F. (2015) 'In situ synthesis of mesoporous manganese oxide/sulfur-doped graphitized carbon as a bifunctional catalyst for oxygen evolution/reduction reactions', *Carbon*, 94, pp. 1028-1036.

Gardella, J.A., Ferguson, S.A. and Chin, R.L. (1986) 'π*← π shakeup satellites for the analysis of structure and bonding in aromatic polymers by X-Ray Photoelectron Spectroscopy', *Applied spectroscopy*, 40(2), pp. 224-232.

Gardner, S.D., Singamsetty, C.S.K., Booth, G.L., He, G.-R. and Pittman Jr, C.U. (1995) 'Surface characterization of carbon fibers using angle-resolved XPS and ISS', *Carbon*, 33(5), pp. 587-595.

Gasteiger, H.A., Kocha, S.S., Sompalli, B. and Wagner, F.T. (2005) 'Activity benchmarks and requirements for Pt, Pt-alloy, and non-Pt oxygen reduction catalysts for PEMFCs', *Applied Catalysis B: Environmental*, 56(1-2 SPEC. ISS.), pp. 9-35.

Gelius, U., Heden, P.F., Hedman, J., Lindberg, B.J., Manne, R., Nordberg, R., Nordling, C. and Siegbahn, K. (1970) 'Molecular spectroscopy by means of ESCA III. Carbon compounds', *Physica Scripta*, 2(1-2), p. 70.

Gierszal, K.P., Jaroniec, M., Kim, T.-W., Kim, J. and Ryoo, R. (2008) 'High temperature treatment of ordered mesoporous carbons prepared by using various carbon precursors and ordered mesoporous silica templates', *New Journal of Chemistry*, 32(6), pp. 981-993.

Gilbertson, L.M., Goodwin, D.G., Taylor, A.D., Pfefferle, L. and Zimmerman, J.B. (2014) 'Toward tailored functional design of multi-walled carbon nanotubes (MWNTs): Electrochemical and antimicrobial activity enhancement via oxidation and selective reduction', *Environmental Science and Technology*, 48(10), pp. 5938-5945.

Gileadi, E. and Gileadi, E. (2011) 'Physical electrochemistry: fundamentals, techniques and applications'.

Giovanoli, R. (1980) 'Vernadite is random-stacked birnessite - A discussion of the paper by F. V. Chukhrov et al.: "Contributions to the mineralogy of authigenic manganese phases from marine manganese deposits" [Mineralium Deposita 14, 249-261 (1979)]', *Mineralium Deposita*, 15(2), pp. 251-253.

Gnana kumar, G., Awan, Z., Suk Nahm, K. and Stanley Xavier, J. (2014) 'Nanotubular MnO2/graphene oxide composites for the application of open air-breathing cathode microbial fuel cells', *Biosensors and Bioelectronics*, 53, pp. 528-534.

Gorlin, Y., Chung, C.J., Nordlund, D., Clemens, B.M. and Jaramillo, T.F. (2012) 'Mn3O4 Supported on glassy carbon: An active non-precious metal catalyst for the oxygen reduction reaction', *ACS Catalysis*, 2(12), pp. 2687-2694.

Gorlin, Y. and Jaramillo, T.F. (2010) 'A Bifunctional Nonprecious Metal Catalyst for Oxygen Reduction and Water Oxidation', *Journal of the American Chemical Society*, 132(39), pp. 13612-13614.

Guo, Y., He, J., Wang, T., Xue, H., Hu, Y., Li, G., Tang, J. and Sun, X. (2011) 'Enhanced electrocatalytic activity of platinum supported on nitrogen modified ordered mesoporous carbon', *Journal of Power Sources*, 196(22), pp. 9299-9307.

Han, X., Zhang, T., Du, J., Cheng, F. and Chen, J. (2013) 'Porous calcium-manganese oxide microspheres for electrocatalytic oxygen reduction with high activity', *Chemical Science*, 4(1), pp. 368-376.

Hantsche, H. (1993) 'High resolution XPS of organic polymers, the scienta ESCA300 database. By G. Beamson and D. Briggs, Wiley, Chichester 1992, 295 pp., hardcover, £ 65.00, ISBN 0-471-93592-1', *Advanced Materials*, 5(10), pp. 778-778.

HaoYu, E., Cheng, S., Scott, K. and Logan, B. (2007) 'Microbial fuel cell performance with non-Pt cathode catalysts', *Journal of Power Sources*, 171(2), pp. 275-281.

Howe, J.Y., Rawn, C.J., Jones, L.E. and Ow, H. (2003) 'Improved crystallographic data for graphite', *Powder Diffraction*, 18(02), pp. 150-154.

Huang, X., Yue, H., Attia, A. and Yang, Y. (2007) 'Preparation and properties of manganese oxide/carbon composites by reduction of potassium permanganate with acetylene black', *Journal of the Electrochemical Society*, 154(1), pp. A26-A33.

Ikeda, T., Boero, M., Huang, S.F., Terakura, K., Oshima, M. and Ozaki, J.I. (2008) 'Carbon alloy catalysts: Active sites for oxygen reduction reaction', *Journal of Physical Chemistry C*, 112(38), pp. 14706-14709.

Inagaki, S., Yokoo, Y., Miki, T. and Kubota, Y. (2013) 'Improvement of electric double-layer capacitance of ordered mesoporous carbon CMK-3 by partial graphitization using metal oxide catalysts', *Microporous and Mesoporous Materials*, 179, pp. 136-143.

Indra, A., Menezes, P.W., Sahraie, N.R., Bergmann, A., Das, C., Tallarida, M., Schmeißer, D., Strasser, P. and Driess, M. (2014) 'Unification of catalytic water oxidation and oxygen reduction reactions: Amorphous beat crystalline cobalt iron oxides', *Journal of the American Chemical Society*, 136(50), pp. 17530-17536.

Jacobson, K.S., Drew, D.M. and He, Z. (2011) 'Use of a liter-scale microbial desalination cell as a platform to study bioelectrochemical desalination with salt solution or artificial seawater', *Environmental Science and Technology*, 45(10), pp. 4652-4657.

James, B.D., Kalinoski, J. and Baum, K. (2011) 'Manufacturing Cost Analysis of Fuel Cell Systems', [Online]. Available at: http://www.hydrogen.energy.gov/pdfs/review11/fc018_james_2011_o.pdf (Accessed: 11 August 2012).

James, B.D., Kevin, N.B. and Andrew, B.S. (2012) *Mass Production Cost Estimation of Direct H2 PEM Fuel Cell Systems for Automotive Applications: 2011 Update*. Inc, S.A. [Online]. Available at: https://www.sainc.com/service/SA%202011%20Update%20of%20Cost%20Analysi

s%20of%20Light%20Duty%20Automobile%20Fuel%20Cell%20Power%20Systems.pdf.

James, B.D., Moton, J.M. and Collela, W.G. (2015) *Mass Production Cost Estimation of Direct H2 PEM Fuel Cell Systems for Transportation Applications: 2014 Update*. Strategic Analysis Inc. [Online]. Available at: https://www.researchgate.net/publication/283505374_Mass_Production_Cost_Estimation_of_Direct_H2_PEM_Fuel_Cell_Systems_for_Transportation_Applications_2014_Update.

James, B.D., Moton, J.M., Collela, W.G. and Whitney, G.C. (2014) *Direct H2 PEM Fuel Cell Systems for Transportation Applications: 2013 Update*.Strategic Analysis Inc. [Online]. Available at: http://energy.gov/sites/prod/files/2014/11/f19/fcto_sa_2013_pemfc_transportation_cost_analysis.pdf.

Janarthanan, R., Serov, A., Pilli, S.K., Gamarra, D.A., Atanassov, P., Hibbs, M.R. and Herring, A.M. (2015) 'Direct Methanol Anion Exchange Membrane Fuel Cell with a Non-Platinum Group Metal Cathode based on Iron-Aminoantipyrine Catalyst', *Electrochimica Acta*, 175, pp. 202-208.

Jasinski, R. (1964) 'A new fuel cell cathode catalyst [13]', *Nature*, 201(4925), pp. 1212-1213.

Jeon, I.-Y., Choi, H.-J., Choi, M., Seo, J.-M., Jung, S.-M., Kim, M.-J., Zhang, S., Zhang, L., Xia, Z., Dai, L., Park, N. and Baek, J.-B. (2013) 'Facile, scalable synthesis of edge-halogenated graphene nanoplatelets as efficient metal-free eletrocatalysts for oxygen reduction reaction', *Sci. Rep.*, 3.

Jiang, C., Guo, Z., Zhu, Y., Liu, H., Wan, M. and Jiang, L. (2015) 'Shewanella-mediated biosynthesis of manganese oxide micro-/nanocubes as efficient electrocatalysts for the oxygen reduction reaction', *ChemSusChem*, 8(1), pp. 158-163.

Jiang, R. and Anson, F.C. (1991) 'The origin of inclined plateau currents in steady-state voltammograms for electrode processes involving electrocatalysis', *Journal of Electroanalytical Chemistry*, 305(2), pp. 171-184.

Jin, S. and Atrens, A. (1987) 'ESCA-studies of the structure and composition of the passive film formed on stainless steels by various immersion times in 0.1 M NaCl solution', *Applied Physics A*, 42(2), pp. 149-165.

Jordan, J.L., Kovac, C.A., Morar, J.F. and Pollak, R.A. (1987) 'High-resolution photoemission study of the interfacial reaction of Cr with polyimide and model polymers', *Physical Review B*, 36(3), p. 1369.

Jun, S., Sang Hoon, J., Ryoo, R., Kruk, M., Jaroniec, M., Liu, Z., Ohsuna, T. and Terasaki, O. (2000) 'Synthesis of new, nanoporous carbon with hexagonally ordered mesostructure [5]', *Journal of the American Chemical Society*, 122(43), pp. 10712-10713.

Kenko, T., Takakuwa, T., Saito, M., Daimon, H., Tasaka, A., Inaba, M., Kadoma, Y., Kumagai, N., Shiroishi, H., Hatai, T. and Kuwano, J. 566 (2013) 'Oxygen reduction catalytic activity of hollandite-type manganese oxides' *Key Engineering Materials*. pp. 253-257. Available at: http://www.scopus.com/inward/record.url?eid=2-s2.0-84883547988&partnerID=40&md5=ebd57c13df8e51622372e343f8631590.

Khilari, S., Pandit, S., Ghangrekar, M.M., Das, D. and Pradhan, D. (2013) 'Graphene supported [small alpha]-MnO2 nanotubes as a cathode catalyst for improved power generation and wastewater treatment in single-chambered microbial fuel cells', *RSC Advances*, 3(21), pp. 7902-7911.

Kim, H., Lee, K., Woo, S.I. and Jung, Y. (2011a) 'On the mechanism of enhanced oxygen reduction reaction in nitrogen-doped graphene nanoribbons', *Physical Chemistry Chemical Physics*, 13(39), pp. 17505-17510.

Kim, J.R., Kim, J.Y., Han, S.B., Park, K.W., Saratale, G.D. and Oh, S.E. (2011b) 'Application of Co-naphthalocyanine (CoNPc) as alternative cathode catalyst and support structure for microbial fuel cells', *Bioresource Technology*, 102(1), pp. 342-347.

Kim, N.D., Kim, W., Joo, J.B., Oh, S., Kim, P., Kim, Y. and Yi, J. (2008) 'Electrochemical capacitor performance of N-doped mesoporous carbons prepared by ammoxidation', *Journal of Power Sources*, 180(1), pp. 671-675.

Kim, T.-W., Kleitz, F., Paul, B. and Ryoo, R. (2005) 'MCM-48-like Large Mesoporous Silicas with Tailored Pore Structure: Facile Synthesis Domain in a Ternary Triblock Copolymer−Butanol−Water System', *Journal of the American Chemical Society*, 127(20), pp. 7601-7610.

Kobayashi, M., Niwa, H., Harada, Y., Horiba, K., Oshima, M., Ofuchi, H., Terakura, K., Ikeda, T., Koshigoe, Y., Ozaki, J.I., Miyata, S., Ueda, S., Yamashita, Y., Yoshikawa, H. and Kobayashi, K. (2011) 'Role of residual transition-metal atoms in oxygen reduction reaction in cobalt phthalocyanine-based carbon cathode catalysts for polymer electrolyte fuel cell', *Journal of Power Sources*, 196(20), pp. 8346-8351.

Kobayashi, M., Niwa, H., Saito, M., Harada, Y., Oshima, M., Ofuchi, H., Terakura, K., Ikeda, T., Koshigoe, Y., Ozaki, J.I. and Miyata, S. (2012) 'Indirect contribution of transition metal towards oxygen reduction reaction activity in iron phthalocyanine-based carbon catalysts for polymer electrolyte fuel cells', *Electrochimica Acta*, 74, pp. 254-259.

Kundu, S., Nagaiah, T.C., Xia, W., Wang, Y., Dommele, S.V., Bitter, J.H., Santa, M., Grundmeier, G., Bron, M., Schuhmann, W. and Muhler, M. (2009) 'Electrocatalytic Activity and Stability of Nitrogen-Containing Carbon Nanotubes in the Oxygen Reduction Reaction', *The Journal of Physical Chemistry C*, 113(32), pp. 14302-14310.

Kurak, K.A. and Anderson, A.B. (2009) 'Nitrogen-treated graphite and oxygen electroreduction on pyridinic edge sites', *Journal of Physical Chemistry C*, 113(16), pp. 6730-6734.

Lee, J., Kim, J. and Hyeon, T. (2006) 'Recent progress in the synthesis of porous carbon materials', *Advanced Materials*, 18(16), pp. 2073-2094.

Lee, J.S., Park, G.S., Lee, H.I., Kim, S.T., Cao, R., Liu, M. and Cho, J. (2011) 'Ketjenblack carbon supported amorphous manganese oxides nanowires as highly efficient electrocatalyst for oxygen reduction reaction in alkaline solutions', *Nano Letters*, 11(12), pp. 5362-5366.

Lee, K., Ahmed, M.S. and Jeon, S. (2015) 'Electrochemical deposition of silver on manganese dioxide coated reduced graphene oxide for enhanced oxygen reduction reaction', *Journal of Power Sources*, 288, pp. 261-269.

Lee, T., Jeon, E.K. and Kim, B.-S. (2014) 'Mussel-inspired nitrogen-doped graphene nanosheet supported manganese oxide nanowires as highly efficient electrocatalysts for oxygen reduction reaction', *Journal of Materials Chemistry A*, 2(17), pp. 6167-6173.

Lepage, G., Albernaz, F.O., Perrier, G. and Merlin, G. (2012) 'Characterization of a microbial fuel cell with reticulated carbon foam electrodes', *Bioresource Technology*, 124, pp. 199-207.

Lewin, E., Persson, P.O.Å., Lattemann, M., Stüber, M., Gorgoi, M., Sandell, A., Ziebert, C., Schäfers, F., Braun, W. and Halbritter, J. (2008) 'On the origin of a third spectral component of C1s XPS-spectra for nc-TiC/aC nanocomposite thin films', *Surface and Coatings Technology*, 202(15), pp. 3563-3570.

Lhoest, J.B., Bertrand, P., Weng, L.T. and Dewez, J.L. (1995) 'Combined Time-of-Flight Secondary Ion Mass Spectrometry and X-ray Photoelectron Spectroscopy Study of the Surface Segregation of Poly(methyl methacrylate) (PMMA) in

Bisphenol A Polycarbonate/PMMA Blends', *Macromolecules*, 28(13), pp. 4631-4637.

Li, B., Li, X., Wang, H. and Wu, P. (2011) 'Pt nanoparticles entrapped in ordered mesoporous carbon for enantioselective hydrogenation', *Journal of Molecular Catalysis A: Chemical*, 345(1-2), pp. 81-89.

Li, J., Li, Z., Tong, J., Xia, C. and Li, F. (2015) 'Nitrogen-doped ordered mesoporous carbon sphere with short channel as an efficient metal-free catalyst for oxygen reduction reaction', *RSC Advances*, 5(86), pp. 70010-70016.

Li, S., Hu, Y., Xu, Q., Sun, J., Hou, B. and Zhang, Y. (2012a) 'Iron- and nitrogen-functionalized graphene as a non-precious metal catalyst for enhanced oxygen reduction in an air-cathode microbial fuel cell', *Journal of Power Sources*, 213(0), pp. 265-269.

Li, Y., Li, M., Jiang, L., Lin, L., Cui, L. and He, X. (2014) 'Advanced oxygen reduction reaction catalyst based on nitrogen and sulfur co-doped graphene in alkaline medium', *Physical Chemistry Chemical Physics*, 16(42), pp. 23196-23205.

Li, Y., Li, T., Yao, M. and Liu, S. (2012b) 'Metal-free nitrogen-doped hollow carbon spheres synthesized by thermal treatment of poly(o-phenylenediamine) for oxygen reduction reaction in direct methanol fuel cell applications', *Journal of Materials Chemistry*, 22(21), pp. 10911-10917.

Liang, J., Jiao, Y., Jaroniec, M. and Qiao, S.Z. (2012a) 'Sulfur and Nitrogen Dual-Doped Mesoporous Graphene Electrocatalyst for Oxygen Reduction with Synergistically Enhanced Performance', *Angewandte Chemie International Edition*, 51(46), pp. 11496-11500.

Liang, Y., Wang, H., Zhou, J., Li, Y., Wang, J., Regier, T. and Dai, H. (2012b) 'Covalent hybrid of spinel manganese-cobalt oxide and graphene as advanced

oxygen reduction electrocatalysts', *Journal of the American Chemical Society*, 134(7), pp. 3517-3523.

Liew, K.B., Wan Daud, W.R., Ghasemi, M., Loh, K.S., Ismail, M., Lim, S.S. and Leong, J.X. (2015) 'Manganese oxide/functionalised carbon nanotubes nanocomposite as catalyst for oxygen reduction reaction in microbial fuel cell', *International Journal of Hydrogen Energy*, 40(35), pp. 11625-11632.

Lin, C.C. and Kuo, C.L. (2013) 'Effects of carbon nanotubes acid treated or annealed and manganese nitrate thermally decomposed on capacitive characteristics of electrochemical capacitors', *Journal of Nanomaterials*, 2013.

Liu, B., Thomas, P.S., Ray, A.S. and Williams, R.P. (2004) 'The effect of sampling conditions on the thermal decomposition of electrolytic manganese dioxide', *Journal of Thermal Analysis and Calorimetry*, 76(1), pp. 115-122.

Liu, G., Li, X., Lee, J.W. and Popov, B.N. (2011a) 'A review of the development of nitrogen-modified carbon-based catalysts for oxygen reduction at USC', *Catalysis Science and Technology*, 1(2), pp. 207-217.

Liu, H., Song, C., Tang, Y., Zhang, J. and Zhang, J. (2007) 'High-surface-area CoTMPP/C synthesized by ultrasonic spray pyrolysis for PEM fuel cell electrocatalysts', *Electrochimica Acta*, 52(13), pp. 4532-4538.

Liu, J., He, W.X., Wei, X.J., Diao, A.Q., Xie, J.M. and Lü, X.M. (2015a) 'Ag-embedded MnO nanorod: facile synthesis and oxygen reduction', *CrystEngComm*, 17(40), pp. 7646-7652.

Liu, L., Deng, Q.F., Agula, B., Zhao, X., Ren, T.Z. and Yuan, Z.Y. (2011b) 'Ordered mesoporous carbon catalyst for dehydrogenation of propane to propylene', *Chemical Communications*, 47(29), pp. 8334-8336.

Liu, L., Xiong, Q., Li, C., Feng, Y. and Chen, S. (2015b) 'Conversion of straw to nitrogen doped carbon for efficient oxygen reduction catalysts in microbial fuel cells', *RSC Advances*, 5(109), pp. 89771-89776.

Liu, N., Yin, L., Wang, C., Zhang, L., Lun, N., Xiang, D., Qi, Y. and Gao, R. (2010a) 'Adjusting the texture and nitrogen content of ordered mesoporous nitrogen-doped carbon materials prepared using SBA-15 silica as a template', *Carbon*, 48(12), pp. 3579-3591.

Liu, R., Wu, D., Feng, X. and Müllen, K. (2010b) 'Nitrogen-doped ordered mesoporous graphitic arrays with high electrocatalytic activity for oxygen reduction', *Angewandte Chemie - International Edition*, 49(14), pp. 2565-2569.

Liu, S.H., Chiang, C.C., Wu, M.T. and Liu, S.B. (2010c) 'Electrochemical activity and durability of platinum nanoparticles supported on ordered mesoporous carbons for oxygen reduction reaction', *International Journal of Hydrogen Energy*, 35(15), pp. 8149-8154.

Liu, X.W., Sun, X.F., Huang, Y.X., Sheng, G.P., Zhou, K., Zeng, R.J., Dong, F., Wang, S.G., Xu, A.W., Tong, Z.H. and Yu, H.Q. (2010d) 'Nano-structured manganese oxide as a cathodic catalyst for enhanced oxygen reduction in a microbial fuel cell fed with a synthetic wastewater', *Water Research*, 44(18), pp. 5298-5305.

Liu, Y., Liu, H., Wang, C., Hou, S.X. and Yang, N. (2013) 'Sustainable energy recovery in wastewater treatment by microbial fuel cells: Stable power generation with nitrogen-doped graphene cathode', *Environmental Science and Technology*, 47(23), pp. 13889-13895.

Logan, B.E., Hamelers, B., Rozendal, R., Schröder, U., Keller, J., Freguia, S., Aelterman, P., Verstraete, W. and Rabaey, K. (2006) 'Microbial fuel cells: Methodology and technology', *Environmental Science and Technology*, 40(17), pp. 5181-5192.

Lu, A., Kiefer, A., Schmidt, W. and Schüth, F. (2003) 'Synthesis of Polyacrylonitrile-Based Ordered Mesoporous Carbon with Tunable Pore Structures', *Chemistry of Materials*, 16(1), pp. 100-103.

Lu, M., Kharkwal, S., Ng, H.Y. and Li, S.F.Y. (2011) 'Carbon nanotube supported MnO 2 catalysts for oxygen reduction reaction and their applications in microbial fuel cells', *Biosensors and Bioelectronics*, 26(12), pp. 4728-4732.

Luo, Z., Lim, S., Tian, Z., Shang, J., Lai, L., MacDonald, B., Fu, C., Shen, Z., Yu, T. and Lin, J. (2011) 'Pyridinic N doped graphene: Synthesis, electronic structure, and electrocatalytic property', *Journal of Materials Chemistry*, 21(22), pp. 8038-8044.

Lyth, S.M., Nabae, Y., Islam, N.M., Kuroki, S., Kakimoto, M. and Miyata, S. (2011) 'Electrochemical oxygen reduction activity of carbon nitride supported on carbon black', *Journal of the Electrochemical Society*, 158(2), pp. B194-B201.

Ma, S.B., Lee, Y.H., Ahn, K.Y., Kim, C.M., Oh, K.H. and Kim, K.B. (2006) 'Spontaneously deposited manganese oxide on acetylene black in an aqueous potassium permanganate solution', *Journal of the Electrochemical Society*, 153(1), pp. C27-C32.

Ma, Y., Wang, R., Wang, H., Key, J. and Ji, S. (2015) 'Control of MnO2 nanocrystal shape from tremella to nanobelt for ehancement of the oxygen reduction reaction activity', *Journal of Power Sources*, 280, pp. 526-532.

Maiyalagan, T., Alaje, T.O. and Scott, K. (2012a) 'Highly stable Pt-Ru nanoparticles supported on three-dimensional cubic ordered mesoporous carbon (Pt-Ru/CMK-8) as promising electrocatalysts for methanol oxidation', *Journal of Physical Chemistry C*, 116(3), pp. 2630-2638.

Maiyalagan, T., Nassr, A.B.A., Alaje, T.O., Bron, M. and Scott, K. (2012b) 'Three-dimensional cubic ordered mesoporous carbon (CMK-8) as highly efficient stable

Pd electro-catalyst support for formic acid oxidation', *Journal of Power Sources*, 211, pp. 147-153.

Mangun, C.L., Benak, K.R., Economy, J. and Foster, K.L. (2001) 'Surface chemistry, pore sizes and adsorption properties of activated carbon fibers and precursors treated with ammonia', *Carbon*, 39(12), pp. 1809-1820.

Mao, L., Zhang, D., Sotomura, T., Nakatsu, K., Koshiba, N. and Ohsaka, T. (2003) 'Mechanistic study of the reduction of oxygen in air electrode with manganese oxides as electrocatalysts', *Electrochimica Acta*, 48(8), pp. 1015-1021.

Martínez Millán, W., Toledano Thompson, T., Arriaga, L.G. and Smit, M.A. (2009) 'Characterization of composite materials of electroconductive polymer and cobalt as electrocatalysts for the oxygen reduction reaction', *International Journal of Hydrogen Energy*, 34(2), pp. 694-702.

Maruyama, J. and Abe, I. (2007a) 'Performance of polymer electrolyte fuel cell formed from Pt-loaded activated carbon with various pore structures', *Electrochemistry*, 75(2), pp. 119-121.

Maruyama, J. and Abe, I. (2007b) 'Structure control of a carbon-based noble-metal-free fuel cell cathode catalyst leading to high power output', *Chemical Communications*, (27), pp. 2879-2881.

Matter, P.H., Wang, E., Arias, M., Biddinger, E.J. and Ozkan, U.S. (2007) 'Oxygen reduction reaction activity and surface properties of nanostructured nitrogen-containing carbon', *Journal of Molecular Catalysis A: Chemical*, 264(1–2), pp. 73-81.

Mayrhofer, K.J.J., Blizanac, B.B., Arenz, M., Stamenkovic, V.R., Ross, P.N. and Markovic, N.M. (2005) 'The impact of geometric and surface electronic properties of Pt-catalysts on the particle size effect in electrocatalysis', *Journal of Physical Chemistry B*, 109(30), pp. 14433-14440.

Mendoza-Sánchez, B., Coelho, J., Pokle, A. and Nicolosi, V. (2015) 'A 2D graphene-manganese oxide nanosheet hybrid synthesized by a single step liquid-phase co-exfoliation method for supercapacitor applications', *Electrochimica Acta*, 174, pp. 696-705.

Meng, Y., Song, W., Huang, H., Ren, Z., Chen, S.Y. and Suib, S.L. (2014) 'Structure-property relationship of bifunctional MnO2 nanostructures: Highly efficient, ultra-stable electrochemical water oxidation and oxygen reduction reaction catalysts identified in alkaline media', *Journal of the American Chemical Society*, 136(32), pp. 11452-11464.

Miller, D.J., Biesinger, M.C. and McIntyre, N.S. (2002) 'Interactions of CO2 and CO at fractional atmosphere pressures with iron and iron oxide surfaces: one possible mechanism for surface contamination?', *Surface and Interface Analysis*, 33(4), pp. 299-305.

Momčilović, M., Stojmenović, M., Gavrilov, N., Pašti, I., Mentus, S. and Babić, B. (2014) 'Complex electrochemical investigation of ordered mesoporous carbon synthesized by soft-templating method: Charge storage and electrocatalytical or Pt-electrocatalyst supporting behavior', *Electrochimica Acta*, 125, pp. 606-614.

Montes-Morán, M.A., Suárez, D., Menéndez, J.A. and Fuente, E. (2004) 'On the nature of basic sites on carbon surfaces: An overview', *Carbon*, 42(7), pp. 1219-1224.

Morozan, A., Campidelli, S., Filoramo, A., Jousselme, B. and Palacin, S. (2011) 'Catalytic activity of cobalt and iron phthalocyanines or porphyrins supported on different carbon nanotubes towards oxygen reduction reaction', *Carbon*, 49(14), pp. 4839-4847.

Mugikura, Y. and Asano, K. (2002) 'Performance of several types of fuel cells and factor analysis of performance', *Electrical Engineering in Japan (English translation of Denki Gakkai Ronbunshi)*, 138(1), pp. 24-33.

'Multi-Year Research, Development, and Demonstration Plan - Fuel Cells', (2016), [Online]. Available at: http://energy.gov/sites/prod/files/2016/06/f32/fcto_myrdd_fuel_cells_0.pdf (Accessed: 11 July, 2016).

Nagaiah, T.C., Bordoloi, A., Sánchez, M.D., Muhler, M. and Schuhmann, W. (2012) 'Mesoporous nitrogen-rich carbon materials as catalysts for the oxygen reduction reaction in alkaline solution', *ChemSusChem*, 5(4), pp. 637-641.

Ndamanisha, J.C. and Guo, L.P. (2012) 'Ordered mesoporous carbon for electrochemical sensing: A review', *Analytica Chimica Acta*, 747, pp. 19-28.

Nie, R., Bo, X., Luhana, C., Nsabimana, A. and Guo, L. (2014) 'Simultaneous formation of nitrogen and sulfur-doped carbon nanotubes-mesoporous carbon and its electrocatalytic activity for oxygen reduction reaction', *International Journal of Hydrogen Energy*, 39(24), pp. 12597-12603.

Niwa, H., Kobayashi, M., Horiba, K., Harada, Y., Oshima, M., Terakura, K., Ikeda, T., Koshigoe, Y., Ozaki, J.I., Miyata, S., Ueda, S., Yamashita, Y., Yoshikawa, H. and Kobayashi, K. (2011) 'X-ray photoemission spectroscopy analysis of N-containing carbon-based cathode catalysts for polymer electrolyte fuel cells', *Journal of Power Sources*, 196(3), pp. 1006-1011.

Nohman, A.K.H., Ismail, H.M. and Hussein, G.A.M. (1995) 'Thermal and chemical events in the decomposition course of manganese compounds', *Journal of Analytical and Applied Pyrolysis*, 34(2), pp. 265-278.

Oh, S.M., Kim, I.Y., Adpakpang, K. and Hwang, S.J. (2015) 'The beneficial effect of nanocrystalline and amorphous nature on the anode performance of manganese oxide for lithium ion batteries', *Electrochimica Acta*, 174, pp. 391-399.

Okamoto, Y. (2009) 'First-principles molecular dynamics simulation of O2 reduction on nitrogen-doped carbon', *Applied Surface Science*, 256(1), pp. 335-341.

Oku, M., Hirokawa, K. and Ikeda, S. (1975) 'X-ray photoelectron spectroscopy of manganese-oxygen systems', *Journal of Electron Spectroscopy and Related Phenomena*, 7(5), pp. 465-473.

Othman, R., Dicks, A.L. and Zhu, Z. (2012) 'Non precious metal catalysts for the PEM fuel cell cathode', *International Journal of Hydrogen Energy*, 37(1), pp. 357-372.

Pašti, I.A., Gavrilov, N.M., Dobrota, A.S., Momčilović, M., Stojmenović, M., Topalov, A., Stanković, D.M., Babić, B., Ćirić-Marjanović, G. and Mentus, S.V. (2015) 'The Effects of a Low-Level Boron, Phosphorus, and Nitrogen Doping on the Oxygen Reduction Activity of Ordered Mesoporous Carbons', *Electrocatalysis*, 6(6), pp. 498-511.

Pichler, T., Knupfer, M., Golden, M.S., Haffner, S., Friedlein, R., Fink, J., Andreoni, W., Curioni, A., Keshavarz-K, M., Bellavia-Lund, C., Sastre, A., Hummelen, J.C. and Wudl, F. (1997) 'On-ball doping of fullerencs: The electronic structure of C59N dimers from experiment and theory', *Physical Review Letters*, 78(22), pp. 4249-4252.

Rahinov, I., Ditzian, N., Goldman, A. and Cheskis, S. (2003) 'NH2 radical formation by ammonia pyrolysis in a temperature range of 800–1000 K', *Applied Physics B: Lasers and Optics*, 77(5), pp. 541-546.

Ramaswamy, N. and Mukerjee, S. (2011) 'Influence of Inner- and Outer-Sphere Electron Transfer Mechanisms during Electrocatalysis of Oxygen Reduction in Alkaline Media', *The Journal of Physical Chemistry C*, 115(36), pp. 18015-18026.

Ramaswamy, N. and Mukerjee, S. (2012) 'Fundamental Mechanistic Understanding of Electrocatalysis of Oxygen Reduction on Pt and Non-Pt Surfaces: Acid versus Alkaline Media', *Advances in Physical Chemistry*, 2012, p. 17.

Rao, C.V., Cabrera, C.R. and Ishikawa, Y. (2010) 'In search of the active site in nitrogen-doped carbon nanotube electrodes for the oxygen reduction reaction', *Journal of Physical Chemistry Letters*, 1(18), pp. 2622-2627.

Raymundo-Piñero, E., Cazorla-Amorós, D., Linares-Solano, A., Find, J., Wild, U. and Schlögl, R. (2002) 'Structural characterization of N-containing activated carbon fibers prepared from a low softening point petroleum pitch and a melamine resin', *Carbon*, 40(4), pp. 597-608.

Robertson, J. and Davis, C.A. (1995) 'Nitrogen doping of tetrahedral amorphous carbon', *Diamond and Related Materials*, 4(4), pp. 441-444.

Roche, I., Katuri, K. and Scott, K. (2010) 'A microbial fuel cell using manganese oxide oxygen reduction catalysts', *Journal of Applied Electrochemistry*, 40(1), pp. 13-21.

Roche, I. and Scott, K. (2009) 'Carbon-supported manganese oxide nanoparticles as electrocatalysts for oxygen reduction reaction (orr) in neutral solution', *Journal of Applied Electrochemistry*, 39(2), pp. 197-204.

Ruvinskiy, P.S., Bonnefont, A., Pham-Huu, C. and Savinova, E.R. (2011) 'Using ordered carbon nanomaterials for shedding light on the mechanism of the cathodic oxygen reduction reaction', *Langmuir*, 27(14), pp. 9018-9027.

Salgado, J.R.C., Alcaide, F., Álvarez, G., Calvillo, L., Lázaro, M.J. and Pastor, E. (2010) 'Pt-Ru electrocatalysts supported on ordered mesoporous carbon for direct methanol fuel cell', *Journal of Power Sources*, 195(13), pp. 4022-4029.

Schulte, K., Wang, L., Moriarty, P.J., Prassides, K. and Tagmatarchis, N. (2007) 'Resonant processes and Coulomb interactions in (C59 N)2', *Journal of Chemical Physics*, 126(18).

Sen, R.K., Zagal, J. and Yeager, E. (1977) 'The electrocatalysis of molecular oxygen reduction', *Inorganic Chemistry*, 16(12), pp. 3379-3380.

Sheng, X., Daems, N., Geboes, B., Kurttepeli, M., Bals, S., Breugelmans, T., Hubin, A., Vankelecom, I.F.J. and Pescarmona, P.P. (2015) 'N-doped ordered mesoporous carbons prepared by a two-step nanocasting strategy as highly active and selective electrocatalysts for the reduction of O2 to H2O2', *Applied Catalysis B: Environmental*, 176-177, pp. 212-224.

Shrestha, S. and Mustain, W.E. (2010) 'Properties of nitrogen-functionalized ordered mesoporous carbon prepared using polypyrrole precursor', *Journal of the Electrochemical Society*, 157(11), pp. B1665-B1672.

Shresthaa, S. and Mustaina, W.E. (2010). Available at: http://www.scopus.com/inward/record.url?eid=2-s2.0-79952688042&partnerID=40&md5=ba8deb2ac54a927034d68a26fcfd8474.

Shypunov, I., Kongi, N., Kozlova, J., Matisen, L., Ritslaid, P., Sammelselg, V. and Tammeveski, K. (2015) 'Enhanced Oxygen Reduction Reaction Activity with Electrodeposited Ag on Manganese Oxide–Graphene Supported Electrocatalyst', *Electrocatalysis*, 6(5), pp. 465-471.

Sing, K.S.W. 57 (1985) 'Reporting physisorption data for gas/solid systems with special reference to the determination of surface area and porosity (Recommendations 1984)' *Pure and Applied Chemistry*. p. 603 4. Available at: //www.degruyter.com/view/j/pac.1985.57.issue-4/pac198557040603/pac198557040603.xml (Accessed: 2016-01-18t16:54:07.046+01:00).

Slanac, D.A., Li, N., Stevenson, K.J. and Johnston, K.P. (2010). Available at: http://www.scopus.com/inward/record.url?eid=2-s2.0-77955991570&partnerID=40&md5=d55c777ae0eee789e3a8b9039857ff27.

Song, J., Xu, T., Gordin, M.L., Zhu, P., Lv, D., Jiang, Y.B., Chen, Y., Duan, Y. and Wang, D. (2014) 'Nitrogen-doped Mesoporous carbon promoted chemical adsorption of sulfur and fabrication of high-Areal-capacity sulfur cathode with exceptional cycling stability for lithium-sulfur batteries', *Advanced Functional Materials*, 24(9), pp. 1243-1250.

Song, X., Ren, H., Ding, J., Wang, C., Yin, X. and Wang, H. (2015) 'One-step nanocasting synthesis of sulfur and nitrogen co-doped ordered mesoporous carbons as efficient electrocatalysts for oxygen reduction', *Materials Letters*, 159, pp. 280-283.

Stańczyk, K., Dziembaj, R., Piwowarska, Z. and Witkowski, S. (1995) 'Transformation of nitrogen structures in carbonization of model compounds determined by XPS', *Carbon*, 33(10), pp. 1383-1392.

Stern, K.H. (1972) 'High temperature properties and decomposition of inorganic salts part 3, nitrates and nitrites', *Journal of Physical and Chemical Reference Data*, 1, pp. 747-772.

Stoerzinger, K.A., Risch, M., Han, B. and Shao-Horn, Y. (2015) 'Recent Insights into Manganese Oxides in Catalyzing Oxygen Reduction Kinetics', *ACS Catalysis*, 5(10), pp. 6021-6031.

Stöhr, B., Boehm, H.P. and Schlögl, R. (1991) 'Enhancement of the catalytic activity of activated carbons in oxidation reactions by thermal treatment with ammonia or hydrogen cyanide and observation of a superoxide species as a possible intermediate', *Carbon*, 29(6), pp. 707-720.

Strohmeier, B.R. and Hercules, D.M. (1984) 'Surface spectroscopic characterization of Mn/Al2O3 catalysts', *Journal of Physical Chemistry*, 88(21), pp. 4922-4929.

Su, D.S., Perathoner, S. and Centi, G. (2013) 'Nanocarbons for the development of advanced catalysts', *Chemical Reviews*, 113(8), pp. 5782-5816.

Su, F., Poh, C.K., Tian, Z., Xu, G., Koh, G., Wang, Z., Liu, Z. and Lin, J. (2010) 'Electrochemical behavior of pt nanoparticles supported on meso- and microporous carbons for fuel cells', *Energy and Fuels*, 24(7), pp. 3727-3732.

Su, Q. (2012) *Graphene based electrode materials for solar cell and electrochemical oxygen reduction*. Johannes Gutenberg-Universität [Online]. Available at: http://ubm.opus.hbz-nrw.de/volltexte/2012/3177.

Subramanian, N.P., Kumaraguru, S.P., Colon-Mercado, H., Kim, H., Popov, B.N., Black, T. and Chen, D.A. (2006) 'Studies on Co-based catalysts supported on modified carbon substrates for PEMFC cathodes', *Journal of Power Sources*, 157(1), pp. 56-63.

Sumboja, A., Ge, X., Goh, F.W.T., Li, B., Geng, D., Hor, T.S.A., Zong, Y. and Liu, Z. (2015) 'Manganese Oxide Catalyst Grown on Carbon Paper as an Air Cathode for High-Performance Rechargeable Zinc-Air Batteries', *ChemPlusChem*, 80(8), pp. 1341-1346.

Susi, T., Pichler, T. and Ayala, P. (2015) 'X-ray photoelectron spectroscopy of graphitic carbon nanomaterials doped with heteroatoms', *Beilstein Journal of Nanotechnology*, 6(1), pp. 177-192.

Szymański, G.S., Karpiński, Z., Biniak, S. and Świątkowski, A. (2002) 'The effect of the gradual thermal decomposition of surface oxygen species on the chemical and catalytic properties of oxidized activated carbon', *Carbon*, 40(14), pp. 2627-2639.

Tammeveski, K., Tenno, T., Rosental, A., Talonen, P., Johansson, L.S. and Niinistö, L. (1999) 'The Reduction of Oxygen on Pt-TiO2 Coated Ti Electrodes in Alkaline Solution', *Journal of the Electrochemical Society*, 146(2), pp. 669-676.

Tan, B.J., Klabunde, K.J. and Sherwood, P.M.A. (1991) 'XPS studies of solvated metal atom dispersed catalysts. Evidence for layered cobalt-manganese particles on alumina and silica', *Journal of the American Chemical Society*, 113(3), pp. 855-861.

Tan, Y., Xu, C., Chen, G., Fang, X., Zheng, N. and Xie, Q. (2012) 'Facile synthesis of manganese-oxide-containing mesoporous nitrogen-doped carbon for efficient oxygen reduction', *Advanced Functional Materials*, 22(21), pp. 4584-4591.

Terrones, M., Jorio, A., Endo, M., Rao, A.M., Kim, Y.A., Hayashi, T., Terrones, H., Charlier, J.C., Dresselhaus, G. and Dresselhaus, M.S. (2004) 'New direction in nanotube science', *Materials Today*, 7(9), pp. 30-45.

Thorum, M.S., Yadav, J. and Gewirth, A.A. (2009) 'Oxygen reduction activity of a copper complex of 3,5-diamino-1,2,4-triazole supported on carbon black', *Angewandte Chemie - International Edition*, 48(1), pp. 165-167.

Toda, T., Igarashi, H., Uchida, H. and Watanabe, M. (1999) 'Enhancement of the electroreduction of oxygen on Pt alloys with Fe, Ni, and Co', *Journal of the Electrochemical Society*, 146(10), pp. 3750-3756.

Town, J.L., MacLaren, F. and Dewald, H.D. (1991) 'Rotating disk voltammetry experiment', *Journal of Chemical Education*, 68(4), p. 352.

Wan, S., Wang, L. and Xue, Q. (2010) 'Electrochemical deposition of sulfur doped DLC nanocomposite film at atmospheric pressure', *Electrochemistry Communications*, 12(1), pp. 61-65.

Wang, J. (2006) *Analytical Electrochemistry*. 3rd Edition edn. New Jersey, USA: John Wiley and Sons Inc.

Wang, K., Zhang, J., Xia, W., Zou, R., Guo, J., Gao, Z., Yan, W., Guo, S. and Xu, Q. (2015a) 'A dual templating route to three-dimensionally ordered mesoporous carbon nanonetworks: tuning the mesopore type for electrochemical performance optimization', *Journal of Materials Chemistry A*, 3(37), pp. 18867-18873.

Wang, X., Lee, J.S., Zhu, Q., Liu, J., Wang, Y. and Dai, S. (2010) 'Ammonia-treated ordered mesoporous carbons as catalytic materials for oxygen reduction reaction', *Chemistry of Materials*, 22(7), pp. 2178-2180.

Wang, X., Li, Q., Pan, H., Lin, Y., Ke, Y., Sheng, H., Swihart, M.T. and Wu, G. (2015b) 'Size-controlled large-diameter and few-walled carbon nanotube catalysts for oxygen reduction', *Nanoscale*, 7(47), pp. 20290-20298.

Wang, Y., Zhang, C., Kang, S., Li, B., Wang, Y., Wang, L. and Li, X. (2011) 'Simple synthesis of graphitic ordered mesoporous carbon supports using natural seed fat', *Journal of Materials Chemistry*, 21(38), pp. 14420-14423.

Watts, J.F. (1994) 'X-ray photoelectron spectroscopy', *Vacuum*, 45(6), pp. 653-671.

Wen, Q., Wang, S., Yan, J., Cong, L., Pan, Z., Ren, Y. and Fan, Z. (2012) 'MnO2–graphene hybrid as an alternative cathodic catalyst to platinum in microbial fuel cells', *Journal of Power Sources*, 216, pp. 187-191.

Wu, J., Wang, Y., Zhang, D. and Hou, B. (2011) 'Studies on the electrochemical reduction of oxygen catalyzed by reduced graphene sheets in neutral media', *Journal of Power Sources*, 196(3), pp. 1141-1144.

Wu, S., Wen, G., Liu, X., Zhong, B. and Su, D.S. (2014) 'Model molecules with oxygenated groups catalyze the reduction of nitrobenzene: Insight into carbocatalysis', *ChemCatChem*, 6(6), pp. 1558-1561.

Wu, Z., Li, W., Xia, Y., Webley, P. and Zhao, D. (2012) 'Ordered mesoporous graphitized pyrolytic carbon materials: Synthesis, graphitization, and electrochemical properties', *Journal of Materials Chemistry*, 22(18), pp. 8835-8845.

Xia, Y. and Mokaya, R. (2004) 'Synthesis of ordered mesoporous carbon and nitrogen-doped carbon materials with graphitic pore walls via a simple chemical vapor deposition method', *Advanced Materials*, 16(17), pp. 1553-1558.

Yang, H., Alonso-Vante, N., Lamy, C. and Akins, D.L. (2005) 'High methanol tolerance of carbon-supported Pt-Cr alloy nanoparticle electrocatalysts for oxygen reduction', *Journal of the Electrochemical Society*, 152(4), pp. A704-A709.

Yang, J. and Xu, J.J. (2003) 'Nanoporous amorphous manganese oxide as electrocatalyst for oxygen reduction in alkaline solutions', *Electrochemistry Communications*, 5(4), pp. 306-311.

Yang, W., Fellinger, T.-P. and Antonietti, M. (2010) 'Efficient Metal-Free Oxygen Reduction in Alkaline Medium on High-Surface-Area Mesoporous Nitrogen-Doped Carbons Made from Ionic Liquids and Nucleobases', *Journal of the American Chemical Society*, 133(2), pp. 206-209.

Yang, X., Zou, W., Su, Y., Zhu, Y., Jiang, H., Shen, J. and Li, C. (2014) 'Activated nitrogen-doped carbon nanofibers with hierarchical pore as efficient oxygen reduction reaction catalyst for microbial fuel cells', *Journal of Power Sources*, 266, pp. 36-42.

Ye, S. and Vijh, A.K. (2005) 'Oxygen reduction on an iron–carbonized aerogel nanocomposite electrocatalyst', *Journal of Solid State Electrochemistry*, 9(3), pp. 146-153.

You, C., Xu, X., Tian, B., Kong, J., Zhao, D. and Liu, B. (2009) 'Electrochemistry and biosensing of glucose oxidase based on mesoporous carbons with different spatially ordered dimensions', *Talanta*, 78(3), pp. 705-710.

You, C., Yan, X., Kong, J., Zhao, D. and Liu, B. (2011) 'Bicontinuous gyroidal mesoporous carbon matrix for facilitating protein electrochemical and bioelectrocatalytic performances', *Talanta*, 83(5), pp. 1507-1514.

Yu, E.H. and Scott, K. (2004) 'Direct methanol alkaline fuel cell with catalysed metal mesh anodes', *Electrochemistry Communications*, 6(4), pp. 361-365.

Yu, J., Guo, M., Muhammad, F., Wang, A., Zhang, F., Li, Q. and Zhu, G. (2014) 'One-pot synthesis of highly ordered nitrogen-containing mesoporous carbon with resorcinol–urea–formaldehyde resin for CO2 capture', *Carbon*, 69, pp. 502-514.

Yuan, Y., Zhou, S. and Zhuang, L. (2010) 'Polypyrrole/carbon black composite as a novel oxygen reduction catalyst for microbial fuel cells', *Journal of Power Sources*, 195(11), pp. 3490-3493.

Zagal, J.H. (1992) 'Metallophthalocyanines as catalysts in electrochemical reactions', *Coordination Chemistry Reviews*, 119(0), pp. 89-136.

Zhang, J., Guo, C., Zhang, L. and Li, C.M. (2013) 'Direct growth of flower-like manganese oxide on reduced graphene oxide towards efficient oxygen reduction reaction', *Chemical Communications*, 49(57), pp. 6334-6336.

Zhang, L., Liu, C., Zhuang, L., Li, W., Zhou, S. and Zhang, J. (2009) 'Manganese dioxide as an alternative cathodic catalyst to platinum in microbial fuel cells', *Biosensors and Bioelectronics*, 24(9), pp. 2825-2829.

Zhang, L. and Xia, Z. (2011) 'Mechanisms of oxygen reduction reaction on nitrogen-doped graphene for fuel cells', *Journal of Physical Chemistry C*, 115(22), pp. 11170-11176.

Zhang, P., Li, K. and Liu, X. (2014) 'Carnation-like MnO2 modified activated carbon air cathode improve power generation in microbial fuel cells', *Journal of Power Sources*, 264, pp. 248-253.

Zhang, P., Lian, J.S. and Jiang, Q. (2012) 'Potential dependent and structural selectivity of the oxygen reduction reaction on nitrogen-doped carbon nanotubes: A density functional theory study', *Physical Chemistry Chemical Physics*, 14(33), pp. 11715-11723.

Zhao, F., Rahunen, N., Varcoe, J.R., Chandra, A., Avignone-Rossa, C., Thumser, A.E. and Slade, R.C.T. (2008) 'Activated carbon cloth as anode for sulfate removal in a microbial fuel cell', *Environmental science & technology*, 42(13), pp. 4971-4976.

Zhou, S., Wu, H., Wu, Y., Shi, H., Feng, X., Jiang, S., Chen, J. and Song, W. (2014) 'Hemi-ordered nanoporous carbon electrode material for highly selective determination of nitrite in physiological and environmental systems', *Thin Solid Films*, 564, pp. 406-411.